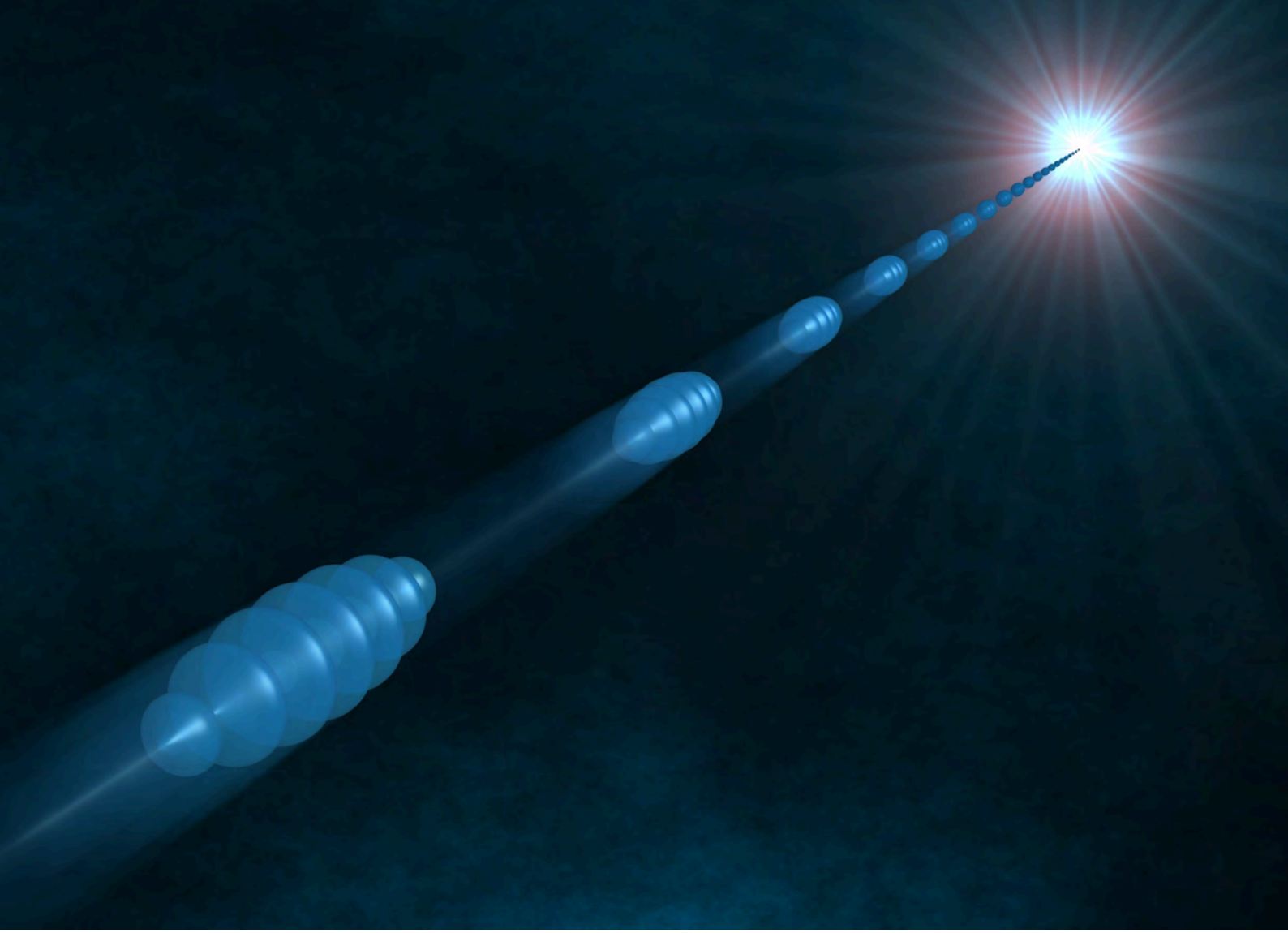

FLASH 2020+

Making FLASH brighter, faster and more flexible
Conceptual Design Report

Deutsches Elektronen-Synchrotron DESY
A Research Centre of the Helmholtz Association

Deutsches Elektronen-Synchrotron DESY

FLASH2020+

Upgrade of FLASH

Conceptual Design Report

Contents

Contributors

Sven Ackermann
Skirmantas Alisauskas
Nicoleta Baboi
Christopher Behrens
Martin Beye
Maciej Brachmanski
Markus Braune
Günter Brenner
Jonathan Correa
Marie Kristin Czwalinna
Stefan Düsterer
Siarhei Dziarzhytski
Nagitha Ekanayake
Benjamin Erk
Bart Faatz
Heinz Graafsma
Vanessa Grattoni
Ingmar Hartl
Wolfgang Hillert
Katja Honkavaara
Barbara Keitel
Marion Kuhlmann
Dmytro Kutnyakhov
Tino Lang
Christoph Lechner
Wim Leemans
Bastian Manschwetus
Erland Müller
Jost Müller
Rui Pan
Georgia Paraskaki
Christopher Passow
Sven Pfeiffer
Elke Plönjes
Juliane Rönsch-Schulenburg
Mabel Ruiz Lopez
Nora Schirmel
Holger Schlarb
Evgeny Schneidmiller
Siegfried Schreiber
Andrey Sorokin
Nikola Stojanovic
Markus Tischer
Kai Tiedtke
Rolf Treusch
Elmar Vogel
Mathias Vogt
Lutz Winkelmann
Lukas Wenthaus
Mikhail Yurkov
Edgar Weckert
Wilfried Wurth
Johann Zemella

In Memory of:

Wilfried Wurth

Special Thanks to:

The members of the Machine, Laser and Photon Science Advisory Committees (MAC, LAC and PSC) for their careful reading of this Conceptual Design Report and their valuable input.

Final Editing and Layout

Martin Beye and Stephan Klumpp

Imprint

Deutsches Elektronen-Synchrotron DESY
Notkestraße 85, D-22607 Hamburg
DOI: 10.3204/PUBDB-2020-00465
ISBN 978-3-945931-30-1

Edition: March 22, 2020

1 Executive Summary

FLASH is the world's first short wavelength free-electron laser (FEL) facility and started user operation already in 2005. It still remains the only high repetition rate free-electron laser in the XUV/soft X-ray regime worldwide. Based on the superconducting accelerator technology developed at DESY, it can provide presently up to 5000 photon pulses per second. Those are delivered to users in pulse trains of up to 500 pulses with a separation of 1 µs repeated 10 times/s (burst mode operation). Experiments at FLASH span diverse fields. Examples are atomic, molecular and optical (AMO) physics, chemistry, condensed matter and nanoscience, life sciences, warm dense matter research and FEL physics and technology. Science at FLASH also drives the development of new methods and instrumentation.

Several hallmark experiments have been performed at FLASH that demonstrated the unique capabilities of short wavelength FELs. There are for example the first single-shot coherent diffractive imaging experiment, the first XUV multi-photon photoionization at ultra-high intensities, the first femtosecond time-resolved magnetic scattering experiment, and the first molecular movie of a gas phase chemical reaction (Rossbach et al. 2019). Key developments in photon diagnostics and beamline instrumentation have been made at FLASH and are now used at many FEL facilities around the world (Rossbach et al. 2019).

Since 2016 FLASH is providing users with pulses from a second FEL line FLASH2 which is operated in parallel to FLASH1. FLASH2 improves the performance for users through variable gap undulators that enable easy wavelength tuning and novel lasing schemes. The progress in creating and measuring ultrashort, fully coherent single-spike SASE pulses, as well as the new state-of-the-art suite of dedicated endstations (operated by the facility) ensure the continuing attractivity of FLASH for users.

FLASH provides outstanding opportunities for time-resolved studies which are based on exquisite pump-probe instrumentation. This includes fully synchronized optical lasers, a variety of X-ray split-and-delay units, a THz source, which is phase stable with respect to the FEL pulses, and sophisticated diagnostics for pulse arrival time and duration. This has led to the fact that now close to 90 % of the experiments performed at FLASH target ultrafast processes down to the range below 100 fs.

Looking at the international landscape of FEL facilities, there are two main distinguishing features between the different facilities besides the wavelength range: FLASH and the European XFEL are based on superconducting accelerator technology and are thus able to provide up to a few 10 000 pulses/s in burst mode. All the other FEL user facilities are driven by normal conducting linear accelerators (linacs) which can only run at significantly lower repetition rates in the range from 50 to a few 100 pulses/s.

The advantage of higher average brilliance of the superconducting machines enables experiments on targets with a very low density such as molecular ions in astro- and atmospheric-chemistry research. Similarly, low hit rate experiments like single molecule imaging would not be possible otherwise due to unfeasible experiment durations. Also a second class of experiments is enabled by the high repetition rate of superconducting machines, namely experiments which require or suffer from a low count rate per pulse. A typical example is time-resolved photoemission spectroscopy on solid targets that has signal constraints. The FEL pulses have to be strongly attenuated to avoid space charge effects in the photoemitted electron cloud. Similarly, time-resolved inelastic X-ray scattering experiments as well as coincidence experiments benefit from high average brilliance. There, a low count rate per pulse is intrinsic to the experimental techniques.

The increasing demand for high repetition rate FELs has led to the proposal of new

facilities such as LCLS-II now being built in Stanford (USA) expected to go online 2021 and the SHINE project in Shanghai (China). Both will push the superconducting technology away from the burst mode operation realized at FLASH and the European XFEL to a quasi-continuous wave operation with pulses evenly spaced in time and repetition rates up to one MHz.

The second major distinguishing factor between the different facilities is the application of external seeding. Currently, there are only two fully externally seeded FEL user facilities, FERMI in Trieste (Italy) operating in the XUV and soft X-ray regime and the new VUV FEL in Dalian (China). Both are low repetition rate FELs. Seeding provides an obvious reduction in pulse-to-pulse variations in comparison to machines based on the self-amplified spontaneous emission (SASE) principle. Improvements in various parameters such as the arrival time jitter and pulse duration, the spectral content and to a lesser degree the intensity are achieved.

More importantly external seeding enables fully coherent FEL pulses and hence the ability to not only control the temporal shape but also the phase of the pulses. This has recently enabled new classes of experiments such as coherent control over ionisation processes (Prince et al. 2016) and the use of higher-order nonlinear processes such as four-wave mixing to probe relaxation processes in solids (Bencivenga et al. 2015). It is anticipated that in particular the concepts in multi-dimensional spectroscopy developed in the optical laser community can be transferred into the XUV and soft X-ray regime with externally seeded FELs.

In the framework of the DESY strategy process for the next decade – DESY2030 – several long-term goals for the future of FLASH have been defined for an upgraded high repetition rate XUV and soft X-ray FEL facility at DESY. The resulting FLASH strategy – FLASH2020+ – outlined in this Conceptual Design Report is based on the FLASH accelerator operating the two independent FEL lines FLASH1 and FLASH2. The presented ambitious development program aims at significantly improving the FEL photon beam properties for users.

Within FLASH2020+ both lines will be equipped with fully tunable undulators being able to deliver photon pulses with variable polarization. Tunable undulators at FLASH1 will allow full parallel operation of the two FEL lines. Up to now this was limited due to the fact that the wavelength requested for experiments at FLASH1 determined the beam energy of the linac. The undulator upgrade will increase the available time for user experiments by almost 40 %. Furthermore, with the new undulator configuration it will be possible to run the accelerator with typically only two beam energy working points. This will significantly reduce tuning time overhead, increase stability and therefore again increase the attractivity and available beamtime for users.

In addition to beam parameter improvements, the FLASH2020+ project will also add new qualities to the provided beams that are strongly requested across the user community. After its completion, FLASH will be in a leading position to explore new science with FELs: One of the two FEL lines shall be fully externally seeded at the full repetition rate that FLASH can provide in burst mode. The other line shall exploit novel lasing concepts based on different undulator configurations. Certain aspects of such improved concepts can currently already be tested and implemented at FLASH2, e.g. harmonic lasing self-seeding (Schneidmiller et al. 2017). Together with an increase in electron beam energy to 1.35 GeV this will extend the wavelength range of fundamental harmonics to the oxygen K-edge, in order to cover the important elemental resonances for energy research and the entire water window for biological questions. With this moderate increase in wavelength range FLASH will stay fully complementary to the European XFEL.

For a facility such as FLASH, where close to 90 % of the experiments are time-resolved and run in some kind of pump-probe scheme, an important request by the user community is to provide pump pulses with a large flexibility in wavelength range. While the condensed matter community is asking for THz and mid-IR pump pulses, experiments targeting molecular reactions mostly would like to have tunable pump sources from the visible to the UV and even VUV. Similar to the requirements for seeding at high repetition rate this requires further efforts into the development of high average power lasers which is part of the FLASH2020+ concept.

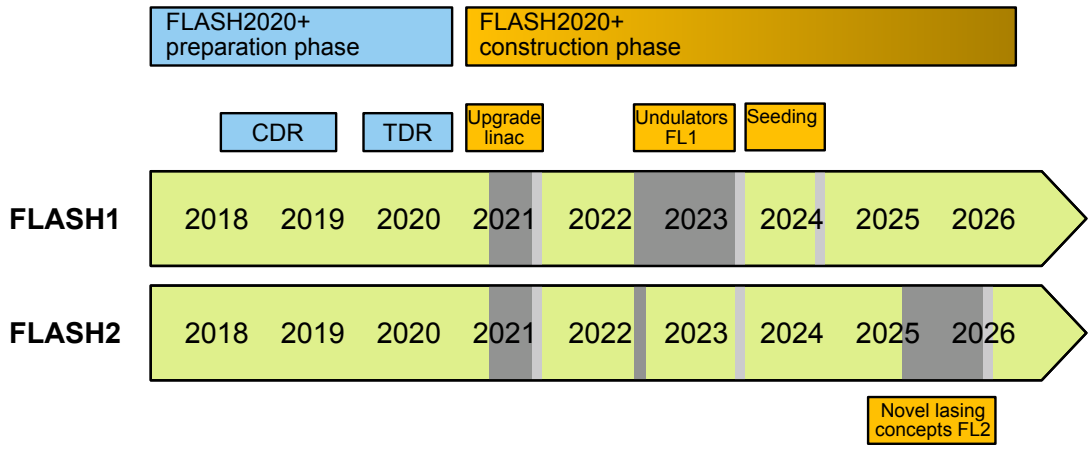

Figure 1: *Overview of the timeline of the FLASH2020+ project.*

There is a strong push from the user side, not only at FLASH but also at the other facilities, to provide even shorter pulses down to the attosecond regime. Single-spike SASE FEL pulses have been recently realized at FLASH and at LCLS pushing the limits in time-resolution towards the few-fs and sub-fs regime (Rönsch-Schulenburg et al. 2014; Huang et al. 2017). Here, synchronization and timing stabilization of the FELs with respect to external lasers will be of key importance for experiments and are constantly being improved at FLASH. However, reaching few hundred attosecond photon pulses requires in particular in the XUV and soft X-ray regime the realization of new concepts based on laser manipulation of the electron bunches. For FLASH2 simulations have predicted pulses shorter than 100 as with nJ pulse energies down to a few nm in wavelength. If this can be achieved with the necessary stability, "attoFLASH" will be superior in pulse energy as well as repetition rate in the wavelength range below 10 nm. This substantially surpasses lab-based laser sources, which rely on high-harmonic generation and have limits in average power (Heyl et al. 2016). FLASH2020+ includes a dedicated R&D program towards this goal.

The user operation mode after the upgrade will follow the established procedures at FLASH. FLASH will continue to have two calls for proposals per year (April 1st, Oct. 1st) with beamtime distributed following a peer review selection process by an international proposal review panel. Beamtime will be allocated in 12h shifts. The total amount of time when the accelerator runs for user experiments will stay at 4500h/year. With tunable undulators at FLASH1 we expect to increase the available time for users by almost 40 % as compared to the current situation. It is anticipated that according to user demands we will schedule dedicated blocks where FLASH runs with fixed accelerator energy at one of the two predefined working points. Prior to beamtimes, we will continue to have preparation meetings with our users which include experts from all FLASH groups (Operations, Beamlines and Optics, Photon diagnostics and Controls) as well as experts from the laser group. During beamtime on-call support will be organized for the most critical components with the goal to provide 24h support. Feedback from the users will be monitored by mandatory beamtime feedback forms.

Figure 1 shows the planned overall timeline of the project (grey boxes indicate anticipated down time followed by commissioning times of the respective FEL line). The project shall proceed in three phases:

Phase 0: Linac Upgrade: Increase of the maximum energy of the linac, change of the FLASH compression scheme, implementation of a transverse deflecting structure (TDS), installation of improved injector lasers and an afterburner undulator at FLASH2 (mid of 2021).

Phase 1: Installation of new undulators with variable gap for FLASH1, upgrade of the FLASH1 photon diagnostics to FLASH2 standards (2023/2024), seeding with high repetition rates of 100 kHz and more (end of 2024).

Phase 2: New configuration of magnet structures at FLASH2 for novel lasing concepts (end of 2025).

	FLASH1 (Seeded)	FLASH1 (SASE)	FLASH2	
Wavelength range	4 – 60	4 – 60	1.3 – 60[1]	nm
Pulse energy	<100	<1000	<1000	µJ
Pulse duration (FWHM)	30	5 – 200	0.1 – 200	fs
Spectral width	Fourier limited	0.5 – 2	0.5 – 2	%
Pulses per second[2]	10 – 5000	10 – 5000	10 – 5000	

Table 1.1: *Parameters of the two FEL lines after the upgrade.*
(1) Including third harmonic. (2) Shared between FLASH1 and FLASH2.

Before analyzing the scientific impact of an upgraded FLASH in the different science areas, we summarize the essential new radiation properties. The upgraded FLASH will combine the established, unique characteristics of FLASH (short and intense XUV to soft X-ray pulses at high repetition rate) with some essential new features that will be very beneficial for scientific studies:

• The improved wavelength tunability of FLASH1 together with the smaller seeded bandwidth will optimize the FLASH1 radiation for high-throughput time-resolved spectroscopy.

• Seeding at FLASH1 will yield fully coherent pulses with completely new scientific applications, e. g. for phase control, interferometric experiments and novel coherent methods.

• Full polarization control at FLASH1 and FLASH2 allows for selectivity to sample symmetries, like orientations of orbitals, chirality or magnetic properties.

• Few- to sub-femtosecond tunable two-color pulses at FLASH2 open unique access to sub-femtosecond dynamics with high resonant selectivity and sufficient intensity, not achievable with alternative sources.

• The extended wavelength range allows one to address the narrowest core-levels (Himpsel 2011) of all elements that are found in the soft X-ray energy region. Therefore, element selective core-level spectroscopies can be performed with smallest lifetime broadening, which is a prerequisite for large information content. Dipole-allowed transitions between element selective core levels and the property-determining valence orbitals are uniquely found in the soft X-ray energy region and can all be addressed with the extended wavelength range employing the fundamental and third harmonic (e. g. 2p-3d transitions at the L-edges of all 3d transition metals).

• Novel opportunities for time-resolved experiments will be created with highly flexible excitation schemes for pump-probe spectroscopy ranging from THz to XUV, which will allow tailored trigger pulses to initiate non-equilibrium dynamics.

• At FLASH2, options will be studied to create pulses with a pulse duration below 100 as with nJ pulse energies in a wavelength regime below 10 nm which will open up new opportunities for attosecond science.

In summary, the FLASH2020+ project envisions developments in FEL technology and the corresponding facility lasers while maintaining the high average brightness. After the upgrade FLASH will again offer unique capabilities to users. FLASH will continue to provide excellent service to users and will stay at the forefront of FEL science and technology. Compared to other major FEL facilities in the world which are either already running, under construction or planned, FLASH will be the only high repetition rate externally seeded FEL facility in the XUV and soft X-ray regime.

References

Bencivenga, F. et al. (2015). „Four-wave mixing experiments with extreme ultraviolet transient gratings“. In: *Nature* 520.7546, pp. 205–208. DOI: 10.1038/nature14341.

Heyl, C. M. et al. (2016). „Introduction to macroscopic power scaling principles for high-order harmonic generation“. In: *Journal of Physics B: Atomic, Molecular and Optical Physics* 50.1, p. 013001. DOI: 10.1088/1361-6455/50/1/013001.

Himpsel, F. J. (2011). „Photon-in photon-out soft X-ray spectroscopy for materials science“. In: *physica status solidi (b)* 248.2, pp. 292–298. DOI: 10.1002/pssb.201046212.

Huang, S. et al. (2017). „Generating Single-Spike Hard X-Ray Pulses with Nonlinear Bunch Compression in Free-Electron Lasers“. In: *Phys. Rev. Lett.* 119 (15), p. 154801. DOI: 10.1103/PhysRevLett.119.154801.

Prince, K. C. et al. (2016). „Coherent control with a short-wavelength free-electron laser“. In: *Nature Photonics* 10.3, pp. 176–179. DOI: 10.1038/nphoton.2016.13.

Rönsch-Schulenburg, J. et al. (2014). „Operation of FLASH with Short SASE-FEL Radiation Pulses“. In: *Proc. of FEL2014 Conf.*, p. 342. Online.

Rossbach, J. et al. (2019). „10 years of pioneering X-ray science at the Free-Electron Laser FLASH at DESY“. In: *Physics Reports* 808, pp. 1–74. DOI: 10.1016/j.physrep.2019.02.002.

Schneidmiller, E. A. et al. (2017). „First operation of a harmonic lasing self-seeded free electron laser“. In: *Phys. Rev. Accel. Beams* 20 (2), p. 020705. DOI: 10.1103/PhysRevAccelBeams.20.020705.

2 Science Case

The science case for FLASH2020+ has been shaped in a series of topical workshops in the last couple of years which culminated in a large user workshop end of 2017. This workshop which featured keynote talks in atomic, molecular, and optical (AMO) science, astrochemistry, catalysis, functional materials, magnetism, imaging, and nonlinear X-ray science followed by break-out sessions resulted in a user list of requirements for a “dream” high repetition rate XUV and soft X-ray FEL facility which is outlined in the

User Wishes

- Wavelength range in the fundamental from ≈60 nm to 2.3 nm covering the full water window up to the oxygen K-edge.
- Accessibility of 3d-transition metal edges with third harmonic radiation.
- Easy wavelength tunability.
- Variable polarization.
- Flexible laser excitation for pump-probe experiments ranging from THz to VUV.
- Fourier-limited FEL pulses.
- Very short soft X-ray pulses ranging from a few fs to sub-fs and even attoseconds.
- Quasi cw-operation with a variable continuous repetition rate up to a maximum of 100 kHz.

Except for the last item on the list, the FLASH2020+ goals are set such that it should be able to fulfill those demands of the user community. In particular, FLASH1 will provide externally seeded Fourier-limited FEL pulses with variable polarization in a wavelength range from ≈60 nm down to about 4 nm with tunable undulators maintaining the high number of pulses achievable with the superconducting accelerator. FLASH2 will be modified such that it can cover the full water window up to the oxygen K-edge in the fundamental as well as the wavelength range down to 1.3 nm with higher harmonics.

FLASH2 will include options for very short pulses from a few femtoseconds to subfemtosecond and even down to the attosecond regime. A very important part of the FLASH2020+ project is also the development of fully synchronized pump laser schemes with greatly enhanced wavelength tunability. The resulting potential for research in different science areas is briefly outlined below. Examples of research and methods that will strongly benefit from the capabilities of FLASH2020+ are presented in colored boxes.

2.1 Atomic, Molecular, and Optical Science and Astrochemistry

In the field of AMO science some of the most important scientific questions that are targeted with free-electron lasers are the fundamental aspects of the interaction of intense short wavelength radiation with small quantum systems. Experiments serve as a benchmark for sophisticated theoretical concepts to describe the quantum mechanics of many-body systems, following ultrafast charge migration and charge transfer processes in molecular systems, and the real-time observation of molecular reactions. To be able to benchmark theoretical concepts for intense ionizing light-matter interaction of small quantum systems, it is required to detect simultaneously electrons and ions upon ionization. Furthermore, such studies rely on full tunability of the wavelength and full control of temporal and spatial pulse shape, and pulse energy.

An externally seeded high-repetition rate FEL such as FLASH1 after the upgrade in combination with dedicated endstations such as e. g. CAMP will provide excellent conditions for research in this field. With the new capabilities of FLASH2020+, even more sophisticated interferometric coincidence experiments which exploit phase control will become feasible.

A very intense area of research is the study of charge transfer and relaxation processes in complex molecular systems such as the primary nucleobases as the building blocks of DNA. Damage and repair mechanisms are of fundamental interest as well as wavepacket motion after controlled excitation. Ideally, the excitation is localized at a specific elemental center and probed at another center with core level spectroscopy.

The latter requires very short pulses in the few femtosecond to attosecond regime and opportunities to do soft X-ray pump/soft X-ray probe experiments with independently tunable two-color FEL pulses: properties of the novel undulator schemes proposed for FLASH2 (see also Section 5). The former will strongly benefit from Fourier-limited tunable XUV and soft X-ray FEL pulses at FLASH1 in combination with fully synchronized external VUV laser sources.

Another very interesting field of research that will strongly profit from the enhanced properties of FLASH after the upgrade is the quest to understand fundamental steps in astrochemical reactions. Reactions in interstellar gas clouds, in close vicinity of star formation, or on small ice and dust particles are very often triggered or influenced by VUV- and XUV-induced creation of molecular ions. To mimic such reactions in a lab environment requires either sophisticated ion sources or the creation of molecular ions directly with FEL radiation and to follow the reaction dynamics with variable delay probe pulses that enable complete analysis of the resulting fragments.

Another area of research, where an upgraded FLASH is beneficial, is a mass spectrometric approach to analyze the composition of molecular fragments after resonantly breaking larger biomolecules. Here, the small bandwidth and tunability of an upgraded FLASH, especially to various carbon, nitrogen or oxygen K-edge resonances of selected functional subgroups of a large molecule, would enable novel approaches to determine photo-sensitivity and chemical structure of such molecules, again with high statistical accuracy.

Through the generation of ultrashort coherent pulses, where the broad bandwidth can create coherent electronic wavepackets at selected sites via resonant excitation at specific elements, the upgraded FLASH can also contribute to our understanding of the photoprotection mechanisms of e. g. the DNA molecule by analyzing the influence of coherent electronic motion onto the energy flow in such molecules as outlined above.

The colored box below outlines concepts for “complete experiments” to follow different classes of light-induced gas phase chemical reactions in real time with a source like FLASH after the upgrade.

Multi-coincidence experiments to follow chemical reactions in real time

An extremely powerful Ansatz to obtain a full picture of light-induced chemical reactions is to ionize the resulting products with an XUV pulse with variable delay and to record all the resulting particles (i. e. electrons and ions) and their momenta in a multi-coincidence experiment. Studies like this require tunable pump lasers for resonant excitation of the reactants as well as easy tunable, ideally Fourier-limited short-pulse XUV probe pulses for product detection. Furthermore, time-resolved multi-coincidence experiments are only feasible with high-repetition rate sources and extremely efficient detection of all fragment channels. This class of experiments will strongly benefit from the unique combination of powerful instrumentation (e. g. the existing ReMi (reaction microscope) endstation) and well-defined Fourier-limited pulses (either seeded or in single-spike SASE operation) available at FLASH after the upgrade.

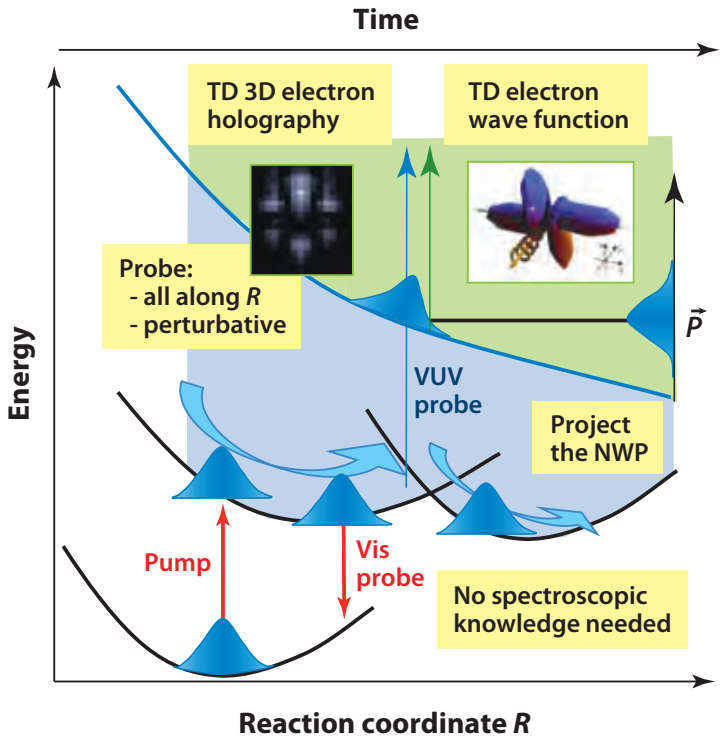

Figure 2.1: *A potential energy landscape is depicted (TD time-dependent; NWP nuclear wavepacket). By multi-coincidence techniques the evolution of the electronic and nuclear wavepackets after a primary excitation can be analyzed using a time-delayed ionizing XUV probe pulse from an FEL. From such a "complete experiment" the excited state potential can be reconstructed without further spectroscopic knowledge.*
Reproduced with permission from (Ullrich et al. 2012). © 2012 by Annual Reviews.

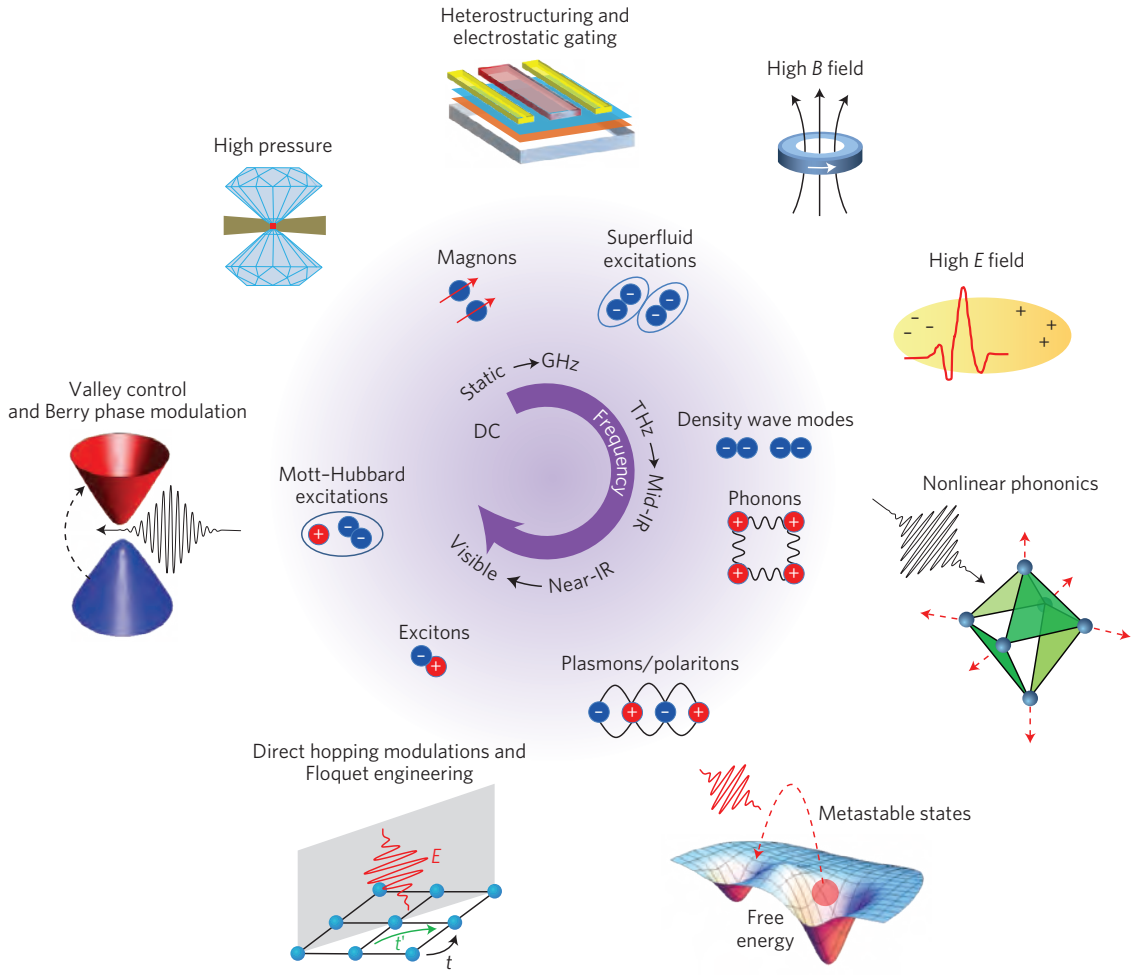

Figure 2.2: *Methods for controlling quantum phases. Elementary excitations in quantum materials and select control techniques arranged (clockwise) in order of ascending frequency. Reproduced with permission from (Basov et al. 2017). © 2017 by Springer Nature Limited.*

2.2 Quantum Materials, Magnetism

Condensed matter systems where quantum effects play an important role show an extremely rich and interesting variety of macroscopic physical properties such as high temperature superconductivity and colossal magnetoresistance as well as a variety of phase transitions such as e. g. metal-insulator transitions and/or different magnetic phases. These fascinating phenomena are caused by a subtle interplay between electronic (charge, orbital, and spin) and lattice degrees of freedom. This interplay leads to various nearly degenerate competing states and hence complex phase diagrams as a function of temperature, doping and external fields.

A possible pathway to understand the microscopic driving forces underlying these phenomena is to probe the relaxation of the relevant electronic states with ultrashort X-ray pulses after the complex systems have been excited out of equilibrium using light pulses from THz-radiation to soft X-rays. The idea is to take electronic structure maps as a function of time after a system is driven out of equilibrium. Here, one can use a well-established static electronic structure tool such as photoelectron spectroscopy which offers great potential when time-resolution in the (sub)-femtosecond range can be added with free-electron laser sources.

X-ray based spectroscopic techniques such as X-ray absorption and X-ray emission specifically allow to investigate the ultrafast response of the electronic structure in a site-selective, element-specific way and hence help to reveal the pathways from microscopic excitations to changes in macroscopic properties in these complex systems. In addition, us-

ing time-resolved resonant elastic and inelastic x-ray scattering techniques one can correlate dynamic electronic structure information with changing structural or electronic order.

Light-induced ultrafast dynamics is not only of interest in the quest for a fundamental understanding of emergent phenomena in quantum materials but also because of the possibility for fast reversible switching between states with different macroscopic properties and controlling quantum phases. Figure 2.2 illustrates how flexible excitations schemes ranging from THz to visible can drive different fundamental excitations which lead to new macroscopic properties.

The search for fingerprints of light-induced transient, metastable phases which could in turn enable one to understand and steer transitions between the different stable phases of the complex materials has attracted tremendous interest recently. For all these studies FLASH will be ideally positioned after the upgrade with flexible pump-probe schemes and unique capabilities to monitor the evolution of electronic structure and fundamental excitations.

A powerful electronic structure tool such as time-resolved photoemission spectroscopy on high density, solid targets requires a low count rate per pulse because the number of emitted photoelectrons emitted in a single ultrashort pulse is constrained due to space charge effects in the photoemitted electron cloud. Other tools intrinsically deliver only low count rates per pulse, such as time-resolved inelastic X-ray scattering.

Both classes of experiments are only possible with the high repetition rates the superconducting machines can provide. In comparison to laser driven high-harmonic generation (HHG-)sources which are very well suited to study time- and angle-resolved photoemission (TR-ARPES) on condensed matter samples in the VUV spectral range with excellent time resolution, high repetition rate FELs such as FLASH are superior because they provide ultrashort pulses in a much broader spectral range from the XUV to the soft and even tender X-ray regime with easy tunability. Higher photon energies for TR-ARPES enable studies which cover an extended range in momentum space. Tunability of the excitation energy gives access to the full 3d momentum information and provides means to study surface vs. bulk phenomena since the inelastic mean free path of the photoelectrons and hence the information depth can be tuned by changing the kinetic energy of the photoelectrons.

Furthermore, using the tunability of the FEL, TR-ARPES studies can be combined with time-resolved X-ray photoelectron spectroscopy (TR-XPS) monitoring local charge state changes and/or time-resolved X-ray photoelectron diffraction (TR-XPD) studies of ultrafast changes in the geometric structure in the same experiment. While time-, angle- and spin-resolved photoemission is already successfully performed and quite heavily demanded at FLASH making use of most efficient detection of the emitted photoelectrons with a momentum microscope these studies will further benefit from a high-repetition rate seeded FEL such as FLASH1 with enhanced spectral stability and decreased spectral bandwidth in combination with Fourier-limited XUV and soft X-ray pulses.

On the other hand, the combination of ultrashort FEL pulses with a time-compensating monochromator at FLASH2 will provide unique new opportunities to achieve a time-resolution of less than 20 fs which is in particular required to follow ultrafast changes in the electronic system in these materials (Hellmann et al. 2012).

FLASH2020+ will also generate excellent opportunities for time-resolved resonant inelastic X-ray scattering studies on quantum materials as outlined in the colored box below.

Resonant inelastic X-ray scattering on quantum materials

Nickel monoxide (NiO) is a material with a half-filled conduction band that should be a good conductor according to simple band theory. Through strong electronic correlations though, it is insulating and exhibits antiferromagnetic order alongside with a distorted bulk unit cell. These interesting properties turn NiO into a fruitful test case for time-resolved experiments: it has been shown, that strong magnonic excitations can be induced by THz or even optical pumping, the electronic correlations can be influenced directly by very strong, transient external fields and the magnetic super-exchange mechanism can be blocked by electron redistributions. All of these properties provide very good experimental benchmarks for modern solid-state theoretical concepts. A deeper exploration of these phenomena requires high resolution studies of the dynamics of electronic excitations through e. g. resonant inelastic X-ray scattering (RIXS). The combination with ultrashort pulses allows to gain such information with femtosecond resolution across phase transitions, where the correlated subsystems transiently decouple. One can thus separate in the time domain which of the different order parameters is more fundamentally stable: the antiferromagnetic order (destroyed by magnons), electronic order (destroyed by optical pumping) or the lattice distortions (which can only follow on longer time scales). In general, though, RIXS is a very photon hungry technique and requires monochromatic, high average flux in small spots to achieve sufficient energy resolution. Especially at FELs, sample damage is largely limiting the usable number of photons in a single pulse. To achieve sufficient resolution, SASE FELs require monochromatization which enhances the fluctuations in the pulse energy on the sample. In order to prevent sample damage, attenuation levels have to be adapted to the highest pulse energy, requiring a large safety margin between the damaging peak and the average pulse energy. This strongly limits the achievable signal levels, results in hour-long acquisition times for a single spectrum and thus effectively limits the accessible parameter space. An externally seeded FEL in contrast delivers more stable, much more monochromatic pulses with the possibility to achieve sufficient resolution even without further monochromatization, which increases typical beamline transmissions by a factor between three and ten. But even if a monochromator is applied, the difference between peak and average pulse energy will be negligible, such that the damage-limited usable flux on the sample can easily be an order of magnitude larger at a seeded FEL than at a SASE FEL.

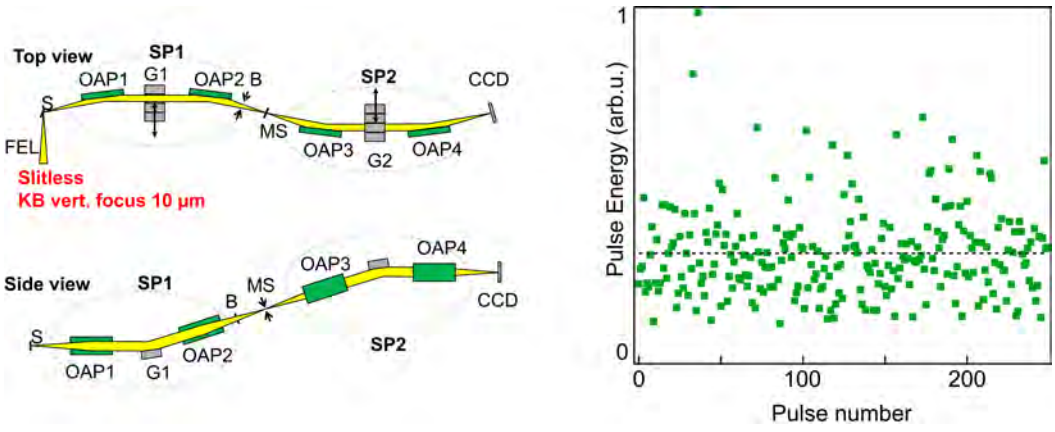

Figure 2.3: *Left: Optical setup of the RIXS spectrometer installed at FLASH1, with design energy resolution <30 meV across the FLASH wavelength range (from (Dziarzhytski et al. 2018)). Right: Simulated relative pulse energies behind a monochromator for SASE pulses around 100 eV with 50 fs pulse length and a total natural bandwidth of 1 eV (FWHM) monochromatized to 100 meV displaying a difference between peak and average pulse energy by a factor of more than three (the average pulse energy is shown dashed).*

2.3 Chemistry, Surface Catalysis and Energy Science

The short pulses at high repetition rates make FLASH the ideal spectroscopy machine to study ultrafast dynamics in photocatalytic processes, heterogenous catalysis on surfaces and charge transfer dynamics in systems relevant for photovoltaics. It turns out that all chemical transformations, i. e. the formation and breaking of chemical bonds, are in general rare events. Each reaction partner is very rarely and for a very short time only in the critical intermediate state of a reaction. It is the availability of short, well-controlled resonant X-ray pulses with high repetition rate in combination with adequate trigger pulses that allows for the study of those rare reaction intermediates to advance our understanding how reactions proceed on their natural femtosecond time scale and how we can choose optimal reaction conditions for more energy- and resource-efficient chemistry.

While for photocatalytic reactions the trigger to initiate a reaction is a femtosecond optical laser pulse ideally resonant to the relevant electronic transition in the molecule, industrially relevant heterogeneous catalytic reactions are in general thermally activated. Here it is important to drive the key reaction pathways with the flexible pump laser pulses in the wavelength range from THz to the visible that will be offered by FLASH so that those reactions can be triggered on an ultrashort time scale, such that a detectable fraction of reactants is found in the intermediate state at the same time.

A key topic that needs experimental exploration is the study of conical intersections: the quantum mechanically coupled crossing of different electronic states in the potential energy landscape of different atomic geometries. Most theoretical descriptions fail at conical intersections (these cannot be described by the ubiquitous Born-Oppenheimer approximation). Nevertheless, it is those crossings that determine which of the possible reaction pathways are taken by the system and a detailed understanding of the dynamics across conical intersections is thus crucial for an optimal tuning of reaction conditions to our needs. Element specific probing with near-edge X-ray absorption or resonant X-ray emission techniques after an ultrashort optical laser pulse has driven a reactant close to a conical intersection allows to directly follow the pathway of the products on the potential energy surfaces. This provides crucial input and benchmarks for the development of novel theoretical concepts.

The current FLASH can directly address the carbon backbone of organic molecules with carbon edge probing, while resonant access to functional blocks containing nitrogen and oxygen is limited. With an upgraded FLASH2, also these core resonances come into reach and allow for efficient probing at the functional side groups of organic molecules.

Adding circular polarization to the FEL probing step even allows to discriminate different molecular chiralities using X-ray absorption dichroism, a field of dynamic studies that is largely unexplored with the high selectivity and information content of X-rays, although very important for everyday life: e. g. only one chirality of a sugar molecule is digestible for humans although the whole molecular composition and all chemical properties are identical between both chiralities. The different effects of molecules with the same composition and bonding structure, while one is the mirror image of the other still provides a large puzzle to our understanding. Full spectroscopic access to the dynamics and the connected insight into how to tailor e. g. catalysts to yield only the product with desired chirality could be uniquely provided by FLASH.

A very powerful technique to probe in particular catalytic reactions at surfaces is time-resolved X-ray photoelectron spectroscopy (TR-XPS). As has been discussed in Section 2.2, time-resolved photoelectron spectroscopy on high density targets requires high-repetition rate FELs. In combination with flexible short-pulse pump lasers, TR-XPS (or time-resolved electron spectroscopy for chemical analysis (TR-ESCA)) provides a fingerprint technique which allows to follow reaction processes in real time and in particular to identify key reaction intermediates.

A seeded high repetition rate FEL such as FLASH1 after the upgrade will be an ideal source for such studies since it will provide spectrally stable Fourier-limited XUV and soft X-ray pulses with a high spectral photon density that allow for very efficient further monochromatization to achieve the necessary resolution to

distinguish between different species present during a surface catalytic reaction.

When those unique analytical features of FLASH are applied using newly available ultrashort pulses in the few femtosecond to subfemtosecond regime, the time resolution in the study of photo-driven charge transfer processes in photocatalytic reactions or in systems relevant for photovoltaics can be lifted to a new level. Even shorter pulses in the attosecond regime with their large bandwidth further allow to resonantly create and study localized coherent electronic wavepackets and their influence onto chemical transformations. With the current absence of sufficiently intense, coherent, and short wavelength pulses, the impact of electronic coherence on the energy flow e. g. in photosynthetic reactions can only be speculated about – with many studies hinting to a larger influence which might become experimentally accessible within FLASH2020+.

2.4 Imaging

Imaging experiments at XUV- and soft X-ray free-electron laser are naturally addressing nanosized objects such as clusters, nanocrystals or domain structures in condensed matter. The spectral and pulse energy stability of a seeded FEL are very beneficial for single-shot imaging experiments. Here, single-shot imaging is mandatory for transient and/or metastable structures as well as statistical sampling of random oriented structures. Recent experiments at FERMI have demonstrated the potential of single-shot imaging of He clusters albeit at low repetition rate (Langbehn et al. 2018).

A high-repetition rate seeded FEL such as FLASH1 after the upgrade provides many more pulses per time in comparison to e. g. FERMI. To exploit this fact for single-shot imaging though, novel imaging detectors for the soft X-ray regime will be required. They are currently under development (see also Chapter 7) and will be available soon.

This will then generate new opportunities for time-resolved studies where the dynamical evolution of nanocrystals and clusters can be studied on femto- to picosecond timescales generating sufficiently large data sets so that novel image analysis tools relying on e. g. machine learning can be applied.

While most of the life science imaging applications at high-repetition rate FELs target structural information at the atomic level and hence require hard X-ray FELs, certain research aspects are well matched to an FEL such as FLASH after the upgrade.

FLASH2 will reach deeper into the water window after the upgrade. The term “water window” characterizes the soft X-ray wavelength region below the oxygen K-edge energy (about 530 eV), where water is largely transparent, but above the carbon K-edge energy (about 280eV), where biomolecules show a large absorption contrast. Statically it has been demonstrated at storage ring sources, e. g. at the Advanced Light Source in Berkeley by the group of Carolyn Larabell, that this wavelength region is very useful for microscopy and tomography of living structures (Ekman et al. 2017).

Here, the high repetition rate of FLASH will enable to record large data sets of single shot images with excellent statistical quality in order to obtain well-sampled information about small, potentially fluctuating structures in the specimen without the need of cryofixation for 3d tomography.

Also here, the developments in XUV and soft X-ray detector technology currently under way will be crucial to the impact of an upgraded FLASH2 in this research field.

2.5 Nonlinear and Attosecond Science

With fully coherent short pulse X-ray sources, there is potential to transfer techniques to the X-ray domain that have been developed in the field of nonlinear spectroscopy and very successfully applied in the IR- and optical spectral regime to study ultrafast relaxation processes. First successful four-wave mixing experiments in the XUV regime have recently been performed at FERMI in an attempt to study coherent phonon dynamics in a region of momentum space not accessible with optical spectroscopy (Bencivenga et al. 2015). The combination of nonlinear spectroscopy techniques, such as e. g. stimulated Raman spectroscopy, with the element selectivity of resonant core excitations would open up a new field with the ability to study electronic wavepacket motion initiated via core excitation at a specific center in the system, e. g. in complex molecules as well as in complex condensed matter systems.

Application of nonlinear spectroscopy to the study of electronic coherences with element selectivity will require independently tunable two-color options for few femtosecond and/or sub-femtosecond FEL pulses in combination with wavelength selective split-and-delay optics which will become available at FLASH2 after the upgrade. As outlined in the colored box below, stimulated processes where resonant or non-resonant core level excitations are involved will compete with the dominant Auger decay processes that determine the lifetime (and the coherence time) of the core excitations. In the soft X-ray regime (carbon, nitrogen, oxygen 1s, 3d transition metal 2p levels) these lifetimes are well below 10 fs.

Application of sub-femtosecond to attosecond pulses to study coherent electronic motion in complex systems such as e. g. biophysically relevant molecules is currently limited by the achievable single pulse energy of laser based high-harmonic generation (HHG-)sources. Of particular interest is the wavelength regime below 5 nm if one wants to exploit the element specificity and chemical selectivity of resonances in the soft X-ray regime. Simulations show that with the upgraded FLASH2 line, in particular using laser manipulation of electron bunches as briefly described in Section 5.3, it should be possible to generate sub-femtosecond pulses with µJ level pulse energies and pulses on the order of 100 attoseconds with a tunable center wavelength in the range of a few nm and nJ pulse energies. Compared to the performance of laser-based HHG sources this would be an improvement of several orders of magnitude (Heyl et al. 2016). Combined with two-color pump-probe schemes this opens up a whole new field of scientific opportunities. An example is given in the colored box below.

Sub-Femtosecond Pulses for Non-Linear Spectroscopies

Non-linear methods hold the promise to improve our ability to study matter by e. g. increasing selectivity, providing information that is complementary but inaccessible to linear methods or just by improving signal levels. Here, it remains especially interesting to use these unique features of non-linear spectroscopy to study ground state valence properties since they are responsible for materials' functionality. A common challenge for all non-linear X-ray spectroscopies though is the separation of the desired direct non-linear process from a sequential process probing highly valence excited states. The Auger process for example transfers the excitation energy from one absorbed X-ray photon into valence excitations within several femtoseconds, such that all following photons will probe an ill-defined highly excited state of the system. Shortening the pulses into the sub-femtosecond region will thus largely enhance the contribution of direct non-linear signals (which scale with the radiation power, fewer photons can therefore be compensated by shorter pulses) as opposed to signals following sequential processes (here, the scaling is mainly with fluence, largely independent of the pulse length). The intense, sub-femtosecond or even attosecond pulses provided by the new FLASH2 thus provide a unique opportunity to perform non-linear spectroscopies.

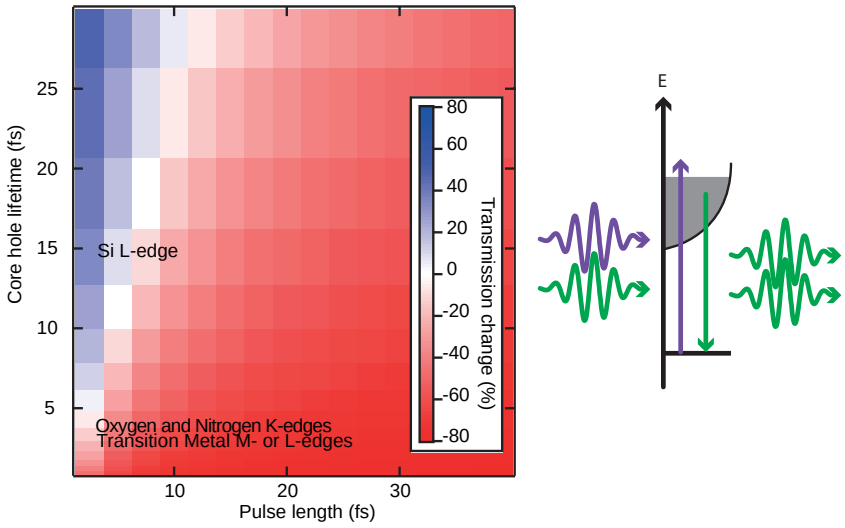

Figure 2.4: *Calculated transmission change as a signature of stimulated emission. Stimulated emission constitutes the simplest and most fundamental non-linear process and can be observed in a two-color experiment by using one (high energy, purple) color to pump core excitations and a second (low energy, green) color to probe the transmission of the sample. An increased transmission (color-coded blue) is a sign of stimulated emission, while a decreased transmission (red) occurs, when a valence excited system is probed. It becomes apparent that pulse lengths have to be substantially shorter than core hole lifetimes to observe stimulated emission. The used rate equation model will fail for pulse length* $< \approx 3$ *fs.*

Attosecond Electron Dynamics in Molecules Dissolved in Water

Tuning two variably delayed attosecond pulses to functional hetero-atom resonances in a biologically relevant molecule, e. g. at the sulphur L-edge around 160 eV and the nitrogen K-edge around 400 eV (using third harmonic radiation), allows to resonantly excite an electronic wavepacket at the sulphur site and probe its real time dynamics across the molecule by studying its arrival at the nitrogen site. The transmission spectrum of a free-flowing µm-thin water solution sheet in vacuum can be measured with the nitrogen edge probe pulse and will contain clear signatures of the presence or absence of additional electron density locally around the nitrogen atom. The sulphur edge pump pulse excites an electron wavepacket locally from the 2p core levels to resonantly selected valence states in the solvated molecule. The flow speed of the jet of typically 40 m/s ensures replacing the excited volume in between the pulses at MHz rate. By making use of recently developed transmission grating based ideal beam splitters (with low line densities, the spatial overlap as well as the ultrashort pulse lengths are preserved) (Brenner et al. 2019), one can produce two copies of the FEL pulses: one to be transmitted through the sample while the other is used for shot-noise limited normalization of SASE fluctuations in spectral pulse energy. With a spectrometer downstream of the interaction region, one separates and analyzes the transmitted spectrum at the nitrogen edge. With this experiment, the attosecond dynamics of an electronic wavepacket can be tracked in real time, together with potential dephasing and scattering mechanisms. This can then uniquely answer fundamental questions around charge transfers on their intrinsic time scale e. g. comparing aromatic systems with unsaturated π-bonded or saturated carbon chains.

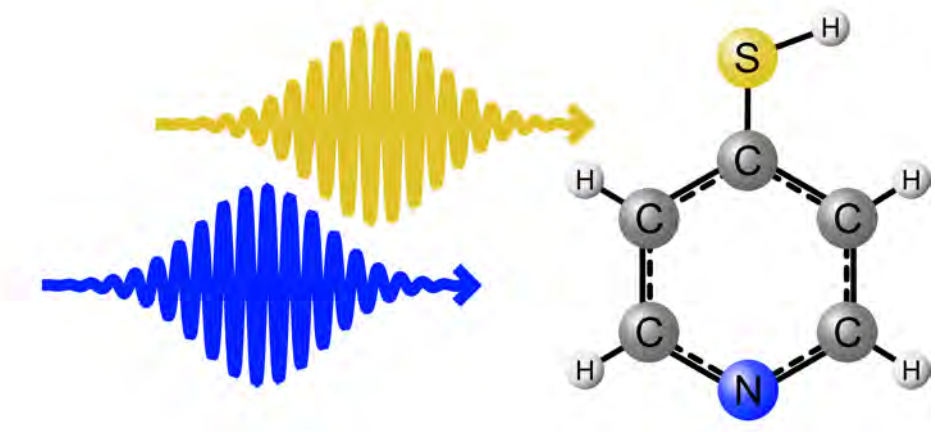

Figure 2.5: *Two variably delayed pulses tuned to the sulphur and nitrogen edges in 4-mercaptopyridine allow to create an electronic wavepacket locally at the sulphur atom and track its propagation across the aromatic π-electron system by analyzing spectral fingerprints at the opposing nitrogen site.*

References

Basov, D. N. et al. (2017). „Towards properties on demand in quantum materials“. In: *Nature Materials* 16.11, pp. 1077–1088. DOI: 10.1038/nmat5017.

Bencivenga, F. et al. (2015). „Four-wave mixing experiments with extreme ultraviolet transient gratings“. In: *Nature* 520.7546, pp. 205–208. DOI: 10.1038/nature14341.

Brenner, G. et al. (2019). „Normalized single-shot X-ray absorption spectroscopy at a free-electron laser“. In: *Optics Letters* 44.9, pp. 2157–2160. DOI: 10.1364/OL.44.002157.

Dziarzhytski, S. et al. (2018). „Diffraction gratings metrology and ray-tracing results for an XUV Raman spectrometer at FLASH“. In: *Journal of Synchrotron Radiation* 25.1, pp. 138–144. DOI: 10.1107/S1600577517013066.

Ekman, A. A. et al. (2017). „Mesoscale imaging with cryo-light and X-rays: Larger than molecular machines, smaller than a cell“. In: *Biology of the Cell* 109.1, pp. 24–38. DOI: 10.1111/boc.201600044.

Hellmann, S. et al. (2012). „Time-domain classification of charge-density-wave insulators“. In: *Nature Communications* 3.1, p. 1069. DOI: 10.1038/ncomms2078.

Langbehn, B. et al. (2018). „Three-Dimensional Shapes of Spinning Helium Nanodroplets“. In: *Phys. Rev. Lett.* 121 (25), p. 255301. DOI: 10.1103/PhysRevLett.121.255301.

Ullrich, J. et al. (2012). „Free-Electron Lasers: New Avenues in Molecular Physics and Photochemistry“. In: *Annual Review of Physical Chemistry* 63.1, pp. 635–660. DOI: 10.1146/annurev-physchem-032511-143720.

3 Accelerator

The FLASH accelerator emerged from the TESLA Test Facility linac (Edwards 1995; The TESLA Test Facility FEL Team 2002) and has been built in the present footprint in 2003. A unique feature of FLASH is its high duty cycle of almost 1/100 thanks to the superconducting technology. RF pulses with a length of up to 800 µs at a repetition rate of 10 Hz are used to accelerate bursts of electron bunches producing thousands of SASE pulses per second.

Major upgrades have been: adding accelerating modules to reach the design energy of 1 GeV in 2007 and 1.2 GeV in 2010, adding 3.9 GHz cavities to linearize the phase space, modifying a section upstream of the SASE undulators for seeding experiments (sFLASH) (Ackermann et al. 2013), and finally a second undulator beamline FLASH2 in 2014 (The FLASH II Team 2010; Faatz et al. 2011; Faatz et al. 2016).

Most components of the accelerator are meanwhile in operation for 15 years and need replacement or refurbishment. An extensive refurbishment program has been started in 2014, after the completion of the 2nd undulator beamline, in order to keep the facility in operation for the next 10 to 15 years, but also to introduce upgrades to keep the facility competitive with soft X-ray FELs worldwide. Table 3.1 shows refurbishment projects and their status. Major upgrades and refurbishment will be discussed in the following sections: energy upgrade, injector laser upgrade, new compression scheme, laser heater, low charge diagnostics, and synchronization. Most refurbishments are required to continue stable and reliable operation of the FLASH accelerator independent of the full or partial realization of FLASH2020+. The full upgrade of the compression scheme and the laser heater however, will only be realized within the FLASH2020+ project.

Table 3.1: *Refurbishment projects. Not ordered by priority.*

	Task	Status		Task	Status
E1	Exchange modules ACC2/3	on-going	E18	Bunch compressor FLASH2	finished
E2	Injector laser	on-going	E19	sFLASH EEHG magnetic chicane	started
E3	Afterburner FLASH2	in design			
E4	Optical synchronization system (incl. BAM)	on-going	E20	Upgrade LLRF	proposed
			E21	Coupler interlocks	on-going
E5	Upgrade RF master oscillator	on-going	E22	RF-gun with higher duty cycle	in preparation
E6	BPM electronics	finished 2017	E23	ACC39 (exchange one cavity)	spare cavity
E7	Toroid system	finished 2016			
E8	Machine Protection	finished 2018	E24	Modulator 3.9 GHz	proposed
E9	Screen stations FLASH1	started	E25	Modulators 1.3 GHz	started
E10	Timing system	finished 2018	E26	Cryogenics refurbishment	proposed
E11	Network switches	on-going	E27	Water pumping stations 1 & 2	proposed
E12	Magnet controls	started			
E13	Vacuum controls	started	E28	Cooling towers	proposed
E14	Fast intra-train orbit feedback	proposed	E29	Radiation shield Bogengang	in preparation
E15	Fast intra-train compression feedback	proposed	E30	Personnel interlock system	proposed
			E31	Absorber FLASH1	proposed
E16	TDS FLASH2	on-going	E32	Cooling water hall 3	started
E17	THz undulator FLASH2	postponed	E33	Repair roof hall 3	finished

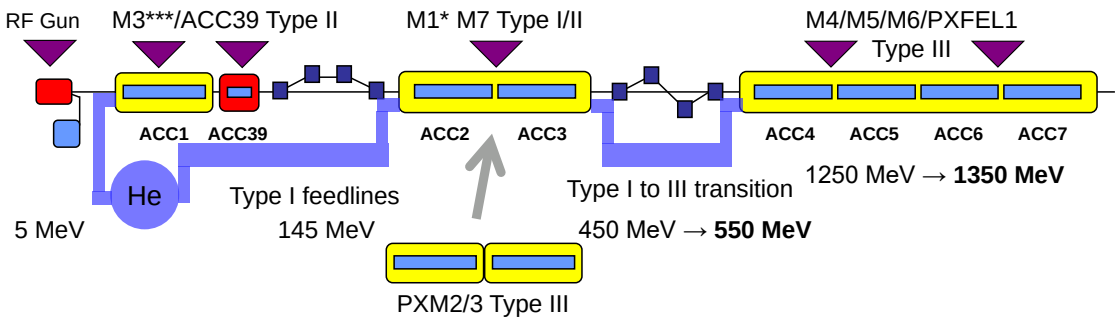

Figure 3.1: *Sketch of the FLASH accelerator showing the accelerating module sections called ACC1 to ACC7 (not to scale). Modules M1* and M7 at ACC2 and ACC3 will be exchanged by modern XFEL-type modules PXM2 and PXM3. The helium feedlines shown in blue will be adapted accordingly. The beam is from left to right. The energies shown are with appropriate compression RF phases under typical SASE conditions.*

3.1 Energy upgrade

FLASH has seven accelerator modules with eight 1.3 GHz 9-cell superconducting cavities each (Pagani et al. 2001; Pagani et al. 1997).

Since a couple of modules have been added and replaced in the last 15 years, several different types of cryogenic modules are in operation. The type I module is from the first generation, type II is an upgraded version of type I. Type III modules have a complete reworked design with reduced diameter of the cryostat and a modified helium feedline to the cavities. XFEL-type modules are very similar to type III modules.

Type I/II modules are not available anymore and their maintenance is meanwhile almost impossible. The module sections called ACC1, ACC2, ACC3, and also ACC39 are equipped with type I/II modules (see Figure 3.1). ACC1 has been refurbished in 2009: module M2* has been exchanged by module M3*** having significant better performances (e. g. higher gradients, less field emission, now with piezo-tuners, magic-T waveguide distribution, remote controlled phase adjustment of single cavities). At the same time, a special module M39 at section ACC39 with four 3.9 GHz cavities has been installed (Edwards et al. 2010).

ACC2 and ACC3 are installed together as a substring of two modules between the first two bunch compressors. Therefore, both modules have to be exchanged at the same time. Two prototype models called PXM2 and PXM3 used for module and cavity tests for the European XFEL are available. The first prototype module PXFEL1 is already installed in position ACC7.

PXM2 and PXM3 however are not ready to be used at FLASH and need a refurbishment on their own. A few cavities can be reused, others need to be replaced. The goal is to install cavities with the highest gradients available. With the refurbished modules we expect to achieve an energy gain of 430 MeV (on-crest). The present modules reach 325 MeV only, because some cavities are operated at reduced gradient due to high field emission.

All new cavities will be equipped with double piezo tuners and XFEL-type power couplers with remote-controllable loaded Q. This is an important improvement compared to the present situation and will significantly contribute to the stability of accelerating gradient and phase along the RF pulse.

The new RF waveguides for ACC2/3 will use the modern magic-T configuration which is already in use for modules ACC1, ACC6 and ACC7, and also at the European XFEL. Compared to the old hybrid splitter configuration, the magic-T system allows optimizing the transmitted RF power for each cavity. This is used to individually adapt the RF power to the quench limit of a given cavity. Otherwise the weakest cavity in an 8-cavity string would determine the accelerating gradient of the whole module and thus would significantly limit their energy gain.

We also plan to upgrade the RF waveguides of modules ACC4 and ACC5 with the magic-T technology. Since stub-tuners will be removed with the waveguide upgrade, this requires for all ACC4 couplers an upgrade to motorized remote-

controllable loaded Qs (presently only manual tuning). With this upgrade we expect to gain another 100 MeV. However, this is only possible with an upgrade of the RF-station for ACC4/5 from the present 5 MW to a 10 MW multibeam klystron. With the present 5 MW klystron we may achieve an increase of at most 50 MeV to 70 MeV.

The RF-station for the refurbished ACC2/3 will be moved from the cryo-annex of the FLASH accelerator hall (100 m away) to a position as close as possible to the modules to minimize the length of the waveguide system. The new RF-station will be equipped with a new modulator, transformer and a 10 MW multibeam klystron.

3.2 Photoinjector

The FLASH electron source is based on a pulsed normal conducting RF-gun (1.3 GHz) operating at high gradients for high brightness electron beams (Schreiber 2005). The RF-gun matches the duty cycle of the accelerator. The present RF-gun is operated with an RF pulse length of 650 µs at 5 MW RF power (10 Hz). An upgrade of the gun is in preparation with an improved heat removal designed for a pulse length of 1 ms at 6 MW (Paramonov et al. 2017). The electron bunches are extracted with UV laser pulses on a Cs_2Te cathode. Besides the RF-gun, the laser pulses determine the quality of the electron beam: transverse and longitudinal shape (in the picosecond range) and timing in respect to the RF field (in the femtosecond range).

The present two main laser systems are in operation since more than 10 years (Will et al. 2011) . Their longitudinal pulse shape is Gaussian and cannot be changed (σ=4.5 ps and 6.5 ps resp.). The bunch pattern in the burst is limited to equal spaced pulses within the pulse train. The development of a new generation photoinjector laser system will have several key advantages. Modern technology will boost the performance in terms of stability. New features like longitudinal pulse shaping will be included. Longitudinal shaping promises to significantly improve the beam brightness. Flexible pulse patterns – including non-equidistant pulses – will be possible. The system will be able to serve two beamlines simultaneously with different pulse shapes and patterns in each beamline. As an option, an upgrade from 1 MHz to 3 MHz or 4.5 MHz intra-train repetition rate is possible. FLASH has developed a technique to produce single-spike SASE pulses. This has been made possible with a third laser system able to produce short laser pulses of 1 ps. This option will also be included in the new photoinjector laser design.

As a common advantage, all DESY operated electron sources especially at FLASH and the European XFEL will profit from the modern laser technology in development. This will ease the management of spare parts and optimize maintenance for all DESY electron sources.

Details of the new laser design are described in Chapter 6.

3.2.1 Laser Rooms

The present laser rooms do not have a sufficiently stable air-conditioning and -cleanliness for a modern high bandwidth laser system. Within a six months shutdown, It seems to be impossible to replace the old rooms with new ones, install the new lasers and commission them. Since there is no space inside the FLASH accelerator hall, we plan to build new laser rooms outside of the hall (Figure 3.2). The rooms for the photoinjector lasers and the laser heater laser will have a total space of 100 m^2. Building the new rooms, installation, and commissioning of the lasers is thus mostly independent of a FLASH shutdown, except the installation of the new laser beamlines.

FLASH will continue to run with the present laser systems until the new systems are ready.

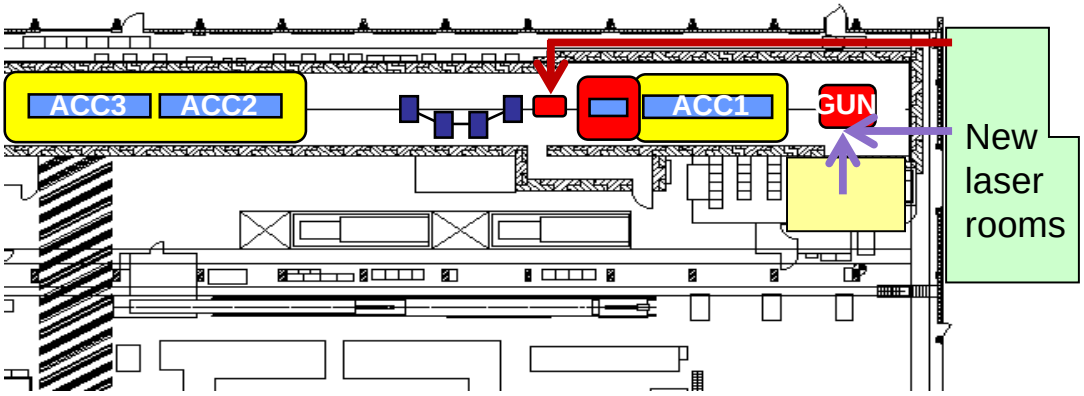

Figure 3.2: *South section of the FLASH accelerator hall showing the injector of the FLASH accelerator starting with the RF-Gun and the first accelerating module ACC1 (beam is from right to left). The new rooms for the photoinjector and laser heater laser systems (green) will be at the south front side outside of the hall. The paths of the laser beams are indicated with violet and red arrows. The old laser room (yellow) will stay in operation until the new lasers are ready.*

3.3 New Bunch Compression Scheme

The electron bunch peak current generated at the electron source is much lower than required for SASE. Therefore, the bunch length is presently compressed by two magnetic bunch compressor chicanes at two different electron beam energies from about 30 A at the source to 2 kA or more in the SASE undulators.

Compression at two energies is needed to balance between space charge effects (better at higher energies) and the required energy chirp along the bunch (better at lower energies). An important ingredient of the compression is the linearization of the phase space using the four 3rd harmonic cavities at 3.9 GHz (ACC39) following the first 1.3 GHz accelerating module (ACC1). ACC1 introduces an energy chirp on the electron bunch, linearized by ACC39 before being sheared in the C-chicane bunch compressor magnets to form a short bunch.

A difficulty occurs due to space charge induced micro bunch instabilities created during the compression process. Together with the emission of coherent synchrotron radiation (CSR) both effects spoil the phase space.

One measure is to reduce the compression at lower energies and to transport a beam with reduced peak current through the extraction beamline to FLASH2. The high peak current will be generated as close as possible to the SASE undulators. This is the main motivation to install an additional C-chicane bunch compressor after the extraction before the FLASH2 SASE undulators.

The same is planned for FLASH1. The present FLASH1 dogleg shaped beamline after the extraction to FLASH2 has been introduced to collimate beam halo in the energy phase space. Collimation of beam halo is required in order to protect the undulators from radiation. At FLASH2, the extraction beamline is used for collimation.

Also for FLASH1 we can reduce space charge and CSR effects by replacing the dogleg with a normal C-chicane bunch compressor. The collimation will then be before and in the dispersive section of the new chicane. Similar to the new FLASH2 chicane, a smoother compression in the low energy part will help to reduce space charge induced micro bunching and CSR effects and will be an advantage for the external seeding options.

An additional advantage replacing the dogleg with a C-chicane is that the exchange will result in a shift of the electron beamline by 40 cm towards the tunnel center. This will significantly ease the installation of new undulators for SASE and seeding, since they are placed farther away from the curved tunnel walls. Furthermore, the horizontal beam shift will allow introducing a mirror system into the photon beamline with horizontal and vertical adjustment features. Presently, only the horizontal direction of the photon beam can be adjusted. In addition,

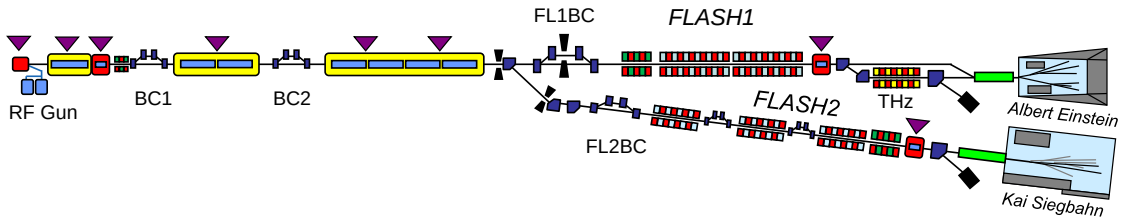

Figure 3.3: *Sketch of FLASH with the new bunch compression scheme. Not to scale. BC1 is modified to include a laser heater, BC2 is now a C-chicane. Each beamline has now a separate compressor FL1BC and FL2BC, respectively, for final compression.*

this gives the possibility to separate the THz-radiation produced by the THz-undulator from the main XUV radiation. For details the reader is referred to Chapter 4.

3.3.1 Details of the New Compression Scheme

In the following, we give details on the new compression scheme and describe the upgrade plans in the first (BC1), second (BC2), and the two final compressor sections (FL1BC and FL2BC), see Figure 3.3.

Bunch Compressor BC1

For a successful seeding in FLASH1 (see Chapter 4.2), we need to mitigate micro bunch instabilities more than achievable with the new compression scheme (Spampinati et al. 2014). Micro bunch instabilities can be reduced by increasing the uncorrelated energy spread of the electron bunch before or during compression (Saldin et al. 2003). Therefore we plan to install a laser heater before the first bunch compressor (see Section 3.4 for details).

In order to generate space for the laser heater, the first bunch compressor chicane BC1 will be shifted downstream from its current position (see Figure 3.4) by 1.5 m. This will require the removal of four quadrupoles while keeping the matching capability of the section. This section is regularly used for beam optics matching of the transverse envelope from the injector into the regular lattice using the four screen method.

For preserving the beam optics matching functionality of this section and at the same time enable adequate beam transport through the accelerator, the remaining quadrupoles will have to be powered one-by-one. Presently, the matching quadrupoles have one common power supply. The bunch compressor itself (dipoles and vacuum chambers) will not be changed. The present nominal bending angle of BC1 is 18° with a range of 15° to 21°. The nominal $R_{56}$is 181.3 mm (range 122 mm to 254 mm). We will use a reduced deflecting angle of 16° with an R_{56} of 140 mm.

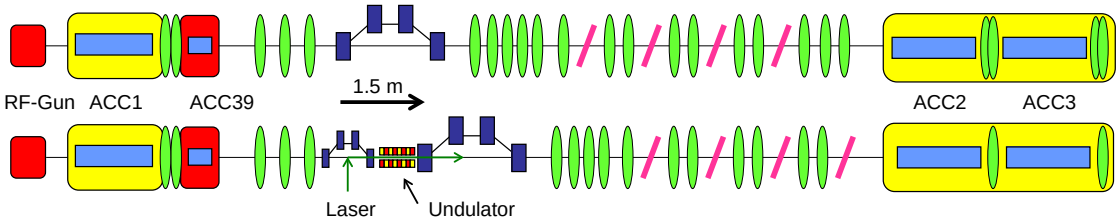

Figure 3.4: *Sketch of the first bunch compressor section BC1. The beam is from left to right. Quadrupoles are indicated as green lenses, chicane dipoles are in blue, screens in magenta. The top sketch shows the present layout, the bottom the new layout. The laser heater undulator together with the laser in-coupling vacuum chamber is placed right before the compressor. The compressor has to move by 1.5 m downstream. The matching section with its four view screens is preserved. The total length of the warm section is 18.5 m.*

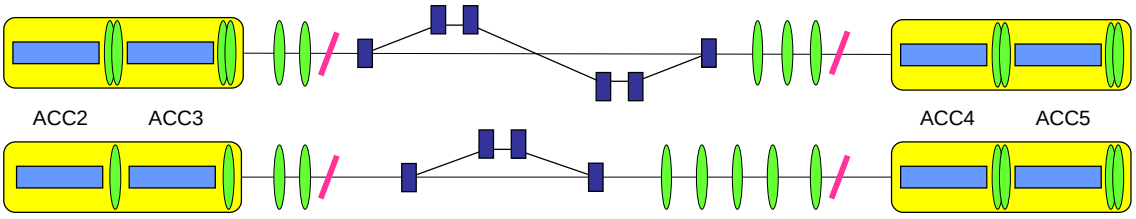

Figure 3.5: *Sketch of the 2nd bunch compressor section BC2. The beam is from left to right. Quadrupoles are indicated as green lenses, chicane dipoles are in blue, screens in magenta. The top sketch shows the present, the bottom the new layout. The S-type chicane is replaced by a compact C-type chicane. This gives space for additional quadrupoles to allow beam optics matching also in this section. The total length of the warm section is 22 m.*

Bunch Compressor BC2

The second bunch compressor BC2 will be modified from the present S-type (6 dipoles) to a C-type (4 dipoles) chicane with an R_{56} of 70 mm and thus shortens by 3.5 m to 10.5 m to generate space for a transverse beam matching section downstream the chicane (Figure 3.5).

In 2003, an S-type chicane has been chosen since simulations showed that the 2nd inverted bend could compensate CSR induced emittance growth (Stulle 2004). Later on it has been experimentally shown, that this is actually not the case. The S-type chicane has in that sense no advantage compared to a C-type, but occupies much more space. The gained space will be used to include a matching section using quadrupole scans on a single screen. Optics matching though is not possible with the present design.

As described in Section 3.1, modules ACC2 and ACC3 will be replaced by modern XFEL-type modules increasing the energy gain by at least 100 MeV. The nominal beam energy in BC2 will thus increase from 450 MeV to 550 MeV (off-crest). The new modules will be equipped with a single quadrupole each, instead of quadrupole doublets. The beam optics will be adapted to this change. The accelerator section following BC2 from ACC4 to ACC7 up to the extraction to FLASH2 remains unchanged.

Bunch Compressor FL1BC

The FLASH1 beamline downstream the extraction section to FLASH2 will be completely rebuilt to replace the present fixed gap undulators with variable gap ones and to include a section to seed the FEL process by an external laser (see Chapter 4). The energy collimator dogleg section will be removed and replaced by a C-type chicane bunch compressor (FL1BC) with a length of 5 m to 6 m, and a maximum R_{56} of 25 mm (Figure 3.3). The removal of the dogleg will result in a horizontal shift of the beamline by 40 cm in direction to the tunnel center (in beam direction left). An energy collimator will be placed between the center dipoles.

FL1BC will have two functions: firstly, an overshearing chicane for EEHG seeding and secondly, a third independent compression stage for SASE operation. The main advantage will be a significant reduction of coherent synchrotron radiation and space charge effects, especially in operation modes which require close to or full compression. This is accomplished by the reduction of compression at lower energy at BC1 and BC2. The final compression is achieved at a higher energy $E = \gamma m_e c^2$ and thus higher beam rigidity which suppresses space charge forces. Space charge forces reduce with $1/\gamma^2$. A compression factor of 4 to 5 is achievable with FL1BC.

In order to measure the compressed phase space, a transverse deflecting structure (TDS) will be installed downstream of the undulators. The present S-band TDS (named LOLA) will be relocated or a new X-band TDS similar to the one developed for FLASH2 will be installed.

A small dogleg will compensate the 40 cm horizontal shift of the beamline and guides the beam into the otherwise unchanged dump section (Figure 3.3).

The overall concept of the beamline is described in Chapter 4.

Bunch Compressor FL2BC

The compressor FL2BC is a C-type chicane with a length of 5 m to 6 m. It is installed after the extraction to FLASH2 and before the undulators (Figure 3.3). The R_{56} of FL2BC will be tunable between 8 and 25 mm.

Table 3.2: *Electron beam energy profile used for the beam optics and compression optimization.*

Section	On-crest energy gain (MeV) present	On-crest energy gain (MeV) after upgrade	RF-Phase (°)	Off-crest energy (integrated) (MeV) after upgrade
GUN	5	5	0	5
ACC1	160	160	5	164
ACC39	−19	−19	−15	146
ACC23	325	430	20	550
ACC45	360	380	0	930
ACC67	420	420	0	1350

Details of Simulations to Design the New Compression Scheme

As a boundary condition we have to consider the achievable energy profile along the accelerator. Especially the achievable gradient in the four 3rd harmonic cavities ACC39 will limit the choice of the compression scheme. The present cavities reach a maximum voltage of 21 MV. In the future, we might be able to replace the weakest cavity by a new one with an improved field gradient. Taking this into account together with a realistic assessment of the attainable gradients of the modules, we have concluded the energy profile for the optics and compression optimization as listed in Table 3.2.

As a first consideration, a smaller bending angle of BC1 would be preferable from the point of RF tolerances. Moreover it would allow imprinting a larger energy chirp on the bunch while preserving the compression in the first stage because of the lower R_{56} of BC1 (see Section 3.3.1). This would also relax the off-crest phase of ACC2/3 while achieving the same compression and thereby enhancing the effective energy gain of ACC2/3. However, reducing R_{56} of BC1 would require a higher gradient in ACC39 to achieve approximately linear compression which is not possible with the present voltage limitation of 21 MV.

A second consideration is the limitation of the peak current to reduce space charge forces (SC) and to preserve a small slice emittance. For higher charges (≈500 pC) the tolerable peak current is higher than for smaller charges (≈100 pC). This is because bunches produced with higher charge already have a larger transverse emittance and therefore a smaller transverse charge density. In addition, the larger bunch length of high charge bunches reduces the density gradient, thereby partly linearizing the SC forces. If we allow a few percent in emittance growth, the peak current limit at BC1 is about 100 A for high charge bunches, and only 30 A for low charge bunches. A similar effect limiting the maximum reasonable peak current holds also at BC2. Because of the new third bunch compressors at final energy, these limitations do not reduce the final peak current required for efficient SASE operation.

The influence of the CSR wake on the bunch depends critically on the Twiss parameters in the corresponding compressor chicane. The reduction of CSR effects requires careful optimization of Twiss parameters in all three chicanes. We have chosen to independently minimize the CSR disruption for each compressor stage. We have performed extensive tracking studies on bunch compression and beam transport simulations.

Four cases of bunch charges have been studied: 500 pC, 250 pC, 100 pC, and 20 pC. The studies were performed using 10 million particles (1 million particles for 20 pC) using the ASTRA code for the photoinjector part and Xtrack for the remaining parts of the beamlines. Compared to the present beamline design with two compression stages, the new beamline design significantly improves the beam quality in terms of transverse emittance, longitudinal linearity, and slice energy spread for all four cases. As an example of the simulations, Figure 3.6 shows a comparison of the longitudinal phase space in FLASH2 at 1.35 GeV, for a bunch charge of 250 pC, and a peak current of 2 kA with and without the 3rd bunch compressor. It clearly shows that space charge and CSR effects are much reduced using the new scheme with three compressors.

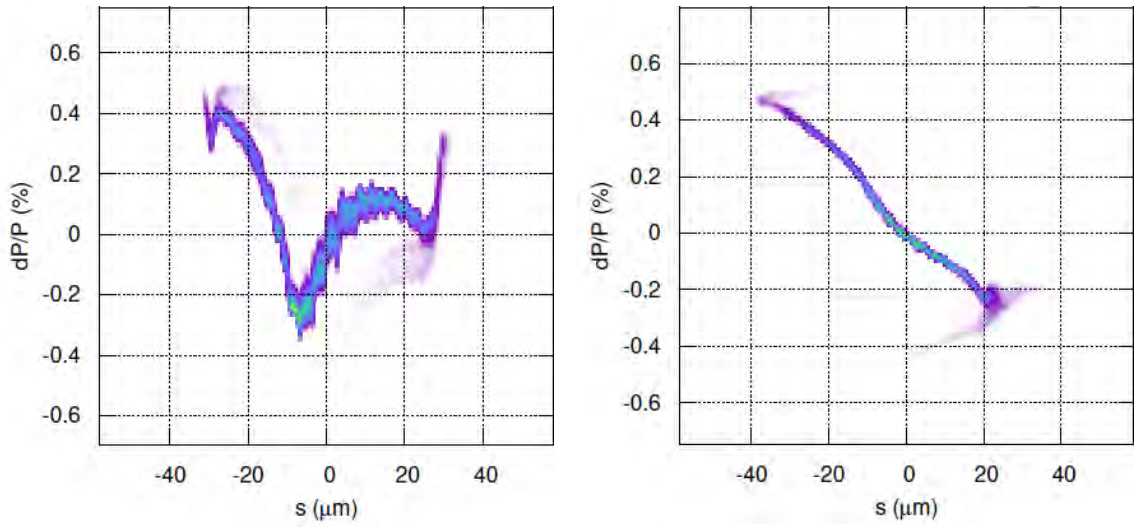

Figure 3.6: *Comparison of the longitudinal phase space in FLASH2 at 1.35 GeV with the present bunch compression scheme using two bunch compressors (left) and with the new scheme using a third compressor (right). The simulation includes space charge and CSR effects. The peak current in both cases is 2 kA, the bunch charge 250 pC.*

In the new design, the compression factors of the 1st, 2nd, and 3rd bunch compressor are 4 to 5, 8 to 10, and 2.5 to 6, respectively. The peak current after BC2 is 250 A to 800 A, while the final peak current is 2 kA. For the 20 pC case, a peak current of 1.5 kA is achieved. In the present two compressor scheme, the slice emittance growth is as large as a factor of 2. For all new cases, the slice emittance growth is small (≈10 %), while the projected emittance growth can be as large as almost a factor of 2.

Table 3.3 summarizes selected beam parameters resulting from start to end simulations from the RF-gun to the FLASH2 beamline. The deflecting angle of BC1 is 16° (R_{56}=140 mm), in BC2 5° (R_{56}=70 mm), and in FL2BC 4.7° (R_{56}=25 mm).

3.4 Laser Heater

Space charge induced micro bunch instabilities spoil the phase space of compressed bunches. This is a severe issue for a successful seeding of the electron beam by an external laser. At best, the phase space of an electron beam for seeding requires a flat energy with a small spread along the bunch.

Even though minimized by the new compression scheme described above, space charge induced micro bunching and coherent synchrotron radiation (CSR) effects still deteriorate the bunch in a non-tolerable way for seeding. Other FEL facilities use a so-called laser heater to mitigate micro bunch instabilities by "heating" up the bunch with an external laser in an undulator field (Spampinati et al. 2014; Huang et al. 2004). The uncorrelated energy spread is increased so that a potential longitudinal space charge (LSC) induced energy modulation is rather smeared out in the compression chicanes than transformed into a charge density modulation. This suppresses the micro bunching instabilities (Saldin et al. 2002a; Saldin et al. 2003).

A start-to-end simulation including the laser heater and its influence on seeding has not yet been carried out. We have studied the beam transport from the RF-gun section to behind the 3rd bunch compressor FL1BC to the EEHG chicane. Studies of the FLASH1 and FLASH2 undulator beamlines including their bunch compressors and GENESIS simulation with realistic bunches are still to be done. The photo injector was simulated with ASTRA and then tracked with Xtrack to the undulator entrance.

The beam was matched to the optimal Twiss functions at the entrance of the bunch compressors. A perfect matching of a symmetric

Table 3.3: *Selected beam properties from the RF-gun to the FLASH2 beamline, along the accelerator for 4 different bunch charges (I_p peak current, ϵ_p projected emittance, ϵ_s slice emittance, δE_s slice energy spread).*

		20 pC				100 pC			
	Energy (MeV)	I_p (A)	ϵ_p (µm)	ϵ_s (µm)	δE_s (keV)	I_p (A)	ϵ_p (µm)	ϵ_s (µm)	δE_s (keV)
GUN	5	5	0.40	0.40	22	8	0.60	0.60	15
ACC1	160	5	0.35	0.30	22	8	0.40	0.40	15
ACC39	145	5	0.35	0.30	22	8	0.40	0.40	15
ACC23	550	25	0.35	0.30	36	35	0.40	0.40	20
ACC45	930	250	0.40	0.30	50	350	0.50	0.40	50
ACC67	1350	250	0.40	0.30	50	350	0.50	0.40	50
EXTR	1350	250	0.40	0.30	50	350	0.50	0.40	50
FINAL	1350	1500	1.00	0.30	250	2000	1.00	0.40	250
		250 pC				**500 pC**			
	Energy (MeV)	I_p (A)	ϵ_p (µm)	ϵ_s (µm)	δE_s (keV)	I_p (A)	ϵ_p (µm)	ϵ_s (µm)	δE_s (keV)
GUN	5	16	0.90	0.90	18	25	1.40	1.20	20
ACC1	160	16	0.70	0.60	18	25	1.10	0.8	20
ACC39	145	16	0.70	0.60	18	25	1.10	0.8	20
ACC23	550	60	0.70	0.60	25	100	1.20	0.8	27
ACC45	930	550	0.80	0.60	50	800	1.20	0.8	50
ACC67	1350	550	0.80	0.60	50	800	1.20	0.8	50
EXTR	1350	550	0.80	0.60	50	800	1.40	0.8	50
FINAL	1350	2000	1.40	0.60	250	2000	1.60	0.8	250

waist between electrons and laser is not possible due to the space requirements for the electron beam optics. The CSR waist in the downstream bunch compressor BC1 is of more importance than the symmetric waist of the electron inside the laser heater undulator. We have found a compromise to achieve a sufficiently small electron beam. This helps to reduce the required laser pulse energy to modulate the electron beam.

For a study with realistic shot-noise driven micro bunching, the macro particle tracking approach is not well suited, since it overestimates the initial granularity. We are pursuing two strategies to overcome this issue.

Firstly, analytical models capable of studying micro bunching beyond first order, and numerical models simulating smooth bunches are being developed. Preliminary results using the well established linear gain approach indicate that the energy spread induced by the laser heater can suppress the micro bunching gain to a large extent. Secondly, a 1-to-1 particle tracking of a finite section of the bunch core with periodic boundary conditions is in preparation.

The best location for the laser heater is before the 1st compression stage BC1, where space charge effects are largest. The energy modulation from the laser heater is oversheared in the subsequent bunch compressor chicane BC1.

We need an additional small chicane for the in-coupling of the laser. We decided not to put the undulator into this chicane. In order to achieve bunch compression in BC1, the electron bunch acquires a negative energy chirp through off-crest acceleration in ACC1. An off-crest accelerated beam has a large correlated energy spread and is transversely spread out via dispersion in the middle of the small in-coupling chicane. This is thus not an ideal place for the laser/bunch interaction in the undulator due to widening and transverse correlations.

The second advantage of our layout is, that we do not expect any trickle heating which is an issue for LCLS.

The external laser beam is reflected via an in-vacuum mirror along the beam path. The laser pulses are synchronized with the electron bunches such that the laser overlaps with the electrons and travels with the bunch through an undulator. The electrons are guided around the in-vacuum mirror by a small C-chicane offsetting the electrons horizontally by 20 mm.

The undulator has 8 to 10 periods and a length of 40 cm. The resonant wavelength is 515 nm matching the wavelength of the laser beam. The laser pulse duration is σ=20 ps (Gaussian), a bit longer than the electron bunches. The required peak power of 1 MW is obtained with a laser pulse energy of 50 µJ. FLASH operates in a burst mode which means that the laser produces pulse trains of 800 pulses spaced by 1 µs (1 MHz) with a repetition rate of 10 Hz. The average laser power is reasonable with 0.4 W. The laser field overlapping with the electron bunch in the undulator imprints an energy modulation with an amplitude of up to 35 keV. The initial uncorrelated energy spread from the RF-gun is about 3 keV. The laser pulse duration is chosen such that the modulation variation along the bunch is not more than 40 %. The bandwidth of the modulation process is about 10 % compared to the maximal RF induced energy chirp of the electron bunch of ≈5 %. This leads to smaller modulation amplitude at the tails of the bunch, which is acceptable. A laser wavelength of 515 nm is chosen to have a better smearing out of the periodically induced energy modulation by the large R_{56} of the following bunch compressor BC1. Even shorter wavelengths, however, would lead to a smaller coupling between the laser field and the electron bunch, which is a disadvantage. The green wavelength is a good compromise. Table 3.4 summarizes basic laser and undulator parameters.

The laser will be located in a laser room together with the photoinjector lasers (see Figure 3.2). The size of the laser room will be large enough to allow further upgrades of the laser system.

We plan to test sophisticated schemes to manipulate the electron bunches with the laser, like transverse pulse shaping including multi-spot techniques and longitudinal pulse stacking. The laser itself is based on the same design as the new photoinjector laser to offer the same flexibility in longitudinal pulse shaping. See Chapter 6 for details.

Table 3.4: *Basic properties of the laser heater laser system and the undulator.*

Laser		
	Wavelength	515 nm
	Single pulse energy	50 µJ
	Pulse duration (Gaussian σ)	20 ps
	Burst mode	800 pulses at 1 MHz
	Repetition rate	10 Hz
Undulator		
	Magnets	Permanent
	Number of periods	8 – 10
	Period length	40 mm
	Gap	16 mm
	K	1.3

3.5 Diagnostics

Beam instrumentation and diagnostics of electron beam properties have been originally designed in 2003 for a bunch charge in the range of 0.5 nC to 2 nC. Already now we use compression schemes which require bunch charges as low as 20 pC, where most diagnostics had either no signal or a very limited resolution. A refurbishment program has already been started in 2013 and is meanwhile mostly finished.

3.5.1 Standard Beam Diagnostics

Standard beam diagnostics comprise the measurement of the charge, beam position, transverse profile, and beam losses.

Beam Charge and Beam Loss Monitors

The toroid system to measure bunch charges along the accelerator including the toroid protection system (TPS) has already been upgraded in 2016. The resolution has improved from 3 pC to better than 0.5 pC. Low noise front-end electronics as well as MicroTCA®-based electronics have replaced the old VME system. The 1 MHz ADCs have been replaced with modern 108 MHz ADCs. This improved tremendously the pulse identification and reliability of the sampling of the toroid pulses to determine the beam charge in a reliable way.

The TPS is an important machine safety feature. It measures the charge transmission along the accelerator and vetoes the beam if a certain single pulse, slice, and/or integrated loss has occurred. In addition to the TPS, local beam losses especially at the undulators are measured with a higher resolution to ensure protection of sensitive beamline components. All beam loss monitors (BLM) along the accelerator have been refurbished as well. This was necessary in order to cope with the two beamline operation, where part of the pulse train is split off and directed to the second undulator beamline FLASH2. The two beamline operation is very flexible; different beam patterns can be used for both beamlines, and also different laser systems. The new protection system (TPS and BLMs) is able to distinguish between losses occurring in one part and/or the other part of the train and vetoes only the part responsible for the losses, not the whole train. This is an important feature to keep the operation of both beamlines as independent as possible.

Beam Position Monitors

Most beam position monitors (BPM) hardware is sufficient to deliver a good resolution also for low charges. However, the original electronics designed for high charge operation failed at charges below 0.3 nC. Therefore, in a first step in 2017, the read-out electronics has been upgraded for all strip-line and button BPMs. The MicroTCA®-based electronics use improved amplifiers and better sampling with the modern 108 MHz ADCs. The cold cavity BPMs inside most modules however could not be upgraded at this point. Two of the six cold cavity BPMs will be replaced by cold button BPMs with the refurbishment of ACC2/3 (see Section 3.1). The resolution of most BPMs is now below 10 µm for a large range of charges. Slow orbit feedbacks have been established profiting from the improved resolution. This is an important step forward to fight against orbit drifts and to stabilize the machine over several hours of operation. Figure 3.7 shows the achieved improvement in resolution especially for low charges (Lorbeer et al. 2018).

All FLASH2 BPMs are already equipped with the new electronics. The FLASH2 cavity BPMs used between the undulators have a very good resolution of down to 1 µm. Their electronics have been provided by Paul-Scherrer-Institute (PSI) in Switzerland. The plan is to replace the present button BPMs in the FLASH1 undulator section by the same type of cavity BPMs when variable gap undulators are installed.

3.5.2 Longitudinal diagnostics

The longitudinal phase space is measured with a variety of diagnostics and instrumentation methods. The bunch length after compression is monitored by bunch compression monitors (BCM) based on the measurement of coherent diffraction radiation. The longitudinal phase space is measured with a transversely deflecting RF structure (TDS). The arrival time of electron pulses is measured by high bandwidth pick-ups in beam arrival time monitors (BAM).

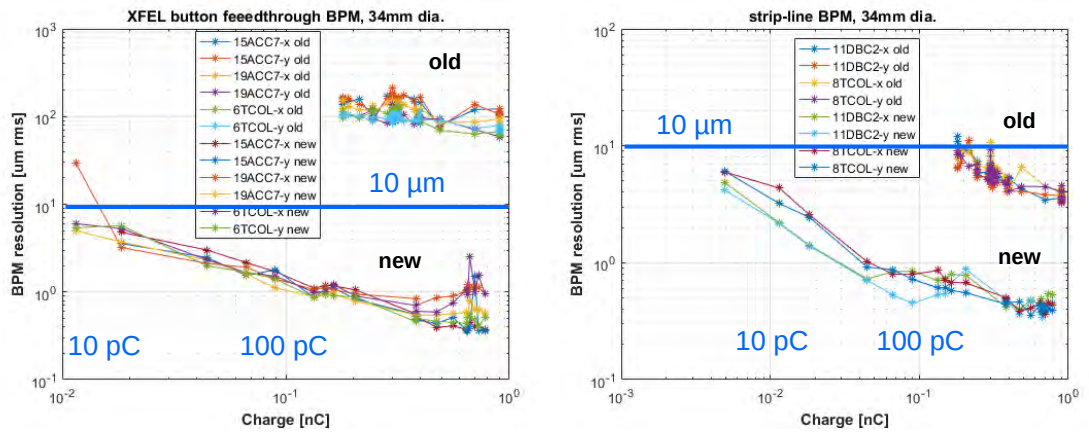

Figure 3.7: *Resolution of the beam position monitors (BPM) after the upgrade ("new") compared to the previous resolutions ("old"). The resolution has significantly improved especially for low charges. The left plot shows the button, the right plot strip-line BPMs.*

Bunch Compression Monitors

The relative compression of bunches is estimated using coherent diffraction radiation emitted by an electron bunch passing through a slit in a screen otherwise used to measure the transverse electron bunch profile using optical transition radiation (Al coated Si-wavers). Two bunch compression monitors (BCM) are installed, one after each bunch compressor. The coherent diffraction radiation is in the THz-range and measured with pyro-electric detectors. The system is laid out to be able to resolve individual bunches in a 1 MHz pulse train with a good resolution. Pile-up corrections and charge corrections are applied. Up to now, the system is used in a slow feedback mode to stabilize the phase of modules ACC1 (BCM in BC1) and ACC2/3 (BCM in BC2). We plan to upgrade the system to make an intra-train fast feedback possible.

In addition to the BCMs, diffraction radiation from off-axis screens are used to measure the radiated spectrum (CRISP4) (Behrens et al. 2012). One electron bunch from a bunch train is kicked to the screen. Three systems are installed, after the last module ACC7, in the FLASH1 and the FLASH2 beamlines. The measurement covers a large spectral range from the near-infrared to THz. From the measured spectral distribution, the duration and shape of electron bunches are estimated. The system is complementary to the transversely deflecting RF structure (TDS) described in the next paragraph and gives a good measurement of the longitudinal phase space of the electron bunch.

Transversely Deflecting Structure

A transversely deflecting structure (TDS) provides a direct measurement of the longitudinal phase space (Behrens et al. 2012). FLASH1 has an S-band RF-structure called "LOLA" with a time resolution of 8 fs (rms) and an energy resolution of $dE/E = 1 \times 10^{-3}$ (rms). LOLA is located after the sFLASH experiment but before the SASE undulators. Unfortunately, during SASE operation, the electron beam optics through LOLA is constrained such that the resolution is reduced to 30 fs at best. We plan to relocate LOLA downstream of the new FLASH1 undulators and adapt the beam optics for better resolution.

In cooperation with CERN and PSI a new type of X-band TDS called "PolariX" is being designed (Craievich et al. 2018). The new design will allow a variable streaking direction (LOLA can streak only in one direction) and a better resolution. We plan to install two PolariX cavities downstream of the FLASH2 undulators. We expect to achieve a time resolution of 4 fs (rms). PolariX is powered by a 12 GHz klystron placed close to the TDS (see Figure 3.8). The X-band RF-station is shared with the TDS prototype in operation at the FLASHForward experiment located in the FLASH3 electron beamline parallel to the FLASH2 line and currently not used for user operation.

Instead of relocating LOLA, we may also use a new PolariX TDS downstream the new FLASH1 undulators.

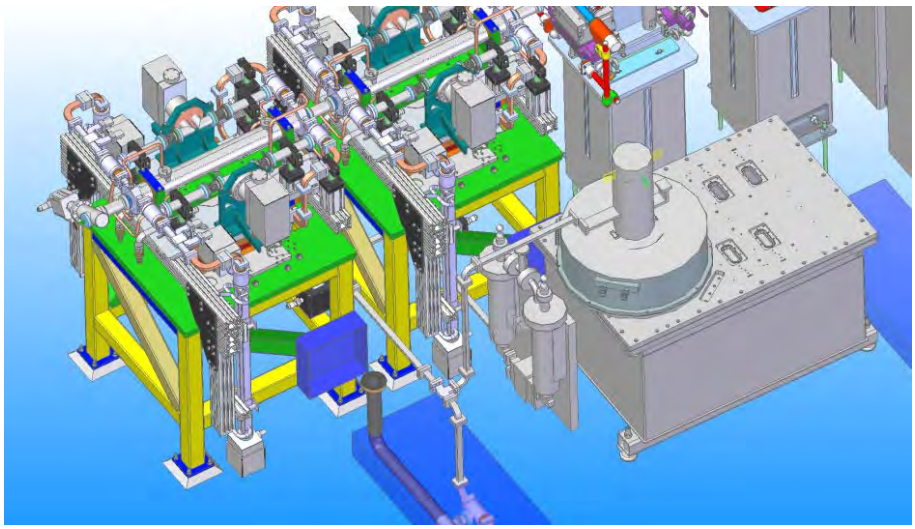

Figure 3.8: *Layout design of the implementation of PolariX, the new X-band transversely deflecting RF structure to be installed in FLASH2. For optimal resolution, two structures are required at a beam energy above 1 GeV. The two cavities are mounted on the green colored tables. The X-band 12 GHz klystron is placed aside.*

Bunch Arrival Time Monitors

The bunch arrival time is an important parameter for pump-probe experiments (Savelyev et al. 2017). The arrival time stability should be less than the photon pulse duration, which may be as short as a few femtoseconds. Therefore considerable effort has been made in order to improve the arrival time stability and its measurement. In collaboration with University Darmstadt, new pick-ups with a bandwidth of 40 GHz and a good sensitivity for low charges have been developed and installed at FLASH (Figure 3.9) (Angelovski et al. 2015). These new bunch arrival time monitors (BAM) are installed before and after each bunch compressor chicane. Instabilities and drifts in arrival time are generated by energy variations of individual bunches or along the bunch train translating into arrival time instabilities or drifts after dispersive sections like bunch compressor chicanes: $cdt = R_{56}dE/E$.

The arrival time is measured by cross-correlating the signal from the pick-up with a reference of the master laser oscillator (MLO). A stabilized optical link realized with the new polarization preserving fibers is running from the synchronization lab to a location as close as possible to the BAM pick-up. For details on the synchronization system see Section 3.6. The cross-correlation is realized in electro-optical modulators (EOM) (Viti et al. 2018).

The new system is presently partially under commissioning. First measurements show an achievable resolution of better than 5 fs at a

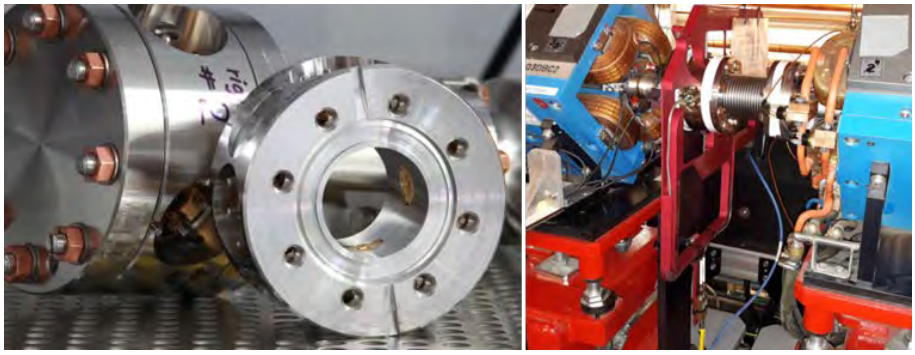

Figure 3.9: *Body of the bunch arrival time monitor (BAM) with its pick-ups (left). As an example, a BAM installed after the 1st bunch compressor is shown. The body with the pick-ups is visible left to the bellow. The cables from the pick-ups are mechanically stabilized using the red-colored support frame.*

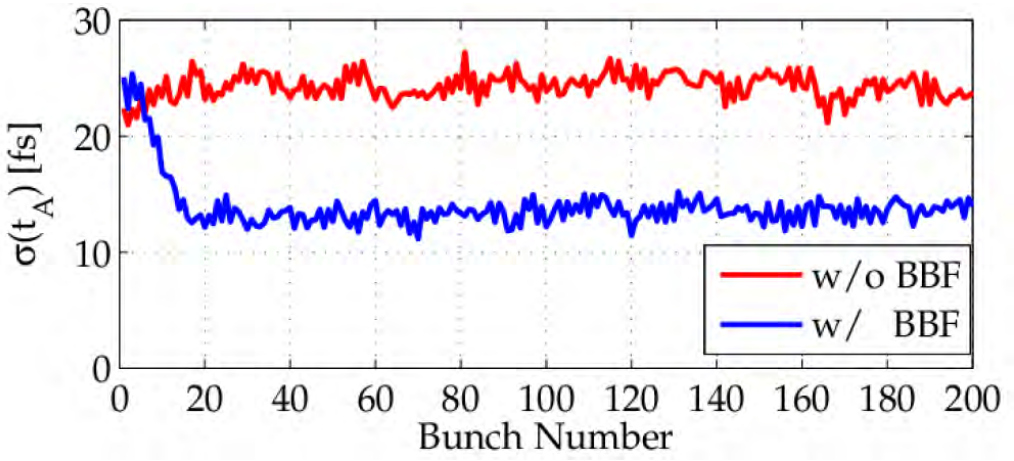

Figure 3.10: *Example of a measurement of the arrival time stability of electron bunches along a bunch train of 200 bunches (1 MHz) with the BAM system (red trace). The fast intra-train feedback improves the stability by a factor of 2 (blue trace). Due to the low bandwidth of the superconducting cavities the steady state is achieved only after 20 µs.*

charge range of 200 pC to 1 nC and less than 10 fs (rms) down to 20 pC. The previous system had a clear cut-off at 200 pC, where the resolution was not sufficient for beam based stabilization with feedbacks.

The BAMs are not only used to measure the arrival time, but also to provide a slow feedback as an average drift compensation and a fast intra-train feedback acting along the pulse train to correct for pulse-to-pulse jitter (Figure 3.10). The arrival time is stabilized by acting on the amplitude of the modules before the bunch compressors. The intra-train feedback is especially important for pump-probe experiments (Schulz et al. 2015). SASE with very short pulses of a few femtoseconds requires bunches with a small bunch charge below 200 pC. For single spike SASE operation, the bunch charge may be as low as 20 pC. Due to its enhanced sensitivity for low charges, the new system allows to use slow and fast feedbacks also for very short SASE pulses, where it is most important.

Beam Arrival Time Feedback Cavity

To improve the arrival time stability, the energy stability of the acceleration amplitude especially before the 1st bunch compressor with its large R_{56} needs to be stabilized as good as possible. Also important in this context is the charge variation which causes variations in acceleration due to beam loading effects. This constrains also the energy and arrival time stability of the photoinjector laser. The superconducting acceleration cavities operated in closed RF feedback loop have a bandwidth of ≈100 kHz. Slow variations along the pulse train and fluctuations from macro pulse to macro pulse can be efficiently regulated. An amplitude stability of $dA/A = 5 \times 10^{-5}$ (rms) and a phase stability of better than 0.01° (rms) is achieved. A stability of $dA/A = 5 \times 10^{-5}$ in ACC1 corresponds to

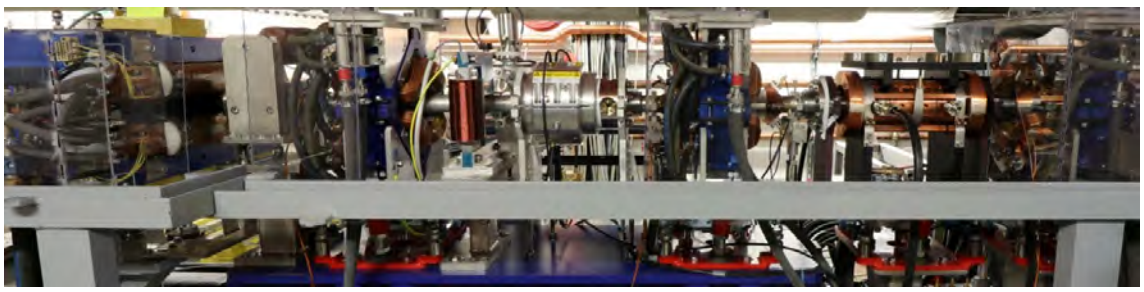

Figure 3.11: *BACCA, the new S-band RF cavity for fast arrival time feedback installed up-stream of the first bunch compressor (copper structure on the right). The first dipole of BC1 (blue) is on the left of the picture.*

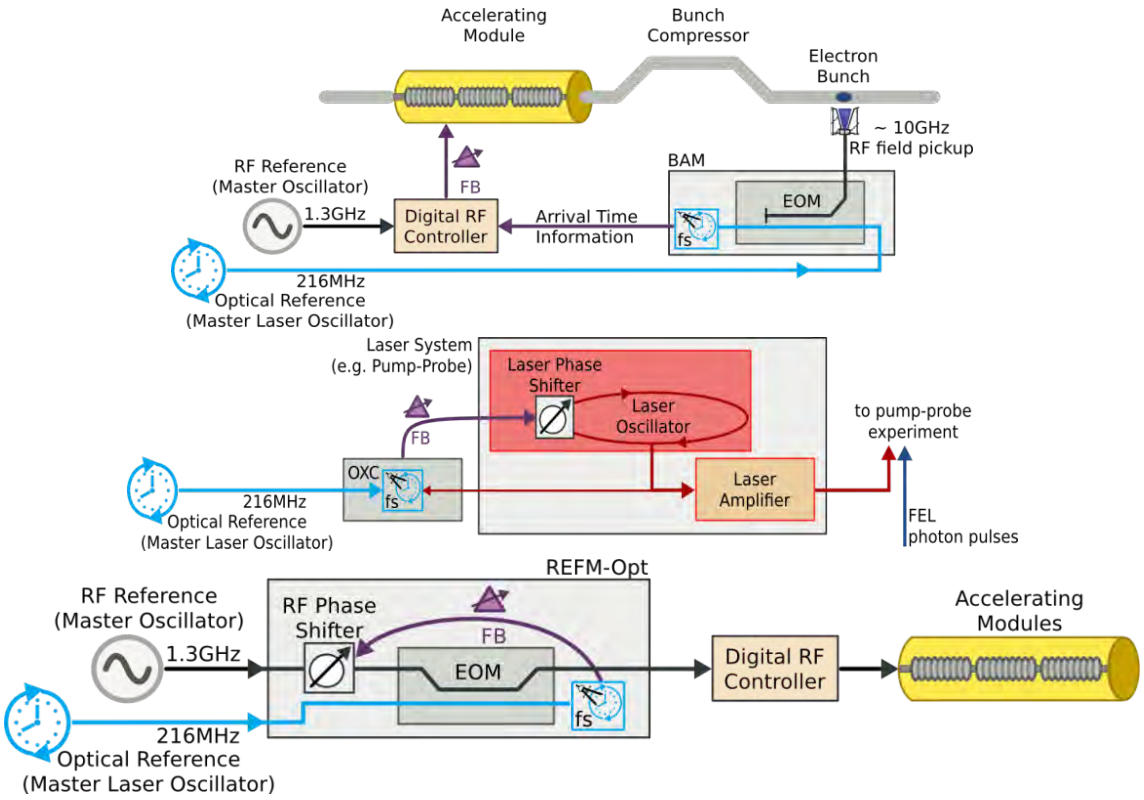

Figure 3.12: *Sketches of the three basic tasks of the optical synchronization system, providing synchronized laser signals for the arrival time measurement, for laser-to-laser synchronization, and to stabilize the RF phase of accelerating modules.*

30 fs arrival time jitter after BC1. In order to improve this, an RF cavity with a higher bandwidth needs to be used.

A warm RF S-band cavity called BACCA has been designed as part of the EuCARD project and is installed after the 1st acceleration module and before the 1st bunch compressor BC1 (Figure 3.11) (Pfeiffer et al. 2019; Pfeiffer 2017). Its bandwidth is 500 kHz to 1 MHz. The arrival time is measured after BC1 with the new improved BAM system and is fed back to BACCA with a low latency of 0.7 µs. BACCA is presently under commissioning. The cavity is driven by a 1 kW amplifier and has an energy modulation range of ±50 keV corresponding to ±200 fs. The sensitivity is 4.3 keV/fs. The goal is to improve the arrival time stability to better than 5 fs.

3.6 Synchronization

Synchronization of the various components of the accelerator as well as synchronization of the electron bunches with external laser systems to the femtosecond level are of utmost importance for stable operation and for time-resolved pump-probe experiments. The synchronization is based on an RF master oscillator (MO) feeding a laser based master (MLO). An ultra-stable master laser oscillator reference is distributed via actively length-stabilized optical fiber links to the various clients (Müller et al. 2019). The synchronization system has three basic tasks: providing synchronized laser signals for the bunch arrival time measurements (BAM), laser-to-laser synchronization, and as a reference for the low-level RF system to stabilize the RF phase of accelerating modules (REFM-Opt). Figure 3.12 shows sketches of the three basic tasks.

The previous system required upgrades in several aspects. The maximum number of eight links is not sufficient to serve all clients. The new system will be more compact and provides 24 links. The timing jitter of the optical links

is significantly reduced from 3 fs to 0.5 fs (rms) by using polarization-maintaining fibers. The residual drift over 24 h is measured to be only 3.3 fs (rms). The jitter of the MLO will be significantly reduced from 30 fs to 3 fs by a new synchronization scheme based on a Mach-Zender interferometer. The synchronization from laser to laser is expected to be reduced from 15 fs to 5 fs.

The upgrade has started in summer 2018. Step by step, new links are being commissioned in the order of priority for FLASH operation. The system is expected to be in full operation by 2020. The plan is to provide links to 3 RF stations, 8 BAMs, and 12 external laser systems.

The master laser oscillator (MLO) is the main optical reference. The laser oscillator is a commercial product, passively mode locked, operating at a wavelength of 1550 nm (standard for telecommunication products). It exhibits ultra-low noise, such that the integrated timing jitter from 10 kHz to 100 kHz stays below 3 fs. Two MLOs are operated in parallel, both synchronized at all time. In case of a failure of one system, switching to the back-up is fast: no link lock will be lost, all timings will be preserved. The synchronization of external laser systems (injector, pump-probe, seed lasers) is firstly based on RF signals from the MO. This is simple and reliable with a jitter of about 20 fs, but exhibits large drifts of hundreds of femtoseconds over hours. To reduce the drifts and also the jitter, laser-to-RF and/or laser-to-laser synchronization is applied (Lamb et al. 2018). The local laser pulses are cross-correlated to the optical reference laser (optical synchronization) and to the RF applied to the local oscillator (RF synchronization). The jitter is reduced to 3 fs (laser to RF) or to 1 fs (rms) with long-term drifts of less than 10 fs (rms). See Figure 3.13 for details.

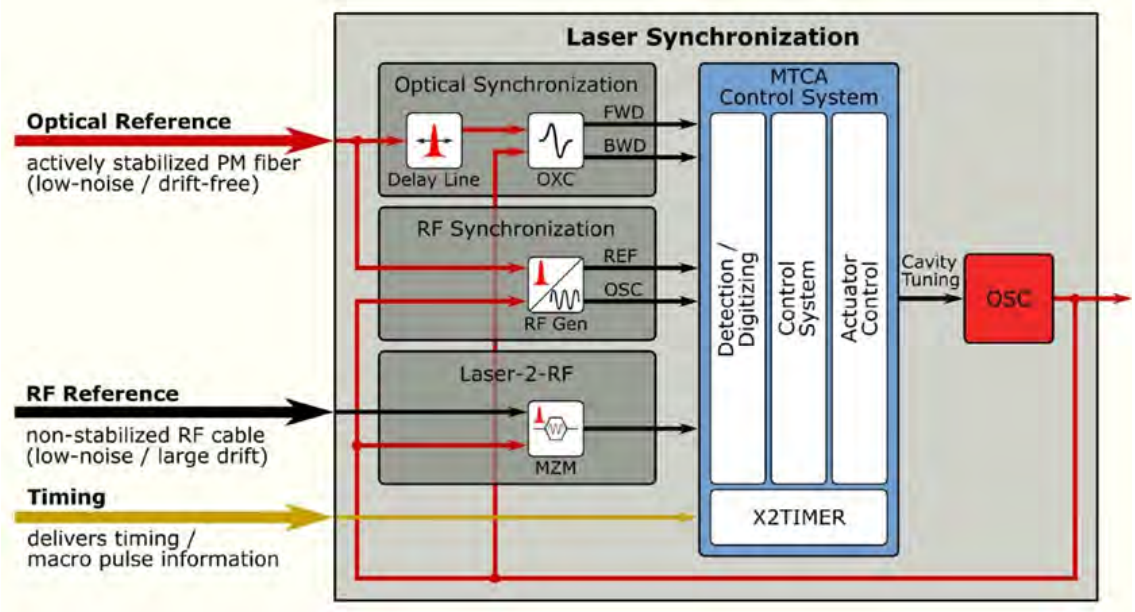

Figure 3.13: *Block diagram of the laser-to-RF and laser-to-laser synchronization options. The laser pulses from the local oscillator are cross-correlated to the reference laser source (optical and RF synchronization) or the reference RF only.*

References

Ackermann, S. et al. (2013). „Generation of Coherent 19- and 38-nm Radiation at a Free-Electron Laser Directly Seeded at 38 nm“. In: *Phys. Rev. Lett.* 111 (11), p. 114801. DOI: 10.1103/PhysRevLett.111.114801.

Angelovski, A. et al. (2015). „Evaluation of the cone-shaped pickup performance for low charge sub-10 fs arrival-time measurements at free electron laser facilities“. In: *Phys. Rev. ST Accel. Beams* 18 (1), p. 012801. DOI: 10.1103/PhysRevSTAB.18.012801.

Behrens, C. et al. (2012). „Constraints on photon pulse duration from longitudinal electron beam diagnostics at a soft x-ray free-electron laser“. In: *Phys. Rev. ST Accel. Beams* 15 (3), p. 030707. DOI: 10.1103/PhysRevSTAB.15.030707.

Craievich, P. et al. (2018). „Status of the Polarix-TDS Project“. In: *Proc. 9th International Particle Accelerator Conference (IPAC'18), Vancouver, BC, Canada, April 29-May 4, 2018* (Vancouver, BC, Canada). International Particle Accelerator Conference 9. Geneva, Switzerland: JACoW Publishing, pp. 3808–3811. ISBN: 978-3-95450-184-7. DOI: 10.18429/JACoW-IPAC2018-THPAL068. Online.

Edwards, D. A. (1995). *TESLA Test Facility Linac Design Report*. Tech. rep. 1995-01. DESY.

Edwards, H. et al. (2010). „3.9 Ghz Cavity Module For Linear Bunch Compression At Flash“. In: *Linear Accelerator Conference LINAC2010, Tsukuba, Japan*, MO304. Online.

Faatz, B. et al. (2011). „Flash II: Perspectives and challenges“. In: *Nuclear Instruments and Methods in Physics Research Section A: Accelerators, Spectrometers, Detectors and Associated Equipment* 635.1, Supplement, S2–S5. DOI: 10.1016/j.nima.2010.10.065.

Faatz, B. et al. (2016). „Simultaneous operation of two soft x-ray free-electron lasers driven by one linear accelerator“. In: *New Journal of Physics* 18.6, p. 062002. DOI: 10.1088/1367-2630/18/6/062002.

Huang, Z. et al. (2004). „Suppression of microbunching instability in the linac coherent light source“. In: *Phys. Rev. ST Accel. Beams* 7 (7), p. 074401. DOI: 10.1103/PhysRevSTAB.7.074401.

Lamb, T. et al. (2018). „Laser-to-RF Synchronization with Femtosecond Precision“. In: *Proc. of International Free Electron Laser Conference (FEL'17), Santa Fe, NM, USA, August 20-25, 2017* (Santa Fe, NM, USA). International Free Electron Laser Conference 38. Geneva, Switzerland: JACoW, pp. 407–410. ISBN: 978-3-95450-179-3. DOI: 10.18429/JACoW-FEL2017-WEB04.

Lorbeer, B. et al. (2018). „High Resolution and Low Charge Button and Strip-Line Beam Position Monitor Electronics Upgrade at Flash“. In: *Proc. 9th International Particle Accelerator Conference (IPAC'18), Vancouver, BC, Canada, April 29-May 4, 2018* (Vancouver, BC, Canada). International Particle Accelerator Conference 9. Geneva, Switzerland: JACoW Publishing, pp. 1923–1926. ISBN: 978-3-95450-184-7. DOI: 10.18429/JACoW-IPAC2018-WEPAF048.

Müller, J. M. et al. (2019). „Large-Scale Optical Synchronization System of the European XFEL“. In: *Proc. 29th Linear Accelerator Conference (LINAC'18), Beijing, China, 16-21 September 2018* (Beijing, China). Linear Accelerator Conference 29. Geneva, Switzerland: JACoW Publishing, pp. 253–256. ISBN: 978-3-95450-194-6. DOI: 10.18429/JACoW-LINAC2018-MOPO121.

Pagani, C. et al. (1997). „TESLA Test Facility (TTF) Cryostat Design and Development“. In: *Workshop on RF Superconductivity, Abano Terme (Padova), Italy*, p. 781.

Pagani, C. et al. (2001). „The TESLA Cryogenic Accelerator Modules“. In: *DESY TESLA* 2001-36.

Paramonov, V. et al. (2017). „Design of an L-band normally conducting RF gun cavity for high peak and average RF power“. In: *Nuclear Instruments and Methods in Physics Research Section A: Accelerators, Spectrometers, Detectors and Associated Equipment* 854, pp. 113–126. DOI: 10.1016/j.nima.2017.02.058.

Pfeiffer, S. (2017). *FLASH NRF cavity and FB system*. Tech. rep. EuCARD2 Deliverable 13.5.

Pfeiffer, S. et al. (2019). „Status Update of the Fast Energy Corrector Cavity at FLASH“. In: *Proc. 29th Linear Accelerator Conference*

(LINAC'18), Beijing, China, 16-21 September 2018 (Beijing, China). Linear Accelerator Conference 29. Geneva, Switzerland: JACoW Publishing, pp. 112–114. ISBN: 978-3-95450-194-6. DOI: 10.18429/JACoW-LINAC2018-MOP0039.

Saldin, E. L. et al. (2002a). „Klystron instability of a relativistic electron beam in a bunch compressor". In: *Nuclear Instruments and Methods in Physics Research Section A: Accelerators, Spectrometers, Detectors and Associated Equipment* 490.1, pp. 1–8. DOI: 10.1016/S0168-9002(02)00905-1.

– (2003). „Longitudinal Space Charge Driven Microbunching Instability in TTF2 linac". In: *DESY TESLA-FEL* 2003-02.

Savelyev, E. et al. (2017). „Jitter-correction for IR/UV-XUV pump-probe experiments at the FLASH free-electron laser". In: *New Journal of Physics* 19.4, p. 043009. DOI: 10.1088/1367-2630/aa652d.

Schreiber, S. (2005). „The Injector of the VUV-FEL at DESY". In: *27th Internation Free Electron Laser Conference, Stanford, CA, USA*, THPP038. Online.

Schulz, S. et al. (2015). „Femtosecond all-optical synchronization of an X-ray free-electron laser". In: *Nature Communications* 6.1, p. 5938. DOI: 10.1038/ncomms6938.

Spampinati, S. et al. (2014). „Laser heater commissioning at an externally seeded free-electron laser". In: *Phys. Rev. ST Accel. Beams* 17 (12), p. 120705. DOI: 10.1103/PhysRevSTAB.17.120705.

Stulle, F. (2004). „A Bunch Compressor for small Emittances and high Peak Currents at the VUV Free-Electron Laser". PhD thesis. Universität Hamburg.

The FLASH II Team (2010). *FLASH II Conceptional Design Report*. Tech. rep. DESY.

The TESLA Test Facility FEL Team (2002). *SASE FEL at the TESLA Facility, Phase 2*. Tech. rep. 2002-01. DESY TESLA-FEL.

Viti, M. et al. (2018). „The Bunch Arrival Time Monitor at FLASH and European XFEL". In: *Proc. of International Conference on Accelerator and Large Experimental Control Systems (ICALEPCS'17), Barcelona, Spain, 8-13 October 2017* (Barcelona, Spain). International Conference on Accelerator and Large Experimental Control Systems 16. Geneva, Switzerland: JACoW, pp. 701–705. ISBN: 978-3-95450-193-9. DOI: 10.18429/JACoW-ICALEPCS2017-TUPHA125.

Will, I. et al. (2011). „Photoinjector drive laser of the FLASH FEL". In: *Opt. Express* 19.24, pp. 23770–23781. DOI: 10.1364/OE.19.023770.

4 FLASH1 FEL Line

The FLASH1 beamline will be completely rebuilt and optimized for seeding. The envisaged wavelength range is 4 nm to 60 nm in the 1st harmonic with variable polarization. As described in Chapter 3, the beam is going straight from the accelerator into the section with modulators, chicanes and radiator undulators. Behind the transverse deflecting structure, which in this geometry can measure the bunch length in dispersive geometry and therefore immediately determine the fraction of the bunch which has overlap with the seed laser (and therefore the absolute length of the radiation pulse), a dogleg is used before entering the THz undulator (see Chapter 3 for details). The layout of the FLASH1 undulator line is shown in Figure 4.1.

The radiator undulator will have an APPLE III type geometry. The standard layout for which all simulations have been performed, assumes 2.5 m long undulators with intersections of about 0.8 m, similar to FLASH2 in its present form. Details can be found in Table 4.1. Further optimization is ongoing. As compared to FLASH2, part of the intersections in the radiator undulator will contain either wirescanners or screens to allow easy matching of the electron beam into the undulator. Instead of phase shifters, chicanes are foreseen. Furthermore, a more advanced design of the undulator is under discussion which would divide the 2.5 m into two 1.2 long sections with chicanes in between. This combination of chicanes and shorter undulators allow also in FLASH1 more advanced schemes to reduce radiation bandwidth, produce superradiant spikes with significantly increased peak powers and harmonic lasing, thus possibly bringing the seeded wavelength further down to cover the complete water window.

Undulator	**APPLE III**
Period	33 mm
Gap	8 mm to 15 mm
Polarization	Variable
Length	2.5 m
Number	12

Table 4.1: *Nominal undulator parameters assumed in this chapter.*

Although the FLASH1 undulator line will be optimized for seeding, it can still be operated in SASE mode. Without a seed to start the amplification process, the saturation length will increase. On the other hand, because the beam can be compressed in a final stage using the EEHG chicane, higher peak currents will be used in SASE mode, thus increasing the pulse energy and shortening the gain length. Therefore, Section 4.1 deals with the simulation of SASE in the radiator undulator. The total number of undulators assumed in the simulations is 12, which is the maximum that fits into the available space. The parameters for SASE are the same as those found in Chapter 3. Section 4.2 is dedicated to detailed seeding simulations. Because for seeding the compression is reduced in order to improve the beam quality, more details on those parameters will be discussed in that section. The final undulator length required to reach saturation with seeding will be shorter. Therefore the minimum wavelength which can be reached with SASE will probably be longer (see Section 4.1 for details).

4.1 Undulator Concept

The simulations in this section have been performed assuming 2.5 m long APPLE III undulators in helical setting with 0.8 m intersections. In this case, the minimum wavelength which can be reached with SASE will be around 4 nm to 5 nm. The space which would become available when less undulators are required for seeding could be used for options such as harmonic lasing or schemes developed at PSI under the name CHIC (chicanes for high power and improved coherence). This effectively increases the wavelength range down to the complete water window with linear polarization, though with reduced pulse energy. The safety margin that should be included to take into account variations of beam parameters or the influence of imperfections in alignment or strength of the quadrupoles is discussed in Section 4.1.2

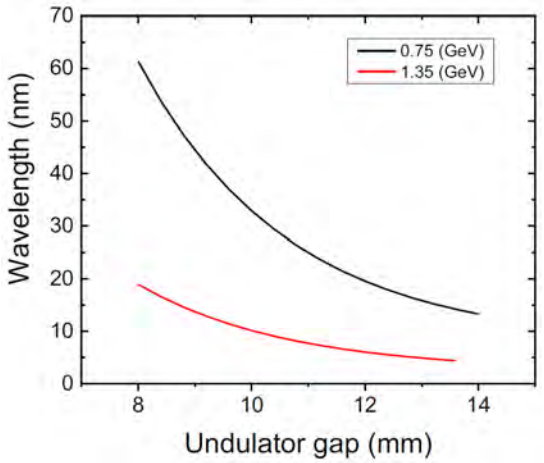

Figure 4.2: *Tunability of the wavelength at two different energies (0.75 GeV and 1.35 GeV). The parameters given in Table 4.1 are assumed. Results are shown for circular polarization and a charge of 250 pC. For 1.35 GeV we have assumed a peak current of 2 kA, and 1.5 kA for 0.75 GeV.*

4.1.1 Achievable Wavelength Range

The wavelength range which can be achieved depends on beam parameters, assumed tolerances and the available length. At the moment, the effective undulator length is estimated based on space needed for seeding and the type of undulators that are built in. For seeding, several chicanes and modulators have been considered, but for example what is needed for diagnostics or characterization of the seed laser is a rough estimate.

In Figure 4.2 and Figure 4.3, the achievable wavelength range, saturation length and saturation power for nominal parameters are shown. For both curves, several steady state and a few time-dependent simulations have been performed. These have been fitted with the Xie-equations to obtain the intermediate values. Since the actual number of undulators will be less (see Section 4.2 on saturation length required for a seeded FEL), the achievable wavelength as a function of the undulator length based on these fits is shown in Figure 4.4.

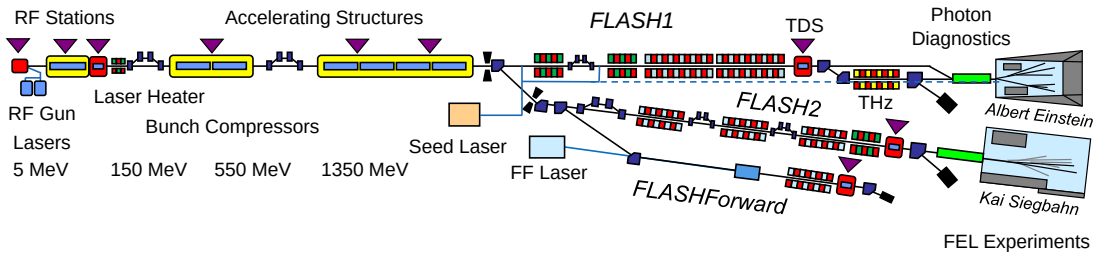

Figure 4.1: *Layout of FLASH1 optimized for seeding with variable gap undulators including circular polarization. Note that the XUV and THz transport is now parallel. The total length of the facility from the electron source to the experimental halls is 315 m.*

Beam parameters	1.35 GeV	0.75 GeV
Emittance	0.4 mm mrad to 1.2 mm mrad	0.4 mm mrad to 1.2 mm mrad
Energy spread	0.1 MeV to 0.5 MeV	0.1 MeV to 0.5 MeV
Peak current	1.5 kA to 2.0 kA	1.5 kA to 2.0 kA
Charge	0.02 nC to 0.5 nC	0.05 nC to 0.5 nC
Bunch length (RMS)	1 µm to 30 µm	1.5 µm to 50 µm

Table 4.2: *Nominal electron beam parameters. It is assumed that the machine runs at two distinct energies only (1.35 GeV and 0.75 GeV).*

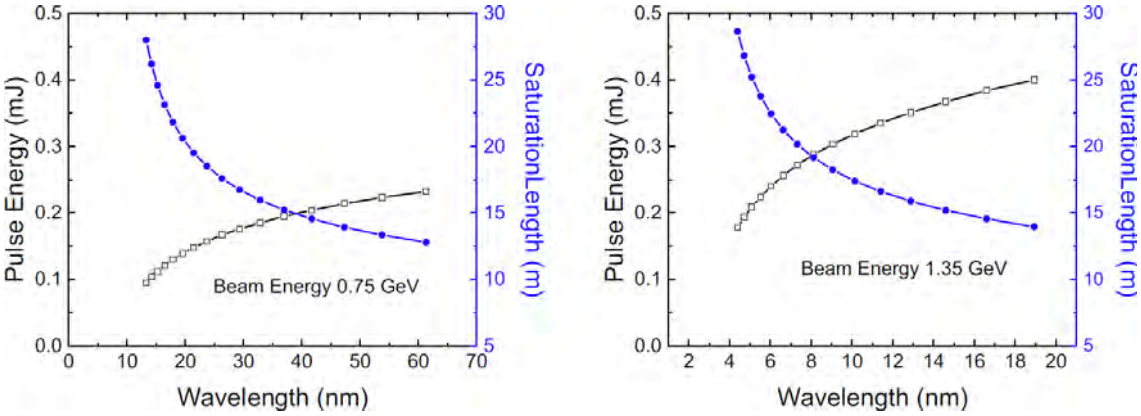

Figure 4.3: *Saturation power and length for 0.75 GeV (left) and 1.35 GeV (right) for parameters given in Table 4.1. Results are shown for circular polarization and a charge of 250 pC. For 1.35 GeV we have assumed a peak current of 2 kA, and 1.5 kA for 0.75 GeV.*

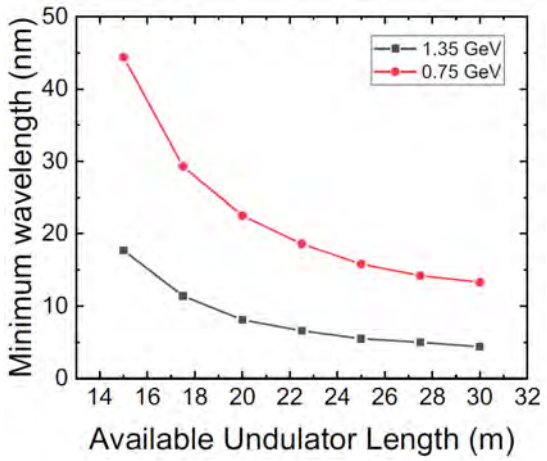

Figure 4.4: *Minimum wavelength that can be achieved as function of the undulator magnetic length.*

4.1.2 Influence of Alignment of Components and Electron Beam

The results of the simulations are shown for nominal parameters. But even for these parameters, the output can vary due to beam jitter or mismatch and due to misalignment of the quadrupoles or non-zero field integrals of the undulator. Furthermore, phase shifter errors can reduce the performance. All this can result in a reduction in pulse energy and an increased minimum wavelength. Simulations in the past have shown that phase shifter and undulator field integrals can be produced such that they hardly influence the FEL performance, at least at the fundamental wavelength. Harmonic lasing will tighten the tolerances, but it still seems likely that they will not dominate the performance.

Here, we only consider the following effects:

- Quadrupole (mis-)alignment
- Orbit jitter
- Beam mismatch

Results in Figure 4.5 show the effect of random errors in quadrupole offsets for the most critical case, which is at 1.35 GeV and K=0.6, which is the minimum K at which saturation can be reached within the given undulator length. The gain length is calculated by taking two points along the undulator (in this case 5 m and 25 m) between startup and saturation in the so-called exponential regime. As can be seen, a quadrupole offset of up to 10 µm in x- and y-plane results in a gain reduction of up to 10 % (inset in Figure 4.5).

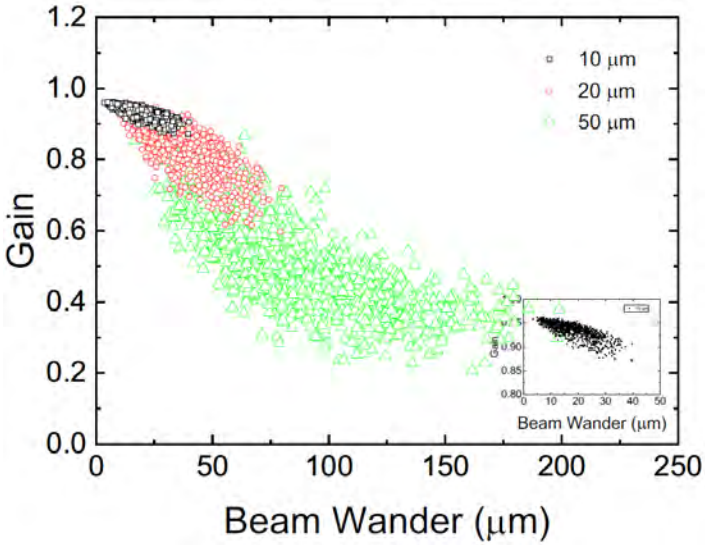

Figure 4.5: *Influence of quadrupole offset on the FEL performance. Results show the inverse gain length for 1.35 GeV and K=0.6 with helical undulator settings. Offsets are random in both x- and y-plane for offsets of 10 µm, 20 µm and 50 µm.*

In Figure 4.6, the influence of a different launch condition of the electron beam is shown. As can be seen, an angle of up to 5 µrad is acceptable, however an angle of 10 µrad already results in a reduction in gain of 20 %. Also a mismatch of the beam inside the undulator of 5 gives a gain reduction of 20 %. The mismatch is defined in the usual way, given in the equation below, where α, β and γ are the Twiss-parameters and "m" stands for the value of a matched beam. This is a rather large mismatch factor, but in practice, this probably means that the quadrupole focusing needs to be adjusted depending on the gap of the undulator.

$$M = \left(\frac{\beta_m \gamma + \gamma_m \beta - 2\alpha_m \alpha}{2} + \frac{\sqrt{(\beta_m \gamma + \gamma_m \beta - 2\alpha_m \alpha)^2 - 4}}{2} \right)^{1/2} - 1$$

It cannot be excluded that due to CSR, microbunching instability and wakefields, the beam quality along the machine will deteriorate more than the expactations based on simulations presented in Chapter 3. Therefore, a number of tolerance studies have been performed looking at peak current, energy spread and emittance. Especially the emittance has a significant influence on what the minimum wavelength is that can be reached. However, this is mainly important for the harmonics or for the advanced concepts in FLASH2, which aims at wavelengths down to 1 nm. It is of far less importance to the design goal of 4 nm and therefore is not discussed here.

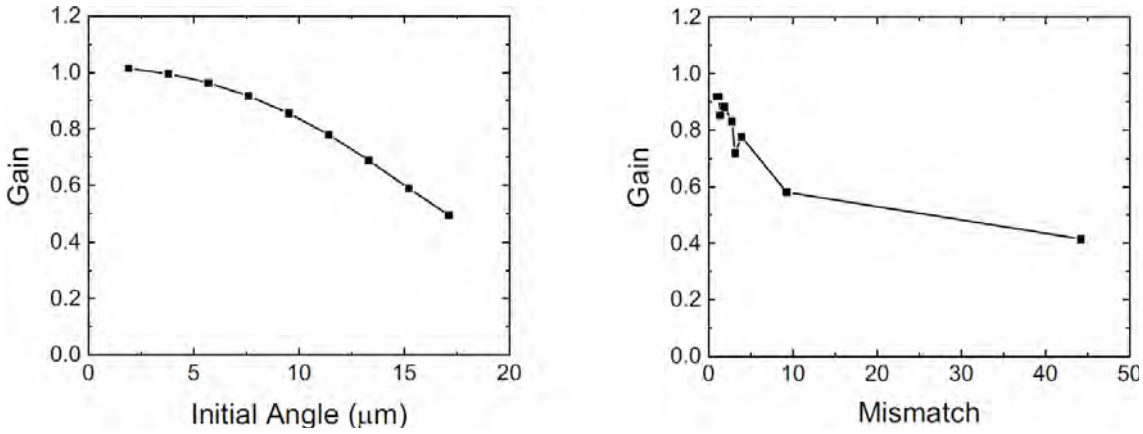

Figure 4.6: *Effect of initial angle (left) and optics mismatch, given by the mismatch parameter M (right) on the FEL performance. Simulations have been performed for 1.35 GeV and the most critical angle, which is in the vertical plane.*

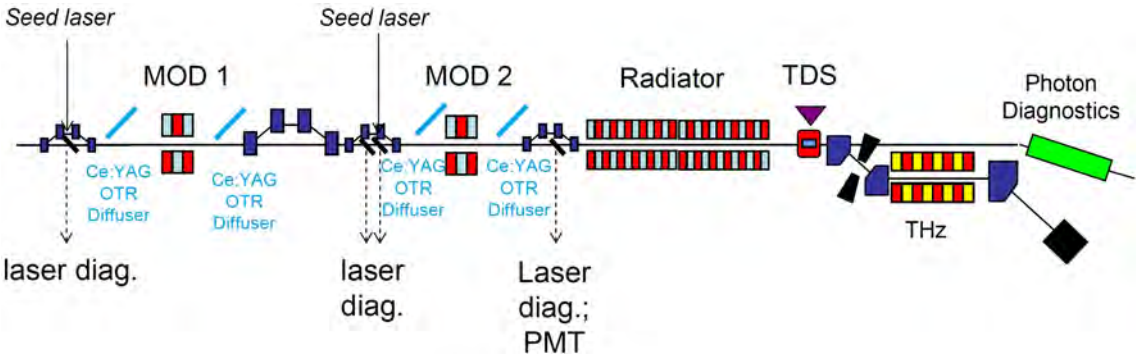

Figure 4.7: *Schematic layout of a seeding section implementing EEHG seeding. From the first modulator on, the quadrupoles (not shown) need to be on quadrupole movers for kick-free operation.*

4.2 Seeding Concept for FLASH1

4.2.1 Seeding of FELs

For externally seeded operation of the FLASH1 undulator beamline in the wavelength range 60 nm to 4 nm we envision a combination of the seeding techniques "high-gain harmonic generation" (HGHG, at the long-wavelength end of the tuning range) (Yu 1991) and "echo-enabled harmonic generation" (EEHG, at wavelengths beyond approx. the 10th harmonic) (Stupakov 2009). HGHG seeding is being applied at the FEL user facility FERMI in user operation since 2012. For HGHG-seeded operation beyond the limitations of single-stage HGHG, which works up to approx. the 15th harmonic, HGHG can be operated as a cascade in which the second HGHG stage is being seeded by radiation emitted from the first stage (Allaria et al. 2013). The advanced scheme EEHG allows reaching the needed high harmonics in a single up-conversion step. In addition to its favorable bunching efficiency at high harmonics, EEHG seeding is expected to mitigate the impact of electron beam imperfections on the properties of the seeded FEL radiation (Hemsing et al. 2014; Hemsing 2018), therefore holding the promise to generate seeded FEL radiation of improved spectral purity. EEHG-seeded FEL operation at 350 nm (3rd harmonic) was demonstrated for the first time at SINAP (Zhao et al. 2012). Currently, FERMI is exploring EEHG seeding at their short-wavelength "FEL-2" beamline and emission of seeded radiation was demonstrated at wavelengths shorter than 10 nm.

4.2.2 Layout of Seeding Section

Figure 4.7 shows the schematic layout of the seeding section. Two independently controllable seed laser pulses are brought into interaction with the electron bunch in two so-called modulators, i. e. variable-gap undulators that are tuned to resonance with the seed radiation. For EEHG seeding, a chicane at the exit of each modulator is required. The chicane at the exit of the first modulator is used to redistribute the longitudinal phase-space distribution of the incoming beam into thin filaments in the longitudinal phase space. The chicane after the second modulator then generates the final longitudinal phase-space distribution optimized for the harmonic of interest. This preconditioned electron beam is then injected into the variable-gap radiator, which is described in Section 4.1.

Reproducible control over the laser-electron interaction is critical for the successful implementation of any seeding scheme. The spatial laser-electron overlap in the two modulators is established using dedicated screen stations installed directly at the entrance and exit of the modulators. Cerium-doped YAG (Ce:YAG) screens will be installed for this purpose. The temporal overlap is established using the established two-step procedure employed at the seeding experiment sFLASH. Initially, the time difference between the electron bunches and the seed laser pulses is reduced down to a few hundred picoseconds. This coarse time is measured by a photomultiplier tube and an oscilloscope. Finally, the precise laser timing is determined by electronically scanning the

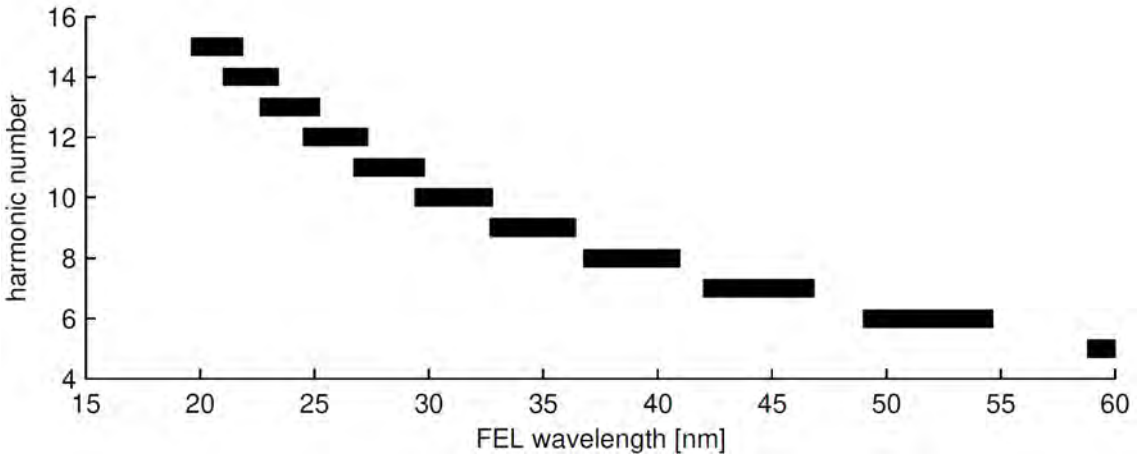

Figure 4.8: *Tunability of the seeded FEL for the seed laser wavelength tuning range 294 nm to 328 nm. For wavelengths shorter than 36.4 nm, continuous, gap-free tunability is achieved.*

laser timing while looking for the signature of the laser-electron interaction in the longitudinal phase-space distribution mapped out by the transverse-deflecting structure (TDS). In addition, by using the TDS, information about the laser-generated modulation amplitude can be obtained. In order to diagnose and optimize the bunching generated by the seeding process, seeded radiation emitted from a single radiator module in the coherent harmonic generation (CHG) process can be used. Dedicated laser diagnostics is planned for the laser pulses arriving via the two seed laser transport lines and for the seed laser pulses extracted from the beamline downstream of the modulators (see also Chapter 6). Wavelength tuning of the seeded FEL radiation will be realized by simultaneously changing the wavelength of the seed laser radiation and re-tuning the accelerator components (modulators, chicanes, radiator modules). The choice of the seed source (see Table 6.1 for a list of potential seed source options) determines the gap-free tuning range. For instance, for the seed source with a tuning range from 294 nm to 328 nm, continuous tuning can be achieved for harmonics $h \geq 9$, i. e. wavelengths shorter than 36.4 nm (see Figure 4.8). On the other hand, for a seed laser tuning range from 300 nm to 230 nm, gap-free tuning of the FEL wavelength would be possible over the entire FEL wavelength range starting at 60 nm.

4.2.3 Simulations

Numerical simulations were performed to study the expected performance of the seeded FEL at the selected operating points listed in Table 4.3. To capture the complex manipulations of the longitudinal phase-space distribution during the process of EEHG seeding, the most recent version 4 of the FEL simulation code “GENESIS 1.3” was used, which is still under active development (Reiche 2019).

As the harmonic up-conversion factor increases, the signal-to-noise ratio of the seeded FEL with respect to SASE start-up deteriorates (Saldin et al. 2002b). Most attractive for the realization of seeded FEL operation at 10 nm or even 4 nm are therefore seeds in the visible or ultraviolet wavelength regions. For a given target FEL wavelength and laser-induced energy modulation amplitudes, the required dispersive strength of the first chicane scales with the seed laser wavelength λ_1 like $R_{56,1} \propto \lambda_1^2$. Moreover, since longer seed laser wavelengths would require higher harmonic up-conversion factors, the operating tolerances of the seeding process (energy modulation amplitudes and control of the chicanes) become more demanding. For these reasons, we focused our simulation studies on ultraviolet seed wavelengths. We studied the EEHG-seeded configurations for target FEL wavelengths of 10 nm and 4 nm. We note that in the 4 nm case, laser-induced energy modulations with an amplitude of 750 keV (both in the first and the second modulator) are exceeding the energy spread tolerances of the FEL amplification process. To mitigate this issue, the first

	60 nm HGHG		10 nm EEHG		4 nm EEHG	
Harmonic Number	5		30		75	
Electron Beam						
Energy / MeV	750		1350		1350	
Energy Spread / keV	150		150		150	
Peak Current / A	500		500		500	
RMS Bunch Length / fs	133		133		133	
Normalized Emittance / mm mrad	0.6		0.6		0.6	
Chicane 1: long. Dispersion / mm	0		3.10		7.04	
Chicane 2: long. Dispersion / µm	47.6		86		81	
Seed Laser						
Wavelength / nm	300		300		300	
Peak Power / MW	0	53	24.5	61.0	25.7	68.0
Waist Size µm	0	763	763	763	763	763
FWHM Pulse Duration / fs	0	50.0	50.0	50.0	50.0	50.0
Peak Laser Modulation Amplitude / keV	0	756	462	748	462	764
Modulators						
Period Length / mm	82.6		82.6		82.6	
Number of Periods	30		30		30	
K-value	5.48		9.97		9.97	

Table 4.3: *Key parameters of the simulated working points. All laser powers are at the interaction points in the respective modulators.*

modulation amplitude was reduced to about 450 keV, which drives up the required dispersive strength of the first chicane. For the long-wavelength end of the wavelength range (60 nm, with an electron beam energy of 750 MeV), we propose the implementation of HGHG seeding. Figure 4.9 illustrates the power profile and spectrum of a 60 nm FEL pulse seeded using a laser pulse with a wavelength of 300 nm. In this simulation result, the peak power of the seeded FEL pulse is approximately 0.6 GW. The remaining radiator is inactive in order to preserve the quality of the seeded FEL pulse. The implementation of pure EEHG seeding in this wavelength range would require the generation of additional energy spread in the laser heater to suppress the HGHG bunching mechanism. Further dedicated studies will be needed to investigate the optimal wavelength or harmonic for the transition from HGHG to EEHG seeding, especially taking into account potential operation of the radiator in a frequency doubling scheme. At short wavelengths beyond the harmonic up-conversion capabilities of HGHG seeding, EEHG seeding is required.

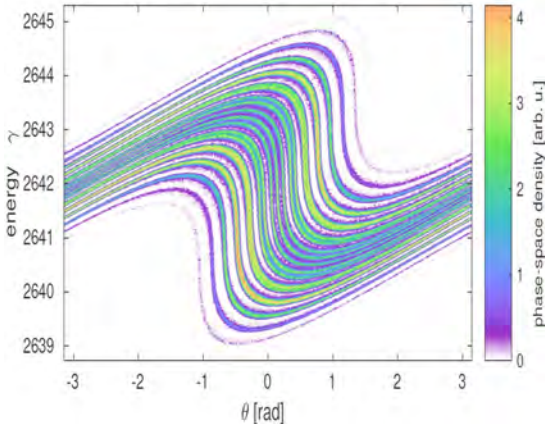

Figure 4.10: *One slice from the final longitudinal phase-space distribution at the entrance of the radiator (10 nm, UV-based EEHG seeding). For this illustration, one slice of the longitudinal phase-space distribution was dumped from the GENESIS simulation.*

The EEHG operating points studied in simulations were prepared by studying the analytical expressions for the EEHG bunching factor (Xiang et al. 2009) in the multi-dimensional configuration space spanned by the peak modulation amplitudes and the longitudinal dispersive strength of the two chicanes. For the peak en-

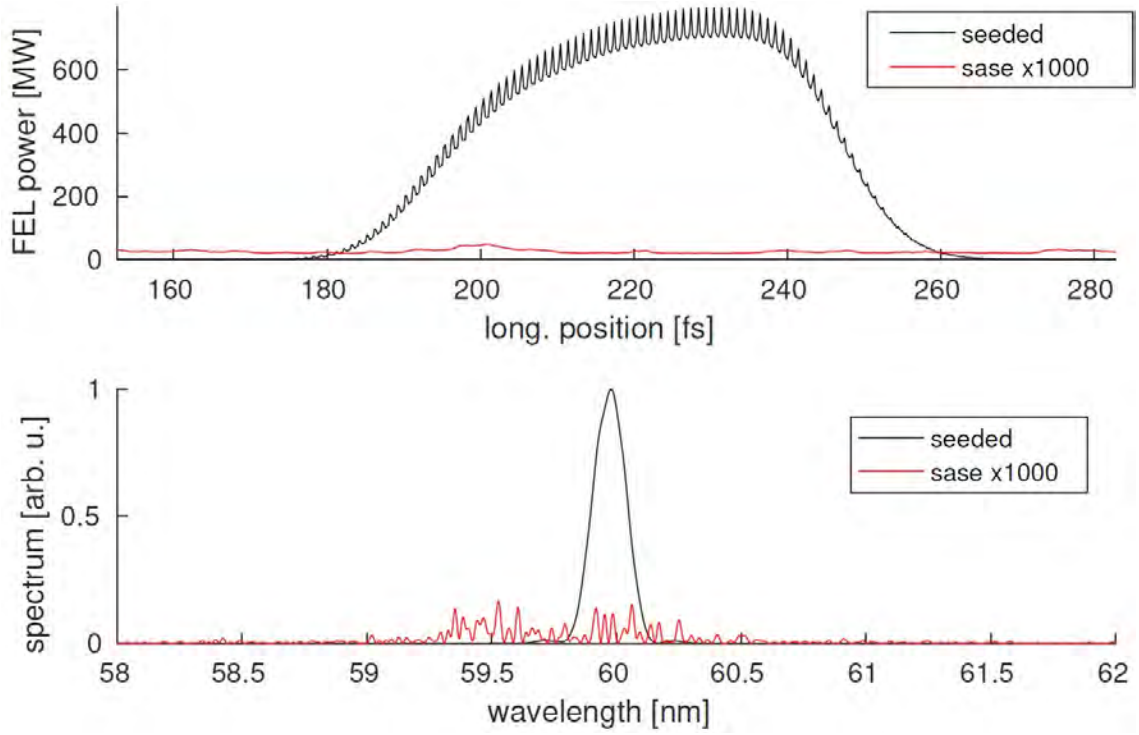

Figure 4.9: *Power profile and spectrum of the HGHG-seeded FEL pulse (wavelength 60 nm) after 4 m of radiator beamline (total undulator length traveled 3.14 m).*

ergy modulation amplitudes generated by the two seed laser pulses, a combination of chicane strengths ($R_{56,1}$,$R_{56,2}$) maximizing the bunching factor for the harmonic of interest was selected. Finally, the seeded FEL performance was optimized with numerical FEL simulations by variation of the longitudinal dispersion of the second chicane.

In the following, the simulation of FEL operation at 10 nm wavelength initiated by EEHG seeding with 300 nm seed pulses is discussed. Figure 4.10 shows the final phase-space distribution at the entrance of the radiator resulting from the aforementioned optimization procedure. In Figure 4.11 the power profile and the spectrum of the seeded FEL pulse after 3 modules of the variable-gap radiator are shown. At this point in the radiator, the power contrast between seeded FEL and SASE FEL exceeds three orders of magnitude. If further radiator modules are active and the gain process is allowed to continue, a superradiant spike develops at the head of the light pulse. Moreover, as the power growth of the SASE still continues, the contrast between SASE and seeded FEL radiation will degrade (Figure 4.13). Figure 4.14 and Figure 4.15 show the simulated FEL power profile, spectrum and gain curve for seeded operation at 4 nm.

4.2.4 Tolerance Considerations

Simulations shown in the previous section were done assuming a Gaussian electron beam and seed laser pulse profile. In reality, all kinds of imperfections play a role, for instance:

- non-Gaussian beams
- jitter of the seed laser and electron beam in position and intensity
- variation or deviation of the R56 of the chicanes, or
- deviations of the laser-generated energy modulation amplitudes from the theoretical optimum.

For more realistic parameters of electron beam and seed laser, start-to-end simulations have been started. Relative laser-electron jitter should not have a big influence, since the transverse profile of the seed laser is almost an order of magnitude larger than that of the electron beam and the region in the electron bunch, supporting FEL lasing, is sufficiently long. Deviations in chicane settings and energy modulation amplitudes will decrease the signal-to-noise ratio, degrading the performance of the seeded FEL.

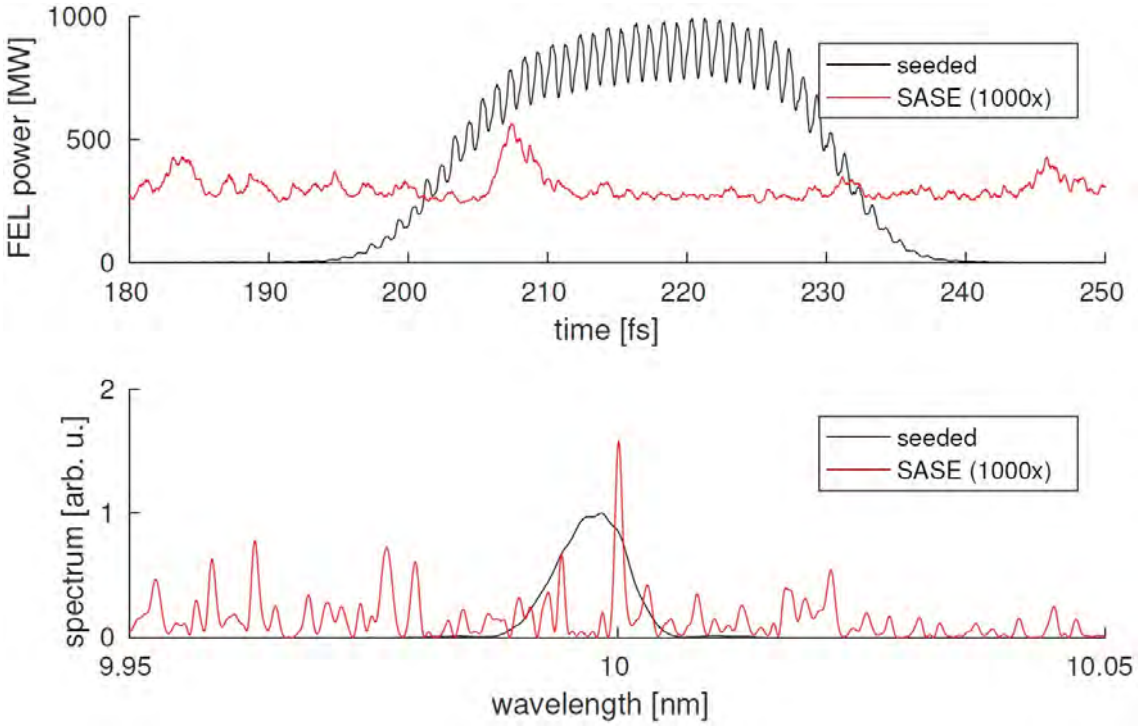

Figure 4.11: *Power profile and spectrum of the EEHG-seeded FEL pulse after 3 modules of the radiator. Also indicated is SASE operation, i. e. with both seed lasers off (note that the SASE power profile was multiplied by 1000 in this figure). Simulation conducted with GENESIS 1.3, version 4.*

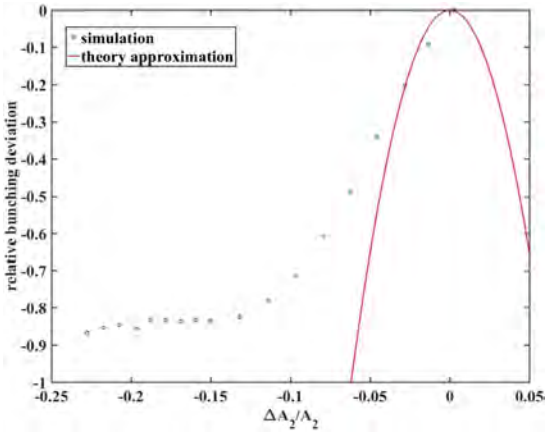

Figure 4.12: *Decrease of bunching at 4 nm versus deviation from the nominal modulation amplitude in the second modulator ($^{\Delta A_2}/_{A_2} = 0$ corresponds to the optimal energy modulation of $A_2 = 5$). Theoretical, approximate curve according to Hemsing et al. 2017.*

For illustration, in Figure 4.12, the impact of a deviation from the ideal amplitude of the second energy modulation

$$A_2(z) = \frac{\Delta\gamma_2(z)}{\sigma_\gamma}$$

(here, normalized to the uncorrelated energy spread σ_γ) is shown for seeded FEL operation at 4 nm. For the parameters studied above, the optimal value for bunching generation at the desired harmonic is approximately $A_2 = 5$ (corresponding to $^{\Delta A_2}/_{A_2} = 0$).

On the other hand, for instance, a slight deviation in modulator settings will have only a small influence, since it has a relatively large bandwidth.

4.2.5 Summary and Outlook

At the studied FEL wavelength of 10 nm, even for conservative beam parameters (500 A current, 1.0 mm mrad normalized emittance, 150 keV slice energy spread), saturation is reached well before the end of the radiator. For this case, the power contrast between seeded operation and SASE operation after 4 radiator modules exceeds 3 orders of magnitude.

The remaining variable-gap undulator modules are fully open to preserve the contrast between seeded signal and SASE.

Only in the 4 nm case, a smaller emittance and/or higher peak current are critical for FEL saturation within the available radiator length,

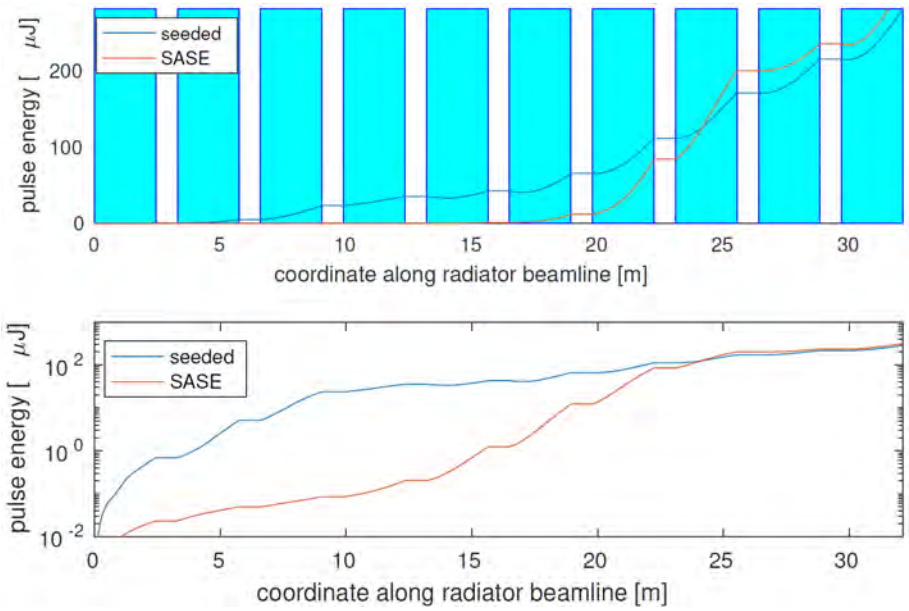

Figure 4.13: *Gain curve of the seeded FEL (simulation for 10 nm FEL wavelength). In the upper panel, the aqua boxes indicate the undulator modules.*

as also predicted by estimations using the Ming-Xie formalism. For the simulations discussed in this chapter, idealized electron bunches were used. The performance of the seeded FEL driven by phase-space distributions obtained from start-to-end simulations still needs to be assessed. Parameter tolerances will be studied in simulations of the seeded FEL at the shortest wavelengths for which the expected tolerances are most critical.

Also, further studies are required on operation schemes of the radiator system, such as transporting the seeded beam along open radiator segments, tapering of the radiator, or lasing in frequency doubling schemes. At the electron beam energy of 1350 MeV the longest achievable FEL wavelength is 18 nm, making EEHG seeding the prime seeding technique for operation at this high-energy operating point. For operation at 750 MeV electron beam energy, one could apply HGHG seeding in combination with frequency doubling (to extend the wavelength range to the long-wavelength limit applicable for 1350 MeV operation). Alternatively, one could start with a shorter seed wavelength or slightly increase the radiator undulator period to increase the maximum wavelength at high energy. Further studies are underway to investigate options which would avoid switching between HGHG and EEHG seeding while running at 750 MeV electron beam energy.

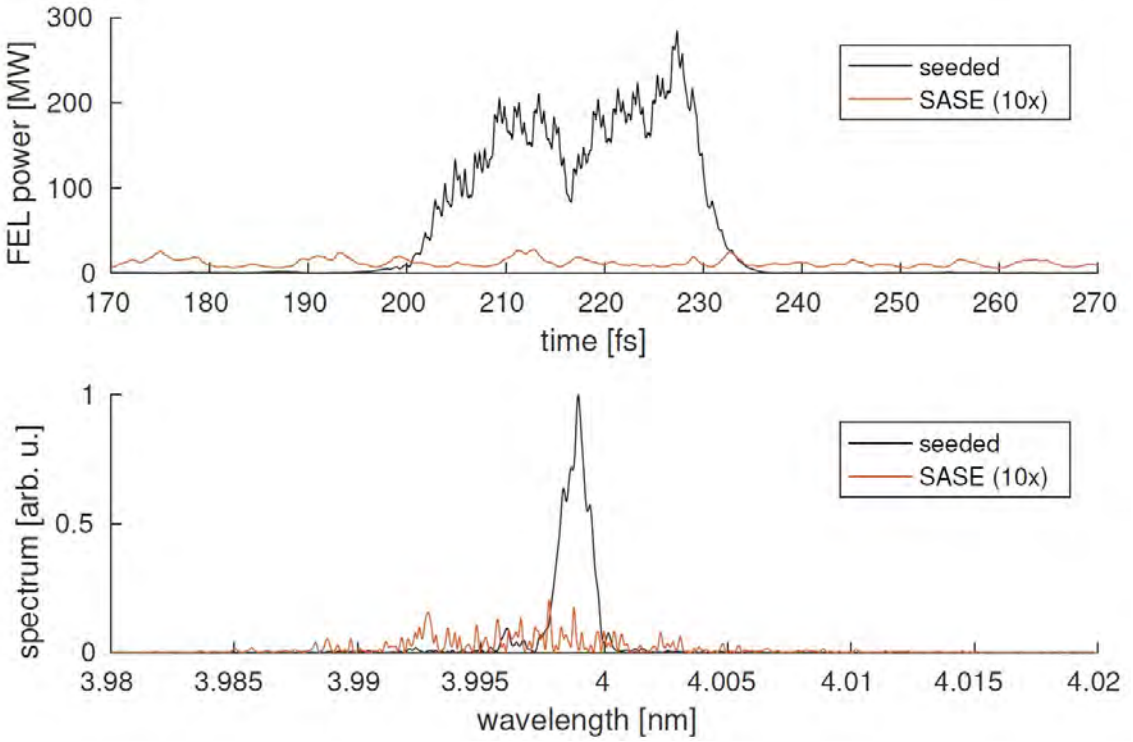

Figure 4.14: *Power profile and spectrum of the EEHG-seeded FEL pulse at 4 nm after 7 modules of the radiator. Also indicated is SASE operation, i. e. with both seed lasers off (note that the SASE power profile was multiplied by 10 in this figure). Simulation conducted with GENESIS 1.3, version 4.*

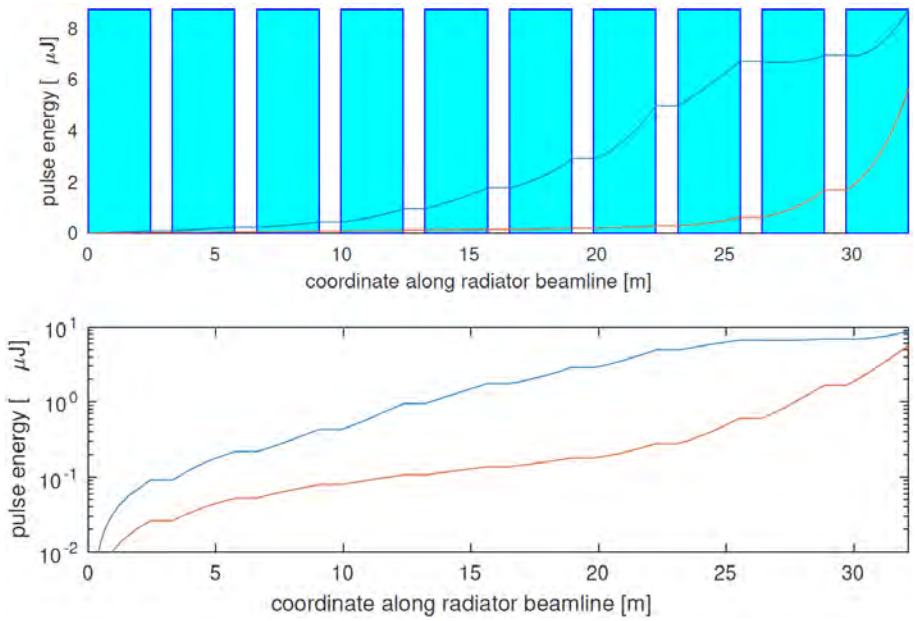

Figure 4.15: *Gain curve of the seeded FEL (simulation for 4 nm FEL wavelength). In the upper panel, the aqua boxes indicate the undulator modules.*

Seeding References

Allaria, E. et al. (2013). „Two-stage seeded soft-X-ray free-electron laser“. In: *Nature Photonics* 7.11, pp. 913–918. DOI: 10.1038/nphoton.2013.277.

Hemsing, E. (2018). „Bunching phase and constraints on echo enabled harmonic generation“. In: *Phys. Rev. Accel. Beams* 21 (5), p. 050702. DOI: 10.1103/PhysRevAccelBeams.21.050702.

Hemsing, E. et al. (2014). „Highly coherent vacuum ultraviolet radiation at the 15th harmonic with echo-enabled harmonic generation technique“. In: *Phys. Rev. ST Accel. Beams* 17 (7), p. 070702. DOI: 10.1103/PhysRevSTAB.17.070702.

Hemsing, E. et al. (2017). „Sensitivity of echo enabled harmonic generation to sinusoidal electron beam energy structure“. In: *Phys. Rev. Accel. Beams* 20 (6), p. 060702. DOI: 10.1103/PhysRevAccelBeams.20.060702.

Reiche, S. (2019). „GENESIS4 source code repository“. In: *Webpage*. Online.

Saldin, E. L. et al. (2002b). „Study of a noise degradation of amplification process in a multistage HGHG FEL“. In: *Optics Communications* 202.1, pp. 169–187. DOI: 10.1016/S0030-4018(02)01091-X.

Stupakov, G. (2009). „Using the Beam-Echo Effect for Generation of Short-Wavelength Radiation“. In: *Phys. Rev. Lett.* 102 (7), p. 074801. DOI: 10.1103/PhysRevLett.102.074801.

Xiang, D. et al. (2009). „Echo-enabled harmonic generation free electron laser“. In: *Phys. Rev. ST Accel. Beams* 12 (3), p. 030702. DOI: 10.1103/PhysRevSTAB.12.030702.

Yu, L. H. (1991). „Generation of intense uv radiation by subharmonically seeded single-pass free-electron lasers“. In: *Phys. Rev. A* 44 (8), pp. 5178–5193. DOI: 10.1103/PhysRevA.44.5178.

Zhao, Z. T. et al. (2012). „First lasing of an echo-enabled harmonic generation free-electron laser“. In: *Nature Photonics* 6.6, pp. 360–363. DOI: 10.1038/nphoton.2012.105.

4.3 THz Sources for the THz-XUV Pump-Probe Facility

In the past decade, THz-XUV pump-probe as well as a limited number of "THz-only" experiments employing the THz undulator at FLASH1 have proven to be a unique addition to the FLASH1 portfolio. Within the FLASH2020+ upgrade, we plan to expand and improve the opportunities for users in this wavelength range. In this section new developments on the THz sources are presented, while the description of a new THz-XUV pump-probe endstation is found in Section 7.1.5, and THz diagnostics are introduced in Section 8.5. The new concept of a limited number of fixed operating points of the FLASH accelerator ranging from 0.75 GeV to 1.35 GeV have implications on the longest wavelength which can be reached by the existing THz undulators. At the highest accelerator energies, it will be limited to ≈30 µm (corresponding to 10 THz). This wavelength is not sufficient to reach most of the excitation modes in the THz spectral range (3 THz to 100 THz) that are of interest for the user community at FLASH (for example soft modes in perovskites, optical phonon modes in dielectrics, or stretching, vibrational or rotational modes in molecules).

Therefore, we propose the development and installation of a new THz undulator source with a novel tuning concept (Vagin et al. 2018) that will make this range fully accessible. In addition, it will enable important new features: variable polarization and pulse synthesis on demand. A maximum length of the magnetic period of 60 cm will allow to reach wavelengths of ≈100 µm (corresponding to 3 THz) even at a 1.35 GeV working point as shown in Figure 4.16. Within the 6 m space available in the FLASH2020+ concept for the machine section containing the THz undulator, it would be possible to include an undulator which produces pulses with a relative spectral bandwidth of about 10 %. To complement the new source, the THz beam transport will be optimized: transmission at longer wavelengths will be improved by increasing the smallest angular acceptance and at shorter wavelengths by utilizing transport with full beam aperture (at FLASH1 the XUV/THz beam separation is performed using a THz mirror with an aperture for the XUV beam). To complement the narrowband tunable THz pulses generated by the THz undulator, we will install a coherent transition radiation (CTR) screen in front of the electron beam dump magnet. This compact device will expand the FLASH spectral range into low THz frequencies (0.3 THz to 3 THz) and enhance the available single-cycle broadband source (edge radiation from the dump magnet) pulse energies by a factor of 10-100. This upgrade will be of high interest to THz field control in solids (e. g. to control of magnetism, where ≈1 T field transients are estimated as needed driving force). CTR screen sources have been used (Hoffmann et al. 2011; Daranciang et al. 2011; Di Mitri et al. 2018)

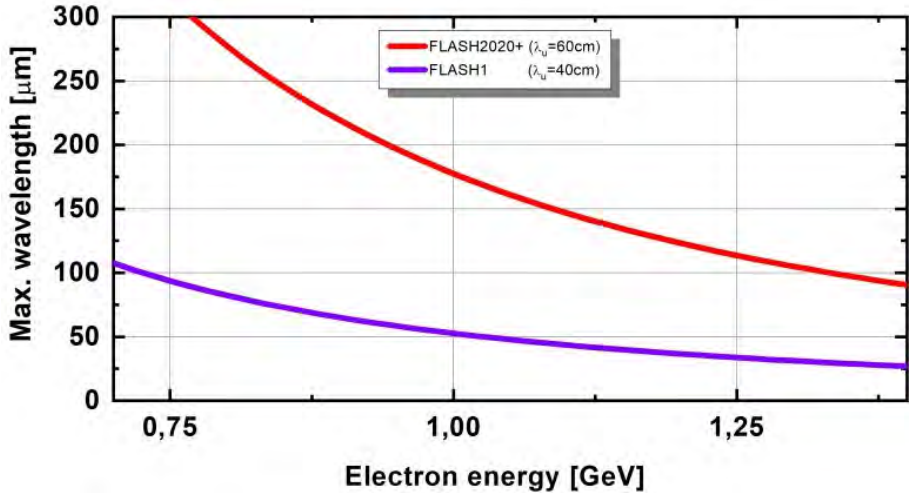

Figure 4.16: *Maximum wavelength that can be reached with the THz undulator at FLASH1 (40 cm period) now and with a proposed FLASH2020+ upgrade to a 60 cm period.*

to generate ultra-broadband single-cycle THz pulses, with energies approaching 1 mJ range at FLASH and other facilities (LCLS, FERMI). The THz sources (undulator and CTR screen) will be installed in the electron beamline parallel to the XUV photon diagnostics section (see Figure 4.17). This will separate the optical transport beamlines from the source point for XUV and THz and will allow completely parasitic operation of "THz-only" experiments from the XUV FEL operation. Therefore, possibilities for new "THz-only" users will open up with unique THz pulses from FLASH in addition to the options for THz-XUV pump-probe experiments described in the next section.

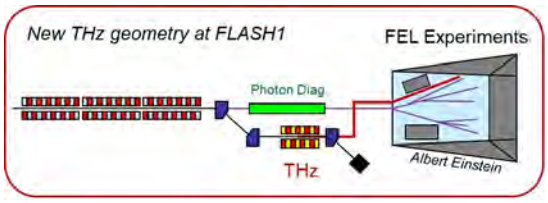

Figure 4.17: *New scheme for the THz section at FLASH2020+.*

4.3.1 THz Doubler at FLASH: Double Pulses for More Flexible Pump-Probe Experiments

In the so called "THz doubler" scheme (Zapolnova et al. 2018), two electron bunches are fed into the accelerator, separated by 21.5 ns. With this scheme, we are tackling the issue that the optical path of the THz is about 7 m (21.5 ns) longer than the XUV beamline. The current solution to "artificially delay" the XUV pulse via a back-reflecting multilayer (ML) mirror with a focal length of ≈3.5 m has a number of drawbacks, such as limited quality and size of the achievable FEL focus and minimal wavelength tunability for the XUV.

The THz doubler scheme is sketched in Figure 4.18. In order to optimize conditions for a typical THz pump - XUV probe experiment, we aim at suppressing XUV lasing of the 1st bunch to 1 % or less of that of the 2nd by appropriate machine settings. Up to now this goal is reached for about 50 % of the pulses and studies to improve this further are ongoing. Despite the fact that this approach now uses two separate pulses for the THz and XUV generation, the relative timing of the two pulses is still very stable. Synchronization of the THz-doubler radiation pulses is measured to be better than 20 fs (rms), and a solution for monitoring arrival times to achieve an even higher temporal resolution has been developed (Zapolnova et al. 2018; Pan et al. 2019). THz pulse energies produced with the doubler concept are currently in the 10 µJ range. In collaboration with partners from the European XFEL, we are developing procedures for FEL optimization (electron bunch charge, compression and chirp) to maximize THz pulse energies for the THz doubler scheme. We foresee to reach similar numbers as in single bunch operation (>100 µJ). Since exploiting the full potential of this scheme also requires precise intensity monitoring of the nanosecond-spaced XUV pulses, the concept will benefit from the upgrade of the gas monitor detectors (GMDs) at FLASH1 to new, faster electronics hardware with a bandwidth of up to 1 GHz (Section 8.1). This will enable pulse energy monitoring of both XUV pulses for post-mortem sorting of the data. In summary, the THz doubler scheme is meanwhile almost mature and will soon be suited to replace the ML mirror approach at the experimental end-station. This will allow implementation of a significantly better and ultimately flexible focusing scheme at the THz-XUV pump-probe beamline as presented in Section 7.1.5. In addition, wavelength limitations of the ML mirror are eliminated, thus wavelength changes on demand (e. g. for scans across a resonance) are no longer hindered. Hence, one can fully profit from the tunable-gap XUV undulators which are in preparation for FLASH1.

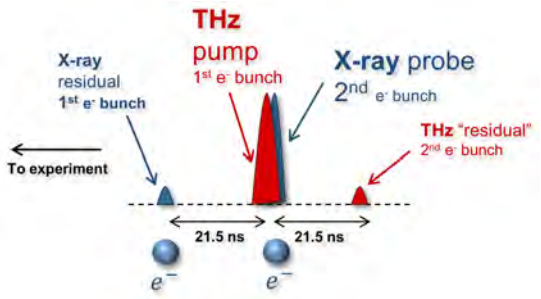

Figure 4.18: *THz doubler scheme: two bunches generate an XUV and THz pulse each. THz from the 1st bunch and XUV from the 2nd bunch are temporally overlapped in the pump-probe experiment (Zapolnova et al. 2018).*

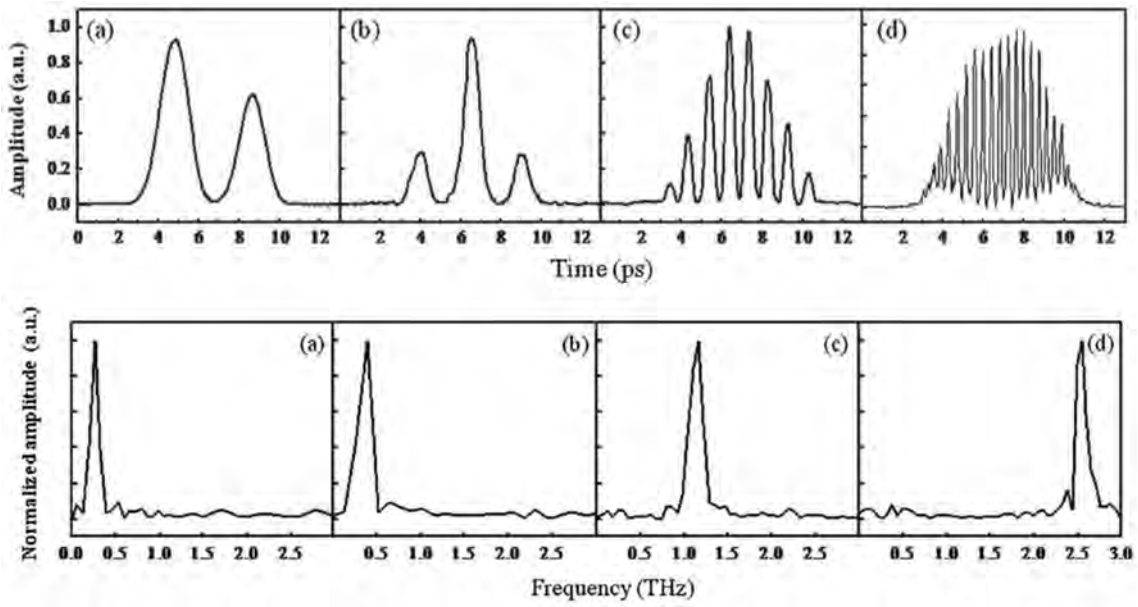

Figure 4.19: *Upper row: Electron density distribution for a temporally modulated electron bunches produced by two delayed laser pulses on the FEL photocathode. Lower row: Spectra of the THz pulses generated by modulated electron bunches irradiating CTR screen. The spectra of THz radiation for time delays (a) 0.4 ps, (b) 0.7 ps, (c) 1.8 ps and (d) 3.6 ps. Reproduced with permission from (Shen et al. 2011). © 2011 by American Physical Society.*

4.3.2 Femtosecond THz-Doubler for Enhanced THz Pulse Energies

The multiple electron bunch scheme will be further utilized to enhance the THz output at FLASH1 following the FLASH2020+ upgrades. This is particularly important for seeded FEL operation that relies on lower peak currents (≈500 A) and a smooth electron bunch, which on its own will generate little to no coherent THz output in the FLASH THz tuning range (3 THz to 30 THz).

In a first step, a double electron bunch will be generated using infrastructure at the FLASH electron gun, that was developed for the FLASH-FORWARD project. The spacing between two short electron bunches will be controlled from 0.1 ps to 10 ps and thus enable coherent enhancement of two closely spaced THz pulses. Once the operating conditions for transport and lasing of such a double electron bunch are established, the concept will be further enhanced towards the generation and lasing of modulated electron bunches (see Figure 4.19). Modulated electron bunches will be produced by two laser pulses interfering on the FEL photocathode (Shen et al. 2011) producing a temporally modulated laser intensity. By careful adjustment of the delay between the laser pulses, multiple electron bunches can be produced with variable spacing that can be chosen to coherently enhance the THz output at the resonant frequency given by the undulator. Utilizing this scheme, the complete electron bunch can be made to coherently contribute to the super-radiant THz pulse generation and we expect THz pulse energies exceeding the 1 mJ level, across the undulator tuning range, which accompanied by improved beamline transport will lead to a pulse energy enhancement by more than one order of magnitude.

THz References

Daranciang, D. et al. (2011). „Single-cycle terahertz pulses with >0.2 V/Åfield amplitudes via coherent transition radiation“. In: *Applied Physics Letters* 99.14, p. 141117. DOI: 10.1063/1.3646399.

Di Mitri, S. et al. (2018). „Coherent THz Emission Enhanced by Coherent Synchrotron Radiation Wakefield“. In: *Scientific Reports* 8.1, p. 11661. DOI: 10.1038/s41598-018-30125-1.

Hoffmann, M. C. et al. (2011). „Coherent single-cycle pulses with MV/cm field strengths from a relativistic transition radiation light source“. In: *Opt. Lett.* 36.23, pp. 4473–4475. DOI: 10.1364/OL.36.004473.

Pan, R. et al. (2019). „Photon diagnostics at the FLASH THz beamline“. In: *Journal of Synchrotron Radiation* 26.3, pp. 700–707. DOI: 10.1107/S1600577519003412.

Shen, Y. et al. (2011). „Tunable Few-Cycle and Multicycle Coherent Terahertz Radiation from Relativistic Electrons“. In: *Phys. Rev. Lett.* 107 (20), p. 204801. DOI: 10.1103/PhysRevLett.107.204801.

Vagin, P. et al. (2018). „Variable Period Undulator with Tunable Polarization“. In: *Synchrotron Radiation News* 31.3, pp. 48–52. DOI: 10.1080/08940886.2018.1460178.

Zapolnova, E. et al. (2018). „THz pulse doubler at FLASH: double pulses for pump–probe experiments at X-ray FELs“. In: *Journal of Synchrotron Radiation* 25.1, pp. 39–43. DOI: 10.1107/S1600577517015442.

5 FLASH2 FEL Line

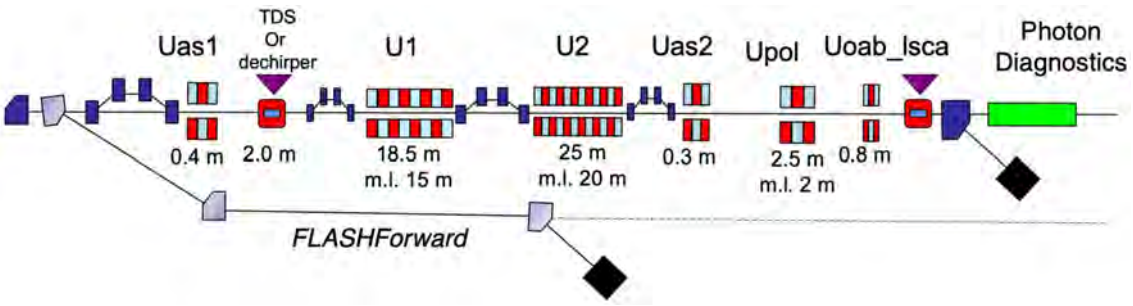

Figure 5.1: *(top) Proposed layout of the FLASH2 FEL line. Abbreviations stand for: U1 and U2 for the main undulators (U1: period 3.5 cm, K_{rms}=2.55; U2: period 2.6 cm, K_{rms}=1.5), TDS for transverse deflecting structure, Uas1and Uas2 for the undulators of the attosecond option, Upol for an afterburner with variable polarization, Uaob_Isca for the optical afterburner undulator.*

5.1 Proposed Layout

The two main goals of the FLASH2 upgrade are:

• to extend the photon energy range with the aim to reach the oxygen K-edge (540 eV) on the fundamental, and 1 keV with the help of advanced lasing schemes (like harmonic lasing)

• to provide a variety of advanced options for user experiments: polarization control, flexible two-color mode of operation with extended pump-probe capabilities, few-femtosecond and attosecond options.

In order to reach these goals, the layout of the FLASH2 FEL line (Figure 5.1) is proposed as follows: The main undulator consists of two sections U1 and U2 with different undulator periods separated by a delay chicane. The undulators are APPLE-type providing full polarization control. The choice of this technology in combination with two different undulator periods allows for a great flexibility in terms of e. g. wavelength range, operation modes, polarization control, and improvement of longitudinal coherence.

The main FEL modes of the scheme in Figure 5.1 will be (electron beam energies: 1.35 GeV and 0.75 GeV):

Harmonic Lasing: 1 nm to 2 nm

Frequency Doubling or Reverse Taper with Harmonic Afterburner: 1.2 nm to 2.3 nm

HLSS: 2 nm to 6 nm @ 1.35 GeV and 6 nm to 20 nm @ 0.75 GeV

SASE: 2.3 nm to 18.5 nm @ 1.35 GeV and 7 nm to 60 nm @ 0.75 GeV

Two colors (SASE @ 1.35 GeV): 4 nm to 18.5 nm (U1) and 2.3 nm to 6 nm (U2)

Two colors (SASE @ 0.75 GeV): 11 nm to 60 nm (U1) and 7 nm to 20 nm (U2)

The bunch compressor (BC) is expected to improve the electron beam quality as described in Chapter 3. In addition, the vacuum chamber of the bunch compressor accommodates an optical in-coupling system for a laser pulse for the attosecond scheme. All the other elements in Figure 5.1 are explained and discussed below in this chapter, some of them have multiple applications.

5.2 Operation Modes and Advanced Lasing Options

For the calculation of undulator lengths and possible photon energy ranges we use the slice parameters of the electron beam simulated for a bunch charge of 100 pC (see Chapter 3). The nominal electron energy after the refurbishment of the accelerator modules will be 1.35 GeV. To increase the accessible range of photon energies, we also consider 0.75 GeV as a second standard energy. Undulator parameters of U1 and U2 are given in Figure 5.1, the undulator gap is assumed to be 8 mm. We now discuss different operation scenarios of the FLASH2 undulator line.

5.2.1 SASE Mode

Self-Amplified Spontaneous Emission (SASE) is the main operation mode that can be realized either in U1 (for longer wavelengths) or in U2 (for shorter wavelengths) or in both undulators tuned to the same wavelength (for an intermediate range). Due to a combination of undulators with two different periods it becomes possible to provide broad tunability at a fixed electron energy, soanning one order of magnitude (to be compared with a factor of three in the present undulator of FLASH2). As mentioned above, for two fixed electron energies, the tunability range in SASE mode will be from 2.3 nm (oxygen K-edge) to 60 nm.

5.2.2 Harmonic Lasing and HLSS FEL

Harmonic lasing in single-pass high-gain FELs (Murphy et al. 1985; Huang et al. 2000; McNeil et al. 2006; Schneidmiller et al. 2012) is due to the FEL instability at an odd harmonic of the planar undulator developing independently from lasing on the fundamental. Contrary to nonlinear harmonic generation (which is driven by the fundamental in the vicinity of saturation) harmonic lasing can provide much more intense, stable, and narrow-band FEL beams. The most attractive feature of saturated harmonic lasing is that the brilliance of a harmonic is comparable to that of the fundamental. Although known theoretically for a long time (Murphy et al. 1985; Huang et al. 2000; McNeil et al. 2006), harmonic lasing in high-gain FELs was not demonstrated experimentally until the pioneering experiments at FLASH2 in which the so-called Harmonic Lasing Self-Seeded FEL (HLSS FEL) (Schneidmiller et al. 2012; Schneidmiller et al. 2013a) worked in the range 4.5 nm to 15 nm (Schneidmiller et al. 2017).

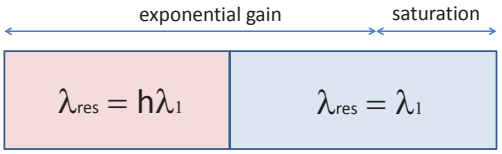

Figure 5.2: *Conceptual scheme of a Harmonic Lasing Self-Seeded FEL (HLSS FEL). (Schneidmiller et al. 2017).*

An undulator is divided into two parts (see Figure 5.2) by setting two different undulator parameters such that the first part is tuned to a sub-harmonic of the second part and the second part is tuned to the wavelength of interest. Harmonic lasing occurs in the exponential gain regime in the first part of the undulator although the fundamental in the first part stays well below saturation. In the second part of the undulator, the fundamental is resonant to the wavelength, previously amplified as the harmonic. The amplification process proceeds in the fundamental up to saturation. In this case the bandwidth is defined by the harmonic lasing (i. e. it is reduced by a significant factor depending on the harmonic number) but the saturation power is still as high as in the reference case of lasing on the fundamental in the whole undulator, i. e. the spectral brightness increases. Application of the post-saturation tapering would allow us to transfer energy from the electron to the photon beam more efficiently than in the case of a standard SASE configuration.

For harmonic lasing operation, undulators U1 and U2 should be tuned to linear polarization mode. Suppression of the fundamental (necessary for harmonic lasing) is achieved by two methods simultaneously: switching between the 3rd and the 5th harmonics (Brinkmann et al. 2014; Penn 2015) and using phase shifters (McNeil et al. 2006; Schneidmiller et al. 2012). One can also use spectral filtering methods by putting, e.g. a filter (suppressing the fundamental but letting the 3rd harmonic go through with

minimal losses) into a delay chicane (see Figure 5.1). Operation between 1 nm and 2 nm for 1.35 GeV will be possible.

In case of HLSS the range would be 2 nm to 6 nm for 1.35 GeV, and 2 nm to 6 nm for 0.75 GeV. In this case U1 can be considered as a "seed" undulator, tuned to linear polarization mode while U2, operating on the fundamental, can provide arbitrary polarization. Bandwidth reduction with respect to the SASE FEL case will depend on the harmonic number in U1. In principle, the bandwidth in HLSS mode can be well below 0.1 % (FWHM) provided that a dechirper is installed and used to minimize the energy chirp in the electron beam.

5.2.3 Reverse Tapering with Harmonic Afterburner

Reverse undulator tapering is a relatively new concept (Schneidmiller et al. 2013b) to be used for polarization control in X-ray FELs. This technique allows to strongly suppress the radiation intensity at the exit of the main (planar) undulator while preserving strong microbunching of the electron beam that produces radiation with a required polarization pattern in a variably polarized afterburner undulator. The concept is routinely used at LCLS (Lutman et al. 2016b) and was successfully tested at FLASH2 (Schneidmiller et al. 2016). Moreover, the afterburner can be tuned to a harmonic of the main undulator as demonstrated at FLASH2 (Schneidmiller et al. 2017).

Polarization control at wavelengths above 2 nm can be achieved by tuning U2 to a desirable polarization mode in SASE or HLSS regimes (in the latter case U1 should be linearly polarized). However, polarization control is especially desired in the range where L-edges of some important magnetic materials are, i. e. typically below 2 nm. In this case U2 (and maybe U1) is tuned to the 2nd or 3rd subharmonic of a desired wavelength. Reverse taper is applied there in order to suppress radiation from this undulator: the fundamental (for any polarization of U2) as well as harmonics (when U2 is in linear polarization mode). However, the fully microbunched electron beam contains strong harmonics in the electron density and can produce powerful radiation in the afterburner Upol, tuned to the resonance with a corresponding (2nd or 3rd) harmonic. The afterburner will be built with the help of the APPLE technology but with a smaller period than U2. It will consist of two sections separated by a phase shifter. Such a configuration is sufficiently flexible and would allow us to produce a desirable polarization pattern.

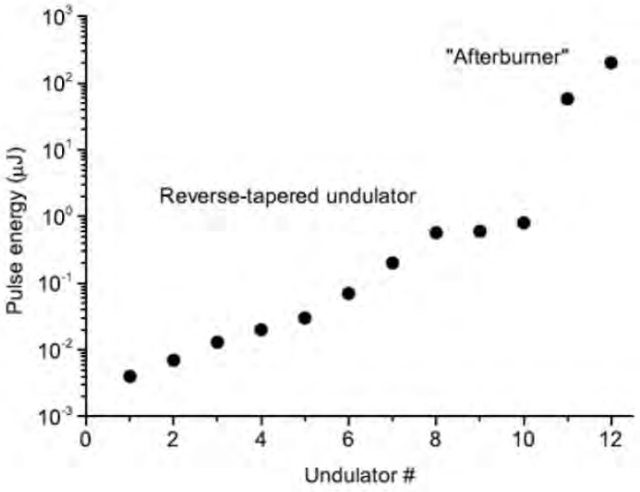

Figure 5.3: *Results from an experiment at FLASH2 where the main part of the undulator was operated in reverse tapering mode while the last two undulators served as afterburner (Schneidmiller et al. 2017).*

5.2.4 Frequency Doubler

The frequency doubler (more generally, frequency multiplier) operates as follows (Bonifacio et al. 1990; Feldhaus et al. 2004). The undulator is divided into two parts. The second part is tuned to twice the frequency of the first part. The amplification process in the first undulator part is stopped at the onset of the nonlinear regime, such that higher harmonic bunching in the electron beam density becomes pronounced, but the radiation level is still too small to significantly disturb the electron beam quality. The modulated electron beam enters the second part of the undulator and generates radiation at the 2nd harmonic. The scheme was tested at LCLS (Nuhn et al. 2010) and at FLASH2 (Kuhlmann et al. 2018). In the latter case the shortest wavelength at FLASH, namely 3.1 nm (this is around the nitrogen K-edge) was achieved (Kuhlmann et al. 2018).

The most efficient use of the frequency doubler assumes the installation of a chicane between two parts of the undulator (or, two different undulators) (Feldhaus et al. 2004). This

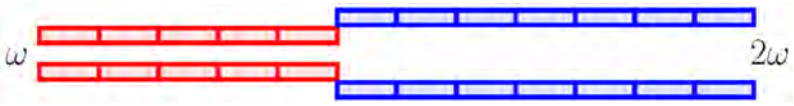

Figure 5.4: *Schematic view of the undulator configuration used when testing the frequency doubler scheme at FLASH2 (Kuhlmann et al. 2018).*

option can be used in the setup shown on Figure 5.1 with the aim to generate an intense soft X-ray beam below 2.3 nm. In this case the undulator U1 is tuned to the second sub-harmonic of the required wavelength, and the energy modulations induced in U1 are converted into density modulations on the second harmonic in the compact chicane behind U2. Then the variably polarized radiation at this harmonic is produced in the afterburner Upol. Thus, the frequency doubler can be an alternative to reverse tapering with the harmonic afterburner. Note, that all considerations of this section can in principle also be applied to the 3rd and higher harmonics, but the scheme becomes less efficient when the harmonic number increases.

5.2.5 Two-color Lasing

Two colors can be produced for different purposes and in different ways. One purpose would be to serve two users at a time. In this case we can employ the principle of a betatron switcher (Brinkmann et al. 2010) kicking some bunches in the pulse train with the help of the extraction kicker. The betatron phase advance can be organized in a way that these bunches oscillate in U1 and do not lase there but after an orbit correction with a static steerer they go straight in U2 and lase to saturation. Non-kicked bunches first go straight in U1 producing SASE there but then they are kicked by the same steerer and do not lase in U2. If the kick is done in a vertical plane, one can organize an orbit kink between the undulators horizontally so that the X-ray beams are spatially separated. Another application of two-color lasing is pump-probe experiments when both colors go to the same user. In this case instead of the extraction kicker one should use a device providing kicks on a femtosecond time scale. This can be either a transverse deflection cavity as suggested in Brinkmann et al. 2010 or a dechirper (Lutman et al. 2016a), see Figure 5.1. The latter method is successfully used at LCLS (Lutman et al. 2016a). To provide a controllable time delay between two X-ray pulses of different colors, one can use a delay chicane shown in Figure 5.1. Wavelength ranges for two-color operation can also be found in Figure 5.1. Note that two-color lasing with alternating tuning of undulator segments to the two colors was recently demonstrated at FLASH2. This option can also be used after the proposed upgrade but then for pump-probe experiments users will need to use a split-and-delay line with spectral filtering as described in Chapter 7. More comfortable for users would probably be the scheme with the chicane, as described above.

5.2.6 Optical Afterburner (OAB)

This concept was proposed in Saldin et al. 2010. It uses the feature of the SASE FEL process, that energy modulations do not only occur on the scale of the resonant wavelength, but also on the scale of the coherence length. If a chicane with a sufficient R_{56} strength (longitudinal dispersion) is installed after the undulator, the FEL induced energy loss modulations can be converted into electron density modulations on the same scale (the modulations are broadband and the central wavelength can be shifted by changing R_{56}). Then the modulated beam radiates in a dedicated afterburner undulator where the bandwidth of the radiation scales as the inverse number of periods.

Two possible applications of this effect were identified in Saldin et al. 2010: production of a second (long wavelength) color for jitter-free pump-probe experiments and measurements of FEL pulse duration (in fact, we obtain an optical replica of the X-ray pulse that can be measured with standard optical methods).

The concept was successfully tested at FLASH1 (Först et al. 2011) and was used in the pulse length measurement campaign (Düsterer et al. 2014). For the considered parameters and proposed layout of FLASH2, the radiation can be produced in the visible and near infrared ranges with the help of the chicane after U2 and the undulator Uoab_lsca. The proposed

undulator consists of five periods with a period length of about 15 cm, but the parameters can be further optimized.

5.2.7 Longitudinal Space Charge Amplifier (LSCA)

The LSCA concept is proposed in Schneidmiller et al. 2010 and is based on the predicted and observed LSC instability in linacs with bunch compressors. LSCA consists of a sequence of focusing channels and chicanes with a radiator undulator at the end. With the suggestion to operate a LSCA in the VUV and X-ray ranges, basic scaling relations were formulated and possible applications were identified. We want to point out that the scheme is a cheap addition to the existing or planned XFEL facilities providing an extension towards longer wavelengths, the production of a second color for pump-probe experiments and the generation of broadband radiation. The latter supports also the generation of attosecond pulses.

Experiments in the visible wavelength range were carried out at SLAC (Marinelli et al. 2013) and recently at FLASH (Lechner et al. 2019). However, operation of a LSCA in the VUV range is still to be demonstrated. The proposed layout of FLASH2, shown in Figure 5.1 would allow to test and to use a VUV LSCA without the installation of any dedicated hardware. Three chicanes are meant to be designed for other purposes, and the undulator Uoab_lsca can be used in two different schemes, namely as OAB (see above) and as LSCA. The expected wavelengths span from a few tens of nm to the visible range, while the bandwidth would be in the range of tens of per cent. Such pulses with a large bandwidth can be interesting for some experiments and they can be produced together with FEL pulses by the same electron bunch.

5.3 Few Femto- and Attosecond Pulses

Short FEL pulses down to ≈1 fs duration can be produced directly with a short electron bunch. "Single-spike lasing" is routinely used at FLASH presently to operate the machine on a 10 fs scale (Rönsch-Schulenburg et al. 2014). The installation of a new bunch compressor right in front of the undulator line and operation at 1.35 GeV will make it possible to produce very short high-quality bunches in low-charge mode (≈10 pC). Another option would be the essentially nonlinear compression of bunches with higher charge in the same way as it has been done in early years of FLASH operation (Ackermann et al. 2007), i.e. producing a bunch with a short lasing part and a long low-current tail. An additional possibility to shape the lasing part would be to use the laser heater. This simple technique has been realized at LCLS to produce attosecond pulses in the hard X-ray regime (Huang et al. 2017). At FLASH, we will be limited to ≈1 fs for shortest wavelengths. Note also, that a short bunch can radiate coherent NIR radiation pulses in the undulator Uoab_lsca. Both pulses will be fully synchronized and can be used for pump-probe experiments.

Another option for the ≈1 fs regime would be to use a standard "long" electron bunch and to apply one of the schemes relying on a laser manipulation of the electron beam, namely the "chirp-taper" scheme (Saldin et al. 2006). In this case the electron beam is modulated by a two-cycle laser pulse in the two-period undulator Uas1 (Figure 5.1) such that there is a slice with the strongest energy chirp. A linear undulator taper is used to compensate for the FEL gain degradation within this slice (Saldin et al. 2006). The rest of the bunch has no strong chirp and suffers from the uncompensated taper. In the case of hard X-rays, the scheme works with Ti:Sa lasers (wavelength 800 nm), and the duration of X-ray pulses can be as low as 200 as (Saldin et al. 2006). For the soft X-ray regime a longer wavelength laser (2 µm to 3 µm) is needed (Fawley 2008) to better match the lasing area and FEL coherence length; here the pulse duration is about 1 fs or longer. In order to further reduce the pulse duration one can make use of the fact that the X-ray pulse is chirped. Thus, it can be either manipulated in the frequency domain by a monochromator or compressed in time in a grating compressor. Also note, that an alternative to the chirp-taper

scheme can be the so called eSASE option (Zholents et al. 2004) with generation of a short high-current spike in the chicane placed in front of U1.

We can also consider a more advanced attosecond option, based on the longitudinal space charge amplifier (LSCA) (Dohlus et al. 2011). The simulations show that soft X-ray pulses with a duration below 100 as can be produced. However, an essential advance in the experimental demonstration of the capabilities of the LSCA concept is required to make a decision on the implementation of the LSCA-based attosecond scheme at FLASH2. In this case some modifications of the layout shown in Figure 5.1 will be required.

Finally, we propose here the most promising FEL-based attosecond scheme. This is a modification of the chirp-taper scheme aiming at a significant reduction of the pulse duration well below the FEL coherence time. The beam is modulated in Uas1 (with two periods and the period length 15 cm) by a CEP-controlled Ti:Sa laser with a pulse duration of 5 fs (FWHM) and a pulse energy in the range of several 100 µJ up to 1 mJ. The chirp-taper compensation is used to maintain amplification within a short slice which is significantly shorter than the FEL coherence length. Due to short-pulse effects the saturation length increases but the undulator is sufficiently long for amplification at wavelengths above 4 nm (U1 and U2 can be used together). The radiation pulse duration is on the order of the coherence time due to the slippage but we propose the following trick to get much shorter pulses: We moderately compress (by 10 % to 30 %) the lasing slice in the chicane after U2, where the microbunching also increases, and let it radiate in a short undulator Uas2 with ten periods and a period length about 3 cm, tuned to the compressed wavelength. The uncompressed part of the bunch is not resonant in this undulator, and the radiation from U2 can be blocked in the chicane. According to our estimates, after Uas2 we get sufficiently clean X-ray pulses with a wavelength of about 3 nm (after compression) or longer, a duration of about 200 as to 300 as and pulse energies in the 100 nJ range.

References

Ackermann, W. et al. (2007). „Operation of a free-electron laser from the extreme ultraviolet to the water window“. In: *Nature Photonics* 1.6, pp. 336–342. DOI: 10.1038/nphoton.2007.76.

Bonifacio, R. et al. (1990). „Large harmonic bunching in a high-gain free-electron laser“. In: *Nuclear Instruments and Methods in Physics Research Section A: Accelerators, Spectrometers, Detectors and Associated Equipment* 293.3, pp. 627–629. DOI: 10.1016/0168-9002(90)90334-3.

Brinkmann, R. et al. (2010). „Possible operation of the European XFEL with ultra-low emittance beams“. In: *Nuclear Instruments and Methods in Physics Research Section A: Accelerators, Spectrometers, Detectors and Associated Equipment* 616.1, pp. 81–87. DOI: 10.1016/j.nima.2010.02.121.

Brinkmann, R. et al. (2014). „Prospects for CW and LP operation of the European XFEL in hard X-ray regime“. In: *Nuclear Instruments and Methods in Physics Research Section A: Accelerators, Spectrometers, Detectors and Associated Equipment* 768, pp. 20–25. DOI: 10.1016/j.nima.2014.09.039.

Dohlus, M. et al. (2011). „Generation of attosecond soft x-ray pulses in a longitudinal space charge amplifier“. In: *Phys. Rev. ST Accel. Beams* 14 (9), p. 090702. DOI: 10.1103/PhysRevSTAB.14.090702.

Düsterer, S. et al. (2014). „Development of experimental techniques for the characterization of ultrashort photon pulses of extreme ultraviolet free-electron lasers“. In: *Phys. Rev. ST Accel. Beams* 17 (12), p. 120702. DOI: 10.1103/PhysRevSTAB.17.120702.

Fawley, W. M. (2008). „Production of ultrashort FEL XUV pulses via a reverse undulator taper“. In: *Nuclear Instruments and Methods in Physics Research Section A: Accelerators, Spectrometers, Detectors and Associated Equipment* 593.1, pp. 111–115. DOI: 10.1016/j.nima.2008.04.051.

Feldhaus, J. et al. (2004). „Two-color FEL amplifier for femtosecond-resolution pump-probe experiments with GW-scale X-ray and optical pulses“. In: *Nuclear Instruments and Methods in Physics Research Section A: Accelerators, Spectrometers, Detectors and Associated Equipment* 528.1, pp. 453–457. DOI: 10.1016/j.nima.2004.04.130.

Först, M. et al. (2011). „Optical afterburner for a SASE FEL: first results from FLASH“. In: *Proc. IPAC2011 Conf.*, p. 3089. Online.

Huang, S. et al. (2017). „Generating Single-Spike Hard X-Ray Pulses with Nonlinear Bunch Compression in Free-Electron Lasers“. In: *Phys. Rev. Lett.* 119 (15), p. 154801. DOI: 10.1103/PhysRevLett.119.154801.

Huang, Z. et al. (2000). „Three-dimensional analysis of harmonic generation in high-gain free-electron lasers“. In: *Phys. Rev. E* 62 (5), pp. 7295–7308. DOI: 10.1103/PhysRevE.62.7295.

Kuhlmann, M. et al. (2018). „Frequency Doubling Mode of Operation of Free Electron Laser FLASH2“. In: *Proc. of International Free Electron Laser Conference (FEL'17), Santa Fe, NM, USA, August 20-25, 2017* (Santa Fe, NM, USA). International Free Electron Laser Conference 38. Geneva, Switzerland: JACoW, pp. 117–120. ISBN: 978-3-95450-179-3. DOI: 10.18429/JACoW-FEL2017-MOP036. Online.

Lechner, C. et al. (2019). „Seeding R&D at sFLASH“. In: *Proc. FEL'19* (Hamburg, Germany). Free Electron Laser Conference 39. JACoW Publishing, Geneva, Switzerland, pp. 230–233. ISBN: 978-3-95450-210-3. DOI: 10.18429/JACoW-FEL2019-TUP076. Online.

Lutman, A. A. et al. (2016a). „Fresh-slice multicolour X-ray free-electron lasers“. In: *Nature Photonics* 10.11, pp. 745–750. DOI: 10.1038/nphoton.2016.201.

Lutman, A. A. et al. (2016b). „Polarization control in an X-ray free-electron laser“. In: *Nature Photonics* 10.7, pp. 468–472. DOI: 10.1038/nphoton.2016.79.

Marinelli, A. et al. (2013). „Generation of Coherent Broadband Photon Pulses with a Cascaded Longitudinal Space-Charge Amplifier“. In: *Phys. Rev. Lett.* 110 (26), p. 264802. DOI: 10.1103/PhysRevLett.110.264802.

McNeil, B. W. J. et al. (2006). „Harmonic Lasing in a Free-Electron-Laser Amplifier“. In: *Phys. Rev. Lett.* 96 (8), p. 084801. DOI: 10.1103/PhysRevLett.96.084801.

Murphy, J. B. et al. (1985). „Collective instability of a free electron laser including space

charge and harmonics“. In: *Optics Communications* 53.3, pp. 197–202. DOI: 10.1016/0030-4018(85)90331-1.

Nuhn, H.-D. et al. (2010). „Characterization of Second Harmonic Afterburner Radiation at the LCLS“. In: *Proc. of the FEL2010 Conference*, p. 690. Online.

Penn, G. (2015). „Simple method to suppress the fundamental in a harmonic free electron laser“. In: *Phys. Rev. ST Accel. Beams* 18 (6), p. 060703. DOI: 10.1103/PhysRevSTAB.18.060703.

Rönsch-Schulenburg, J. et al. (2014). „Operation of FLASH with Short SASE-FEL Radiation Pulses“. In: *Proc. of FEL2014 Conf.*, p. 342. Online.

Saldin, E. L. et al. (2006). „Self-amplified spontaneous emission FEL with energy-chirped electron beam and its application for generation of attosecond x-ray pulses“. In: *Phys. Rev. ST Accel. Beams* 9 (5), p. 050702. DOI: 10.1103/PhysRevSTAB.9.050702.

– (2010). „Optical afterburner for an x-ray free electron laser as a tool for pump-probe experiments“. In: *Phys. Rev. ST Accel. Beams* 13 (3), p. 030701. DOI: 10.1103/PhysRevSTAB.13.030701.

Schneidmiller, E. A. et al. (2010). „Using the longitudinal space charge instability for generation of vacuum ultraviolet and x-ray radiation“. In: *Phys. Rev. ST Accel. Beams* 13 (11), p. 110701. DOI: 10.1103/PhysRevSTAB.13.110701.

– (2012). „Harmonic lasing in x-ray free electron lasers“. In: *Phys. Rev. ST Accel. Beams* 15 (8), p. 080702. DOI: 10.1103/PhysRevSTAB.15.080702.

– (2013a). „Harmonic Lasing Self-Seeded FEL“. In: *Proc. of FEL2013 Conf.*, p. 700. Online.

– (2013b). „Obtaining high degree of circular polarization at x-ray free electron lasers via a reverse undulator taper“. In: *Phys. Rev. ST Accel. Beams* 16 (11), p. 110702. DOI: 10.1103/PhysRevSTAB.16.110702.

– (2016). „Reverse undulator tapering for polarization control at XFELs“. In: *Proc. IPAC2016 Conf.*, p. 722. Online.

Schneidmiller, E. A. et al. (2017). „First operation of a harmonic lasing self-seeded free electron laser“. In: *Phys. Rev. Accel. Beams* 20 (2), p. 020705. DOI: 10.1103/PhysRevAccelBeams.20.020705.

Zholents, A. A. et al. (2004). „Proposal for Intense Attosecond Radiation from an X-Ray Free-Electron Laser“. In: *Phys. Rev. Lett.* 92 (22), p. 224801. DOI: 10.1103/PhysRevLett.92.224801.

6 Lasers

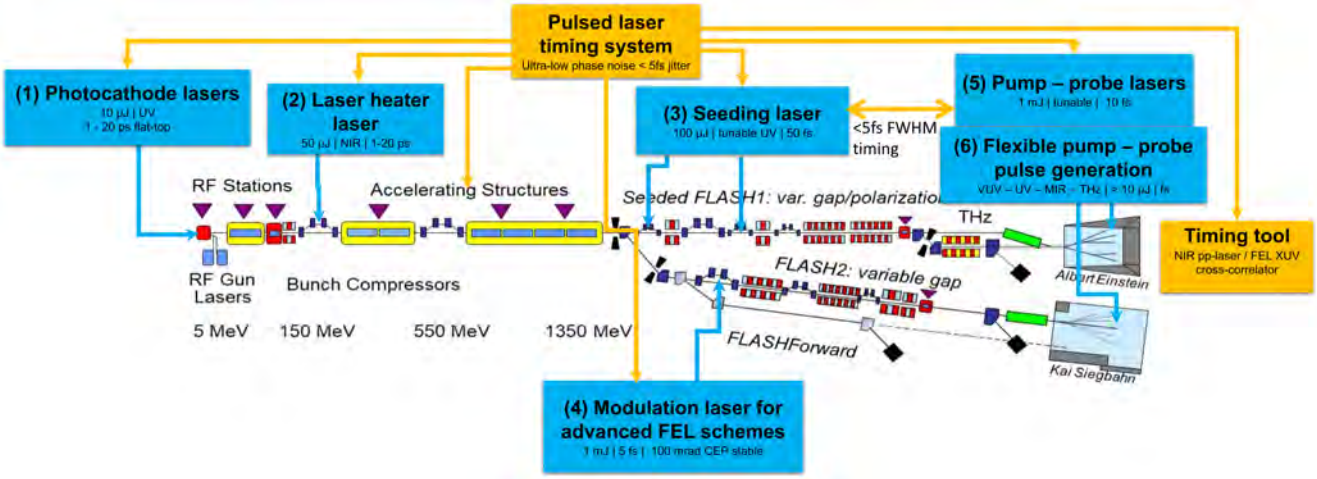

Figure 6.1: *Overview of the FLASH2020+ ultrafast optical laser systems (blue boxes, blue arrows) and the corresponding optical timing and synchronization links (yellow boxes, yellow arrows). The following chapters describe the concepts for the FLASH2020+ ultrafast laser systems.*

Ultrafast optical lasers play an essential role in any X-ray and XUV FEL user facility. An overview of their installations in FLASH2020+ is shown in Figure 6.1. They include (1) photocathode lasers which generate the photoelectrons to be accelerated in the linac, (2) the laser heater laser, (3) the seed laser, (4) modulation lasers which are all needed to modulate the electron beam energy for tailored FEL performance and finally (5) pump-probe lasers and (6) their corresponding setups for flexible pump-probe generation which allows one to fully exploit the capabilities of the FLASH2020+ facility for investigations of ultrafast dynamics in matter. The required tight synchronization and timing between ultrafast optical laser pulses and electron or XUV FEL pulses is provided by length-stabilized fiber-optic timing links for feedback controls to laser oscillators and timing diagnostics in timing tools (compare Chapter 3 for details). All laser systems follow the burst-mode pulse structure of FLASH2020+ with 10 Hz bursts of approximately 1:99 burst-to-space ratio and 100 kHz to 1 MHz intra-burst pulse repetition frequency.

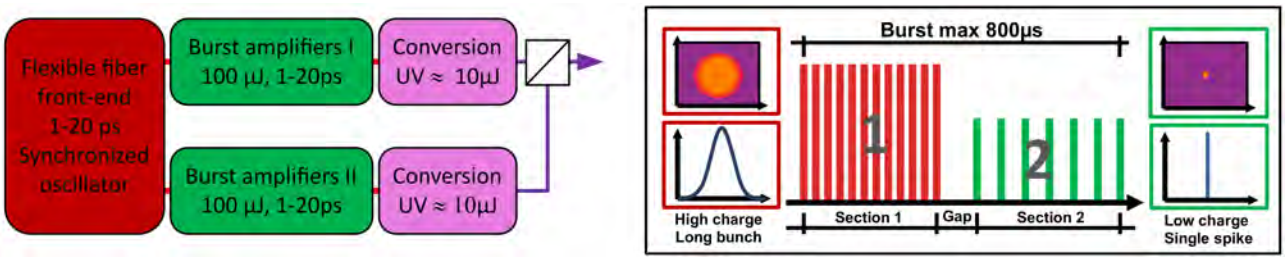

Figure 6.2: *Left: Simplified schematic of the photocathode gun drive laser for FLASH2020+. Right: Intra-burst structure required for different operational regimes of FLASH1 and FLASH2.*

6.1 Photocathode and Laser Heater Lasers

Currently, the FLASH RF photocathode gun is driven by three photocathode lasers emitting deep UV picosecond pulses. Two of them are used for routine operations (Will et al. 2005), while one of them produces shorter pulses for single spike SASE FEL operation (Christie et al. 2017). We will replace these more than ten years old laser systems by a flexible photocathode laser system consisting of a Yb:fiber oscillator and pre-amplifiers, Yb:YAG power amplifiers, a fourth harmonic generation stage, polarization beam combining, spatial shaping and beam transport. A schematic setup of the proposed laser system is shown in Figure 6.2, together with a schematic of an example burst structure.

The system is developed in-house using a front-end very similar to the one developed for the European XFEL (Winkelmann et al. 2018) and commercial Yb:YAG gain blocks. It allows for two burst segments serving the FLASH1 and FLASH2 FEL beamlines of adjustable burst length, inter-burst repetition rate and gap between segments. The total length of both bursts combined including gap can be up to 1 ms. The laser system is equipped with a computer-controlled spectral phase and amplitude pulse shaper which can provide adjustable pulse durations of Gaussian shape from 1 ps to 20 ps. Currently, an R&D project is exploring advanced pulse-shapes, such as temporal flat-top shapes which can improve accelerator emittance (Krasilnikov et al. 2012). The laser system will be located in a newly constructed laser room, attached to DESY building 28 close to the FLASH electron gun (see Section 3.2.1). This new construction was favored over tearing down and replacing the existing laser room for risk mitigation. It allows the current FLASH photocathode lasers still being operational while the new systems are being commissioned.

The laser heater is described in Chapter 3. It is essential to suppress microbunching instabilities for seeded operation of FLASH. Table 3.2 summarizes the requirements: An ultrafast laser pulse train of 50 µJ energy per pulse, 515 nm or 532 nm center wavelength, 20 ps pulse duration at up to 1 MHz rate is required in the interaction region. We expect less than 3 dB insertion loss to beam-transport and coupling to the electron beamline, leading to a requirement of 100 µJ second harmonic output of the laser system. The laser heater laser will be based on the laser system developed for the European XFEL (Winkelmann et al. 2018) comprising of a Yb:fiber front end and Nd:YVO4 power amplifiers. The forth-harmonic generation stage will be replaced by a second-harmonic generation stage. The 20 ps pulse duration requirement can be achieved by spectral filtering or pulse stretching.

The existing XFEL photocathode laser system was designed for a 50 µJ, 4.5 MHz pulse train and has demonstrated the capability to produce 100 µJ level NIR pulses. At a reduced repetition rate of 1 MHz we expect to reach the required pulse energies for FLASH without or with only minimal design changes.

The laser system will be located in another newly constructed laser room outside DESY building 28. The room will be sufficiently large to hold additional laser systems for future novel electron beam manipulation schemes, for example slicing. For coupling to the electron beam, a coupling chicane will be considered (compare Section 3.3.1: Bunch compressor BC1)

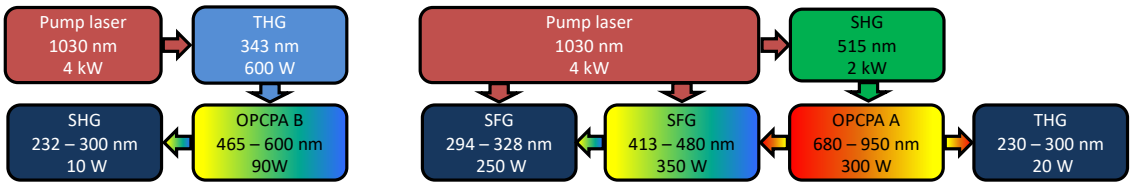

Figure 6.3: *Illustration of possible nonlinear frequency conversion schemes; left: OPCPA B (343 nm, 1 ps pump pulses) with subsequent broadband SHG; right: OPCPA A (515 nm, 1 ps pump pulses) with subsequent cascaded sum frequency conversion stages using the 1030 nm, 1 ps pump laser beam. All powers in the figure refer to average powers within a 1 ms burst.*

	Average power in 1 ms burst (compressed before beam transport) (W)	Compressed pulse energy at 100 kHz before beam transport (mJ)	Compressed pulse energy at 1 MHz before beam transport (mJ)	Tunability (nm)
Pump laser as reported in Pergament et al. 2016	4000	40.0	4.00	1030
OPCPA A (515 nm pump, as reported in Pergament et al. 2016)	300	3.0	0.30	690 – 900
OPCPA B (343 nm pump, alternate concept, simulation)	90	0.9	0.09	465 – 600
Visible output OPCPA A (sum frequency simulation)	350	3.5	0.35	413 – 480
UV output – OPCPA A (cascaded sum frequency, simulation)	250	2.5	0.25	294 – 328
UV output – OPCPA A (THG, simulation)	20	0.2	0.02	230 – 300
UV output – OPCPA B (SHG, estimation)	10	0.1	0.01	232 – 300

Table 6.1: *Expected output parameters of the parametric amplifiers and subsequent frequency conversion stages. For an illustration of the possible nonlinear conversion schemes see Figure 6.3.*

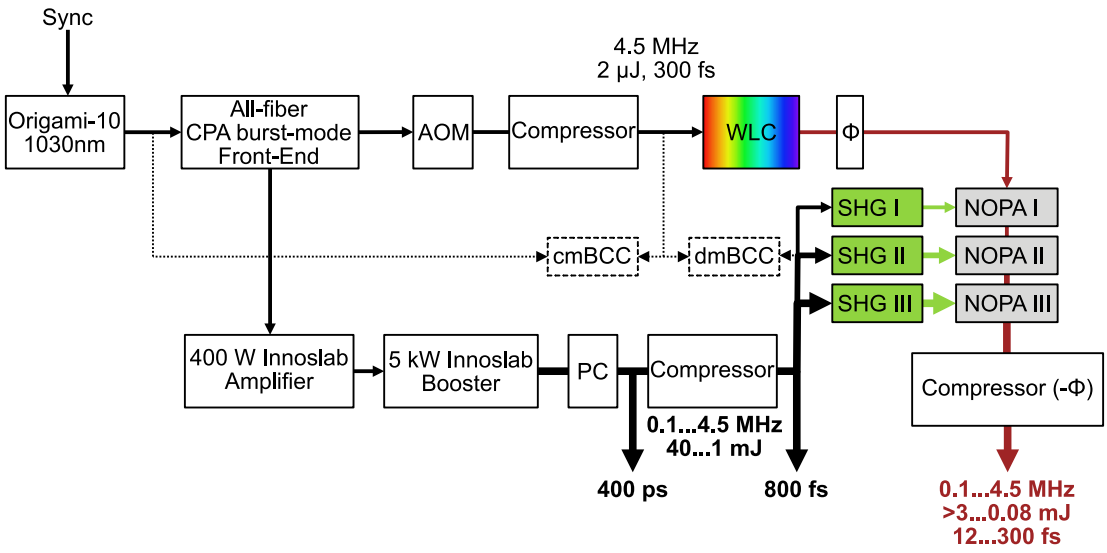

Figure 6.4: *Schematic of the pump-probe laser system of the European XFEL, for details see (Pergament et al. 2016).*

6.2 Seed laser

The concept for the seeded FLASH1 FEL beamline in FLASH2020+ capable of both high gain harmonic generation (HGHG) and echo enabled harmonic generation (EEHG) seeding is described in detail in Chapter 4. In the following sections we will focus on the laser technology which provides broadly tunable seed laser pulses in the UV (or visible) spectral range to the seeding modulators.

6.2.1 Requirements and Challenges

As shown by theoretical considerations and simulations for HGHG and EEHG seeding, seed laser pulses of 50 fs duration and peak powers of up to 25 MW (first stage) plus 70 MW (second stage) are required at the interaction region with the electron beam (see details in Chapter 4). This corresponds to single pulse laser energies of 5 µJ, however the simulations do so far not include any imperfections of electron and laser beam. With an additional factor of 10 for imperfections and an estimated insertion loss of 3 dB for beam transport and coupling, the required pulse energies at the output of the laser system will be approximately 100 µJ.

Instabilities in seeded XUV pulse energy can be caused by laser pulse energy fluctuations but also by fluctuations in spatial and temporal overlap between laser pulses and electron pulses. To achieve high XUV energy stability, the requirements for the laser system are: beam quality near the diffraction limit, excellent energy and pointing stability as well as excellent stability in timing jitter and low timing drifts. For a seeded FLASH1 beamline the requirements for the laser system in terms of availability and remote control capability are high, similar to the photocathode laser system. However, since the seed laser system is of higher complexity than the photocathode laser system, this requirement is very challenging. Note: A change in FEL wavelength requires simultaneous seed laser wavelength tuning, to be performed remote-controlled by the FLASH operator in the control room.

An additional challenge are the requirements for the optics for laser beam transport and coupling into the electron beam vacuum. We require dielectric UV mirrors of high damage threshold, high reflectivity over a large bandwidth and low dispersion. This combined requirement is at the edge of current coating technology. To mitigate risks we will immediately start to evaluate vendor capabilities and we will plan for two parallel laser beam transport lines which can be fitted with optics for different spectral regions.

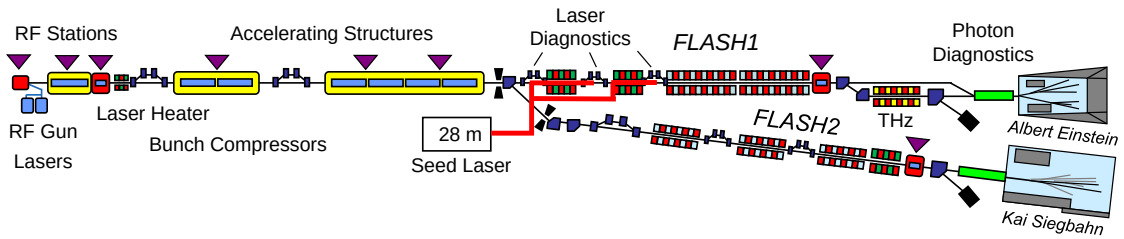

Figure 6.5: *Sketch of the location of the seed laser room (labeled 28m) and the laser beam transport to the modulation undulators (red lines) for HHGH and EEHG seeding.*

6.2.2 Laser Concept

The seed laser system will be based on Optical Parametric Chirped Pulse Amplification (OPCPA) technology (Dubietis et al. 1992), the only laser technology capable of providing the required wavelength tunability, spectral bandwidth and average power (or repetition rate).

We will implement an OPCPA as close as possible to the pump-probe lasers of the European XFEL (Pergament et al. 2014; Pergament et al. 2016) (compare Figure 6.4). This laser system comprises of an ultra-stable 1 µm femtosecond oscillator, Yb:fiber amplifiers, supercontinuum seed pulse generation and Yb:YAG InnoSlab amplifiers for high energy pump pulse generation for three OPCPA amplifier stages. It uses chirped mirrors for stretching and bulk silica for compression of the broadband pulses.

The experience at the European XFEL shows that such a laser system can be reliably operated on a long term. Our simulations show that the output parameters of this laser system allow for deep UV seeding at 100 kHz with sufficient headroom in pulse energy. For seeding at 1 MHz an upgrade of the pump-laser average power capability during the 1 ms burst by a factor 4 from currently 4 kW to 16 kW is required. This is beyond currently developed technology and requires additional R&D efforts. To mitigate risks, we will initially seed FLASH1 at 100 kHz and simultaneously explore options for pump-laser power scaling in close collaboration with potential suppliers.

The OPCPA system provides pulses in the NIR spectral range, tunable between 700 nm and 950 nm. Those pulses need to be converted to the UV spectral range by third harmonic generation (THG) or cascaded sum frequency mixing (SFG). For SFG the remaining depleted NIR pump pulse after second harmonic generation (SHG III in Figure 6.4) will be used.

As an alternative concept the OPCPA stages NOPA I-III in Figure 6.4 can be pumped by the third harmonic (343 nm) of the InnoSlab pump-amplifier chain. This alternative concept would allow to directly generate visible pulses, tunable between 465 nm and 600 nm, which can be converted to UV by a simple SHG stage. We performed OPCPA and nonlinear conversion simulations for the above described concepts using the software package chi3D (Lang 2019). The results of the simulations are shown in Table 6.1.

We will perform experimental studies to validate the simulations for our final selection of the best concept. As mentioned above, for an upgrade from 100 kHz to 1 MHz seeding an upgrade of the pump-laser is required. We expect that the nonlinear conversion stages can be adapted to higher repetition frequencies with relatively little effort.

6.2.3 Laser Room and Laser Beam Transport

The seed laser will be located in an already existing room in building 28m. Figure 6.5 illustrates the location of the seed laser room within the FLASH facility together with the laser transport beam line. The seed laser beams for the two modulation undulators will be transported in vacuum onto stable coupling platforms next to the electron beamline. We will evaluate different options for beam transport: relay imaging using (1) transmissive and (2) reflective optics as well as (3) collimated beam transport with active beam stabilization.

Each platform can hold pulse compressors, mode matching optics, beam diagnostics and beam controls. After each modulator, the laser pulses will be coupled out of the electron beamline. Here, additional beam diagnostics will be installed.

Our power budget and damage requirements only allow for dielectric mirror coatings in the laser beam transport. As already mentioned above, the availability of suitable large bandwidth femtosecond mirror coatings in the UV spectral range is unclear. To mitigate this risk we will implement spatial multiplexing of different spectral regions in parallel beamlines in one vacuum tube. The beam diameter at the input coupling mirror and the vacuum window is given by mode-matching to the electron beam. This leads to a small laser beam size on those optics, they are therefore most critical in terms of laser-induced damage.

We plan for a metallic mirror outside the electron beam vacuum under grazing incidence followed by a coated window or an uncoated window in Brewster's angle. This is most likely the only feasible method to increase the effective beam area sufficiently to avoid mirror damage. We will also test the effects of self-phase modulation and of two-photon absorption of the window. We will investigate the option for lead shielding of the input coupling windows for protection against radiation darkening. Before finalizing the design, we will study the limits for coupling into the electron beam pipe and perform damage tests. After interaction with electrons, the laser beam will be coupled out of the electron beam pipe and used for online diagnostics.

6.3 Pump-Probe Lasers

Approximately 60 % of all recent user experiments at the FLASH facility required ultrafast optical lasers in a pump-probe configuration. A typical physical phenomenon under investigation in these experiments occurs on picosecond to femtosecond timescales, requiring laser pulse durations on a similar or shorter timescale and exactly controllable (or at least exactly measurable) temporal separation between XUV FEL and optical laser pulses. Ultrafast optical pump-probe pulses should be on the one hand controllable but on the other hand also stable and reproducible in parameters such as pulse energy, polarization, pointing, wavelength, bandwidth, focus size and pulse duration.

The specific requirements strongly depend on the experiment and need to be individually evaluated for each single experiment. Here, typically trade-offs between simultaneously desired pulse parameters have to be made. Advanced experiments will require more than one optical pulse per FEL pulse, for example an additional pulse to align molecules immediately before the interaction occurs. To meet all this requirements, our design concept for optical pump-probe lasers for FLASH2020+ will provide the most flexible set of optical pump-probe pulses possible which at the same time is capable of maintaining high stability, availability, reproducibility and user-friendliness to the operators.

An overview of the infrastructure for optical pump-probe capabilities in the FLASH2020+ facility is shown in Figure 6.6. The experimental halls for the FLASH1 and FLASH2 beamlines are each equipped with a laser hutch containing a state of the art OPCPA laser system. Each hutch is very well controlled in temperature, humidity and particle count. The femtosecond pulses generated by these laser systems will be transported in refractive relay imaging beamlines to modular optical delivery (MOD) stations, close to the instruments. The MODs comprise mode-matching telescopes, pulse compression, wavelength conversion, polarization rotation, attenuation, pulse diagnostics and active beam stabilization setups. For beam delivery from MOD to the instruments or experimental endstations, we will typically install multiple setups which are directly attached to the instruments.

We will install the additional MOD station MOD 2.0 without access to an instrument so that preparations, tests and development of setups for future user-beamtimes can be performed even during on-going user-experiments when the laser hutches cannot be accessed. This station will be essential for developing flexible pump-probe schemes during the FLASH2020+ project phase. Its presence will later during the FLASH2020+ operation phase reduce the "tooling time" for novel beam-time specific setups which can be pre-aligned in the MOD 2.0 station and later transferred to the relevant MOD station for the beamtime.

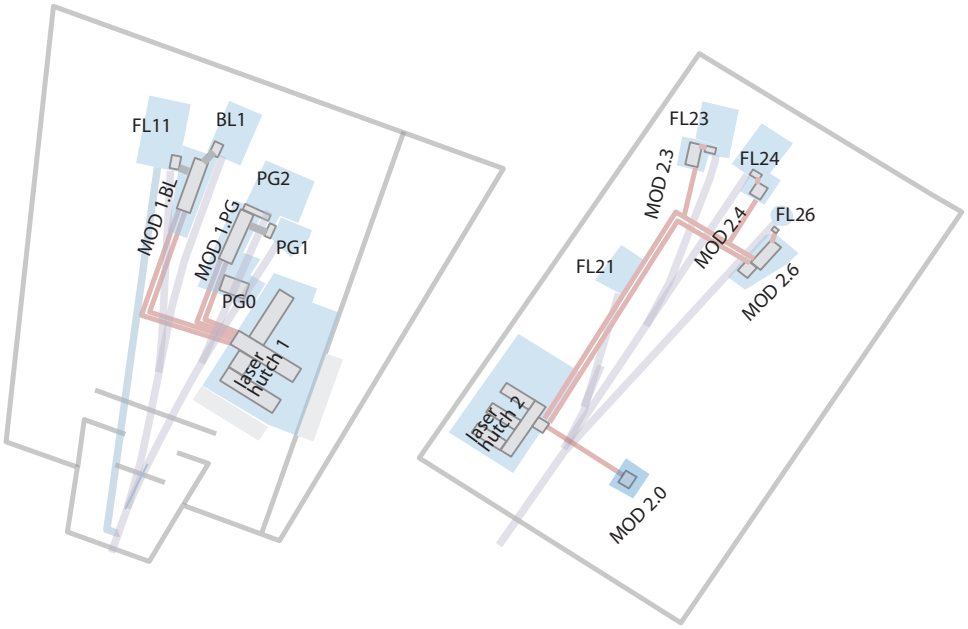

Figure 6.6: *Overview of optical ultrafast pump-probe infrastructure in the experimental hall of the FLASH facilities (left: FLASH1, right: FLASH2). MOD: Modular optical delivery station. Laser transport beamlines are shown in red, laser safety enclosures in light blue, laser tables in light gray, FEL XUV beamlines in light purple. Purpose of MOD 2.0 is development and test of setups for future FEL beamtimes. The developed setups will be transferred to other MODs close to instruments for use during FEL beamtimes.*

6.3.1 OPCPA Pump-Probe Laser Systems

As already described in Section 6.2.2, OPCPA technology is the only laser technology which can provide ultrashort pulses at the required pulse energy and repetition rate. For the pump-probe laser development we will also rely on the experience gathered at both DESY and the European XFEL in building OPCPA burst-mode laser systems. Those already developed lasers can provide tunable NIR wavelengths (650 nm to 900 nm) and tunable pulse durations (<15 fs to >100 fs) (Pergament et al. 2016).

To meet the requirements for FLASH2020+ the following measures will be taken:

1. Setup R&D laser system: We will combine existing InnoSlab amplifiers and a new fiber-laser front-end to establish a development laser system for R&D on OPCPA and nonlinear conversion schemes in our laser development lab. This measure is enabling us to test planned concepts and pre-align systems which would not be possible in the FLASH experimental hall due to the high demand for lasers for user experiments. This measure also ensures short shut-down times, since it allows installation of pre-tested configurations in the FLASH facility. Since the setup of this R&D lab and also the MOD 2.0 station is critical for the FLASH2020+ project we will start those efforts immediately.

2. Replacement of pump-probe lasers in laser hutch 1: Laser hutch 1 contains outdated laser systems. We will replace these systems with a system similar to the European XFEL pump-probe laser (Pergament et al. 2016). The performance of the laser system is summarized in Table 6.1. This measure will require major reconstructions: Tear down and reconstruction of laser hutch 1 including the air-conditioning system, new beam transport pipes and new installation of all MOD stations MOD 1.BL and MOD 1.PG and coupling to the instruments in the FLASH1 experimental hall. To allow user operation during reconstruction of the laser hutch 1 and setup of the new pump-probe lasers we will install interim lasers in MOD 2.BL and MOD 2.PG with adequate performance to accommodate the most important beamtimes. We consider for Mod 2.BL the existing 10 Hz Ti:sapphire laser, which will be moved from laser hutch 1 to Mod.BL and for MOD.PG a Yb-based burst mode system with spectral broadening and recompression.

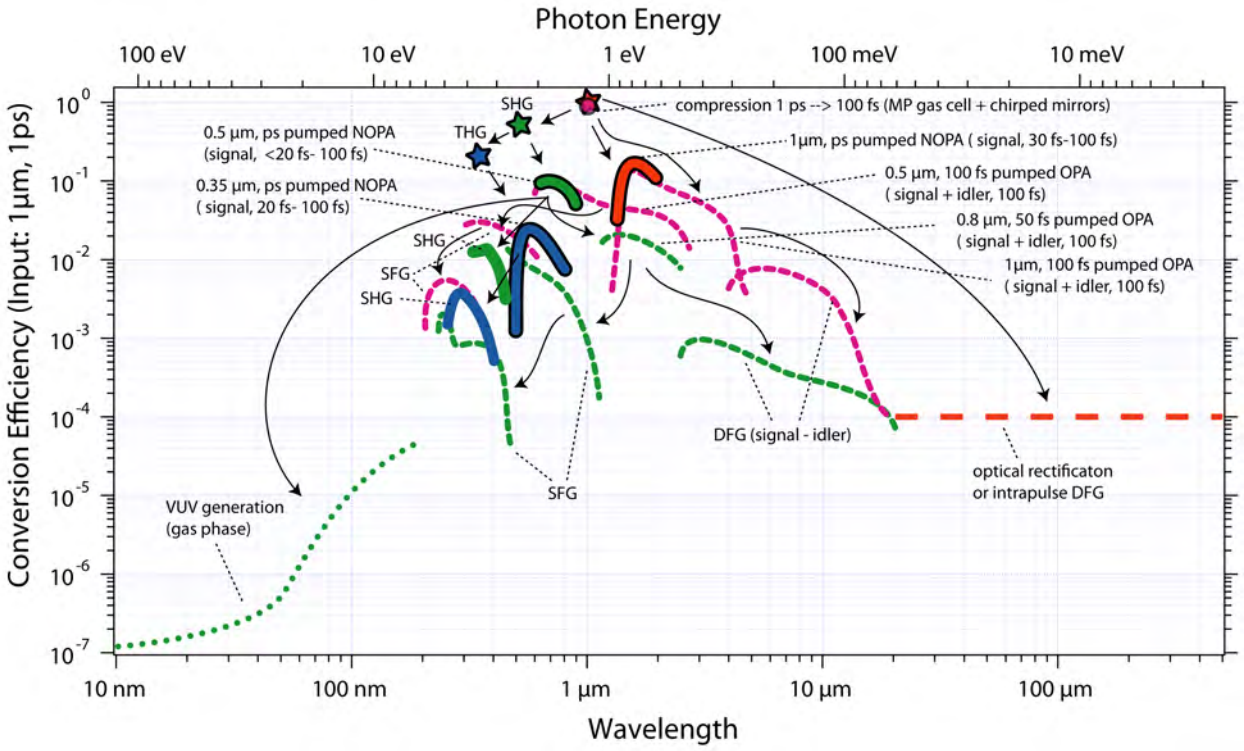

Figure 6.7: *Illustration of the spectral coverage of the pump-probe lasers and their estimated efficiency with respect to the 1 ps 1030 nm pump laser (pump laser power after upgrade: 40 mJ at 100 kHz, 4 mJ at 1 MHz) via several nonlinear conversion schemes described in the text. The green dashed and dotted lines indicate nonlinear conversion starting from a SHG-pumped non-collinear OPCPA, pink dashed lines indicate what would be possible if multi-pass cavity pulse compression is available. The red dashed line is the estimated THz conversion efficiency using 1 µm ps pump pulses. Note: Transmission of beam-transport and coupling to the instruments is not included in the efficiency estimation. The OPA efficiency estimation is based on in-house OPCPA experiments and published data of commercial available OPAs (Light Conversion 2019a; Light Conversion 2019b).*

3. Upgrade of fiber-laser front-end and pump-laser in laser hutch 2: Laser hutch 2 contains a modern OPCPA laser system, which was developed at DESY during the past years. However, its pump-laser has only 10 % of the energy and average power (400 W) of the system above (4 kW). We will upgrade the pump-laser system by a 4 kW version to meet future wavelength-flexibility demands by providing sufficient pulse energy for frequency conversion at the highest repetition frequency. The existing system also comprises a prototype fiber-laser front-end and pump-pulse compressor. Both components drift and are difficult to align. We will upgrade those components to state-of-the-art technology to improve stability and availability of the system.

4. 20 Hz pump-laser, alternately pumping two OPCPA chains: At the European XFEL a fast galvo-scanner was developed which can distribute 20 Hz rate pump-laser pulses alternating to two OPCPA amplifier chains (Palmer et al. 2019). This allows simultaneous delivery of ultrashort pulses to two MODs, with one of them capable to be synchronized to the FEL. This measure will dramatically improve setup and preparation possibilities for upcoming user experiments and for the development of new features. Parallel to a running pump-probe experimental beamtime at one instrument, the ultrafast optical laser can be delivered to a second instrument for setup, alignment and test experiments. For development of new optical laser features, such as advanced wavelength conversion schemes, this second set of 10 Hz burst pulses can also be delivered from laser hutch 2 to MOD 2.0.

5. External compression of ps-pump pulses by a factor 5-10: Very recently, an interesting new technology has become available which may significantly alter the ultrafast pump-probe options at FLASH2020+. Promising efficient spectral broadening and re-compression schemes for 100 fs level pulses using gas-filled multipass cells or gas-filled capillaries were demonstrated (Fritsch et al. 2018; Jeong et al. 2018). Our simulations show that similar methods are also capable of reducing the pulse duration of our ps-pump-pulses by a factor 5-10. This is confirmed by recently published results, which have demonstrated spectral broadening and re-compression of 18 mJ, 1.3 ps pulses to 41 fs in a gas-filled multi-pass cell with 90 % efficiency (Kaumanns et al. 2018). A commercial pulse-compression product using this technique with specified input pulse durations between 150 fs and 1 ps has also become available (Amplitude Systems 2019). We will start a research program exploring these options. If this is successful, we plan to immediately implement these schemes in both laser systems (FLASH1 and FLASH2). This would allow us to deliver multi mJ-level 100 fs level pulses at MHz repetition rates centered at 1030 nm to the MODs and instruments, opening up new opportunities for both experiments and wavelength conversion stages. At the MOD stations then 100 fs, 1 µm pulses of 10-times higher energy than the previously used 50 fs, 800 nm pulses would be available for pumping widely tunable OPAs. In a wide spectral range, this would lead to an approximately tenfold increase in pulse energy available to the instruments (compare the purple and green dashed lines in Figure 6.7).

6. 343 nm and 1030 nm pumped OPCPA: While we will initially install non-collinear OPCPA amplifier chains pumped by the second harmonic (515 nm, 1 ps) of our powerful pump-lasers, we will start R&D efforts on 343 nm and 1030 nm pumped OPCPAs. Those will allow us to generate with high efficiency and good stability the entire spectral band from 0.5 µm to 4.2 µm, due to the now newly available high-energy ultrashort pulses in the spectral range between 500 nm to 700 nm (for 343 nm pumping) and 1.5 µm to 4.2 µm (for 1030 nm pumping. Note: we will use the idler beam only in a last collinear stage here). Those options will further increase our wavelength flexibility. Wavelengths above 1.5 µm for example allow THz and MIR generation in modern highly efficient materials like DAST or ZGP (Hauri et al. 2011; Schunemann 2017).

We will continuously follow novel developments on laser technology and evaluate options before starting a specific development. Especially progress in pump-laser power and energy scaling is of great importance and – as we have seen above – required for seeding of FLASH at MHz rates. While currently InnoSlab technology (Russbueldt et al. 2015; Schmidt et al. 2017) is the only proven pump-laser technology which can provide 4 kW, 1 ms bursts of pump pulses, we will evaluate competing technologies such as thin disk multipass amplifiers (Dietz et al. 2018; Nagisetty et al. 2018), coherent combining of fiber lasers (Müller et al. 2016; Müller et al. 2018) and cryogenic amplifiers (Zapata et al. 2018) for new installations.

6.3.2 Beam Transport and Dispersion Management.

For laser beam transport from laser hutches to the MOD stations we will build on technology developed for the FLASH2 pump-probe laser system. We will use positive (normal) dispersion stretching, relay imaging in evacuated beam pipes using refractive optics and negative dispersion compressors using either chirped mirrors (for pulse durations between 10 fs and 30 fs) or transmission gratings (for bandwidth limited pulse durations above 30 fs). The beam pipes allow for transport of multiple beams spatially multiplexed with different beam paths fitted with wavelength-specific optics. Motorized mirrors both in a beam switch yard in the laser hutch and in T-crosses allow rapid switching between experiments. We plan for the transport of OPCPA output pulses (500 fs stretched 600 nm to 900 nm, 1 mJ) and NIR pump pulses (1030 nm, 1 ps, 10 mJ) with later upgrade options for 500 nm to 700 nm (343 nm OPCPA pumping) and 1.5 µm to 4.2 µm (1030 nm OPCPA pumping). Active beam-stabilization at the MODs will correct for spatial beam drifts.

Instrument →	FL11	BL1	PG1	PG2	PG0	FL21	FL23	FL24	FL26	
Wavelength	MOD		MOD				MOD	MOD	MOD	MOD
in µm↓	1.BL		1.PG				2.3	2.4	2.6	2.0
<0.24	O							O	O	
0.24 – 0.3	✓		O				O	✓	✓	✓
0.35 – 0.45	✓		✓				✓	✓	O	✓
0.45 – 0.7	O							O		✓
0.7 – 0.9	✓		✓				✓	✓	✓	✓
0.9 – 1.5	O		✓				✓	✓		✓
1.5 – 4.2			✓				✓	✓		✓
4.2 – 15			O				O	O		✓
>15			O				O	O		✓

Table 6.2: *Assessment of demands for wavelength flexibility at different instruments. We identified the green options (✓) as to be realized first, followed by the blue (O) options. Setups will be tested in MOD 2.0 before installing at an instrument. Note: The yellow shaded frequency range will be available directly out of the laser hutches after implementation of 323 nm and 1030 nm pumped OPCPAs.*

6.3.3 Wavelength Conversion and Flexible Pump-Probe Schemes

Compared to the current FLASH facility where with few exceptions only harmonics of the 800 nm center wavelength laser systems were available, FLASH2020+ will dramatically improve experimental capabilities by providing flexible pump-probe schemes with optical pump-probe pulses covering the entire spectral range from VUV to THz. In the following paragraphs we will describe a multitude of nonlinear conversion schemes which allow this large spectral coverage. An illustration of the wavelength coverage and the conversion efficiency is shown in Figure 6.7.

Our primary strategy is here to extend the wavelength coverage of the OPCPA laser systems to the spectral range from 0.5 µm to 4.2 µm (see item 5 in Section 6.3.1) and to transport this wavelength range to the MODs where further wavelength-conversion can occur (sum frequency generation (SFG), third harmonic generation (THG), optical parametric amplifiers (OPA) or rectification for THz). We can especially cover most of the important UV spectral range by straight forward SHG and THG of the widely tunable OPCPA output. As a fallback strategy, we will also consider transporting only near-infrared radiation (either centered at 800 nm or centered at 1 µm) to the MOD stations and do all wavelength conversion steps inside the MOD stations.

The spectral range above 4.2 µm is impractical to be transported over long distance due to absorption in non-evacuated beam paths and required apertures and optics. The wavelength range >15 µm will be generated close to the instrument by optical rectification (or intra-pulse DFG) using either the OPCPA output around 800 nm or the 1 µm ps OPCPA pump laser as driver, where either single-cycle or narrow band pulses can be generated (Carbajo et al. 2015; Hirori et al. 2011).

The wavelength range between 4.2 µm and 15 µm can only be covered by either a low efficient OPA at the MOD (DFG between signal- and idler beams) or by transporting two intense beams (OPCPA output and OPCPA pump) to the MOD for DFG generation at the MOD. The feasibility of the latter concept needs to be experimentally verified, since transporting two beams over long distances is challenging due to the high requirements on stability for spatial and temporal overlap between both beams at the conversion stages at the MOD. Here, the availability of above mentioned novel highly efficient compression schemes for the 10 mJ, 1 ps, 1030 nm OPCPA pump pulse would dramatically change the situation, since now low-efficient OPA schemes could provide sufficient pulse energy for most experimental needs in and beyond the 4.2 µm to 15 µm spectral range.

Our implementation strategy is to proceed in steps of increasing complexity:

1. Installation of SHG and THG of the 515 nm pumped OPCPA output at the MODs (→350 nm to 450 nm and 200 nm to 300 nm, respectively).

2. Wide spectral tunability by installation of commercial OPAs pumped by the OPCPA output at the MODs (green dashed lines in Figure 6.7). This step is also relatively straight forward to implement, however, can only provide low pulse-energies and pulse-durations of 100 fs and above. Higher pulse energies can be achieved by 1 µm pumped OPAs (purple dashed lines in Figure 6.7). Implementation of this method requires successful pulse compression schemes of the OPCPA pump laser (see item 4 in Section 6.3.1), since commercial OPAs require 100 fs to 200 fs level pump pulses.

3. Development of 343 nm and 1030 nm pumped OPCPAs (see item 5 in Section 6.3.1) with SHG and THG stages at the MODs. This measure provides a pulse energy boost of a factor of 10 at potentially shorter pulses compared to step 2 above.

4. Development of advanced frequency conversion schemes for extended wavelength coverage and shorter pulses.

The implementation of above schemes at the specific instruments will be strongly driven by user and science demands. Our current assessment of needs for the instruments is summarized in Table 6.2. Our concept allows for tests and preparation for future setups in MOD 2.0 (compare Figure 6.6). Science demands also drive the R&D efforts on advanced frequency conversion schemes and their future implementation.

Possible promising concepts for advanced schemes are:

- VUV generation via high-harmonic generation. There is an on-going R&D project for this scheme at FL26, financed by a university BMBF project.

- DUV (150 nm to 250 nm) generation via perturbative harmonics in gases (Fuji et al. 2007; Kida et al. 2011; Wallmeier et al. 1988) or gas-filled fibers (Köttig et al. 2017; Mak et al. 2013; Winters et al. 2018) or solid state setups (Homann et al. 2008).

- UV (250 nm to 350 nm) pulses below 20 fs via broadband nonlinear mixing schemes (Baum et al. 2004; Varillas et al. 2014).

- Long-mid-infrared pulse generation (5 µm to 15 µm) using two beam transport to the MODs or compressed 1 µm pump pulses.

- THz generation – both single cycle and narrow bandwidth.

6.3.4 Coupling to the Instruments

Coupling of the ultrafast pump-probe laser to the instruments will be in collinear (or close to collinear) geometry for wavelengths shorter than 4.2 µm. In collinear geometry we will use a flat in-vacuum metallic mirror reflecting the optical beam and transmitting the XUV beam via a hole drilled into the mirror. MIR and THz delivery is performed in a 90° geometry due to required large aperture and a focusing parabola close to the interaction point. Optical laser generated VUV pulses will be coupled in grazing incidence geometry next to the XUV beam in an already existing setup at MOD 2.6.

We plan to install the focusing optics in a vacuum chamber directly connected to the instrument. This chamber can also host the last frequency conversion stage to deep UV or mid-IR. With vacuum coupling to the instrument, no dispersion-issues with UV vacuum windows and no molecular absorption in air exist. An optional beam transport from the MOD stations to an optical setup provided by the user experiment is also possible.

6.4 Modulation Laser for Advanced FEL Schemes

Advanced FEL schemes in the FLASH2 beamline for water-window attosecond pulse generation (compare Chapter 5) require a CEP stable NIR laser delivering two cycle 1 mJ pulses with 100 mrad to 200 mrad pulse to pulse phase stability. For initial R&D projects and to verify the predictions from theory and simulations, we will operate at 10 Hz, where suitable laser technology exists and is in part commercially available. Technology includes CEP stable Ti:sapphire regenerative amplifiers with spectral broadening in hollow core fibers and re-compression and DFG sources with passive CEP stability. One major challenge will be the transport of the CEP stable laser beam from the laser lab to the undulator hall (approx. 20 m) and to maintain the CEP stability in a non-temperature-controlled environment. Most likely the required phase stability can only be preserved during beam transport if additional air-conditioning and climate control is added for the optical beam path. A further challenge will be the coupling of the optical laser beam to the modulator, where commercially available windows and mirrors need to be operated close to optical damage.

Since here the laser requirements are very demanding, a dedicated R&D phase will start as soon as the details of the electron beam manipulation concept and corresponding FEL beamline and modulation laser requirements are better defined.

6.5 Synchronization and Timing

Precise and controllable timing between XUV pulses and ultrafast optical laser pulses is the most important enabling requirement for the study of ultrafast phenomena in pump-probe experiments.

FLASH is equipped with a pulsed laser synchronization system over length stabilized fibers (compare Chapter 3). In a previous campaign at the FLASH1 facility an out-of-loop timing jitter of (28 ± 2) fs rms. was measured. Details of this measurements and a description of the FLASH all-optical synchronization system can be found in (Schulz et al. 2015). The FLASH2020+ synchronization and timing system for optical ultrafast lasers will build on DESY's existing worldwide leading system and add several improvements. With the availability of a seeded FEL, the XUV photon arrival time is governed by the seed laser from which we expect a further reduction in timing jitter. Currently, all laser oscillators are stabilized via length-stabilized fibers to the master laser oscillator of the facility. Drifts of the laser amplifiers with respect to the laser oscillator are partly compensated by feedback control. However, the OPCPA amplifier and the laser beam delivery timing relies currently only on passive stability and is not actively timing drift corrected. For the FEL XUV photons, the arrival time of the electrons is stabilized, while the XUV beam pipes are not timing drift corrected. A very rough estimation of expected uncompensated timing drifts over 24 hours is shown in Table 6.3. Major drifts are expected outside the laser hutch in the transport beamline and the MODs where climate control is inferior to the laser hutch.

We also expect in the experimental hall jitter due to acoustic noise and mechanical vibrations. MODs are enclosed by laser safety curtains without any acoustic isolation to the FLASH experimental halls where for example vacuum pumps may cause significant noise levels.

6.5.1 FLASH2020+ Timing and Jitter Improvement Projects

Currently, most of the actual timing drifts are estimations only. In previous measurement campaigns it was often unclear if the timing of the FEL XUV beam is drifting or if the timing of the ultrafast laser system is drifting.

In Schulz et al. 2015, the majority of jitter is attributed to the FEL XUV beam.

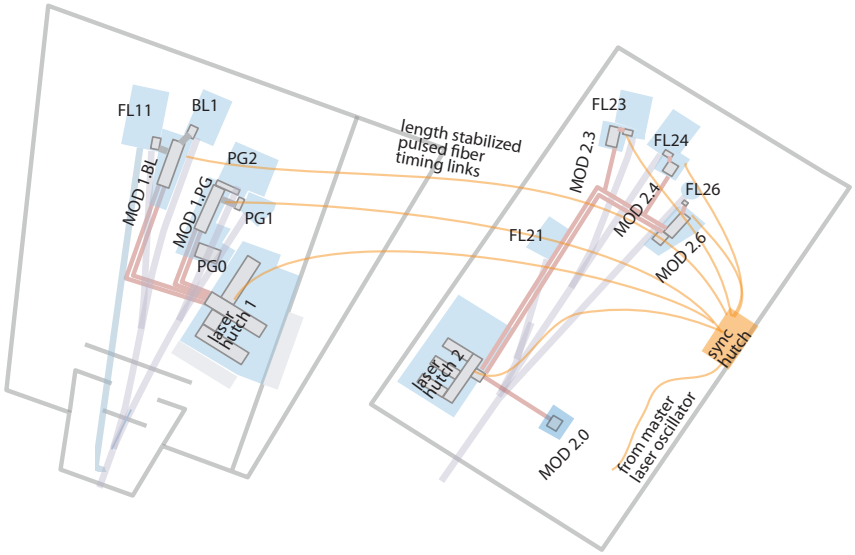

Figure 6.8: *Overview of synchronization sub-distribution and length stabilized fiber links for pump-probe experiments (orange).*

Material	Drift coefficients from temperature or humidity change	Drift per day, laser hutch (air: ΔT: 0.15 °C, Δhum: 1.5 %, Δp: 0.5 kPa)	Drift per day, laser beamlines and MODs: (air: ΔT: 0.8 °C, Δhum: 5 %, Δp: 0.5 kPa
Optical fiber	temp: 4 fs/m/0.1K, hum : 5 fs/%hum/m	All fibers are in feedback control typical compensation: 1.5 ps	
Aluminum breadboard	7.7 fs/m/0.1K	0.2 ps	0.4 ps (mainly multi-pass chirped mirror compressor – 6 m beam path)
Steel table	3.7 fs/m/0.1K	0.2 ps	0.4 ps
Concrete floor	4 fs/m/0.1K		1.3 ps (40 m beam transport)

Table 6.3: *Rough estimation of currently uncompensated timing drifts at FLASH due to temperature, humidity or pressure changes. The numbers are most likely over-estimated, since they do not account for the (often very slow) time constants in between a change in environmental properties to a change in material properties.*

To improve timing and jitter we will pursue the following measures:

Synchronization sub-distribution for pump-probe experiments. The maximum number of fiber-optics synchronization links is limited due to space constraints. For supplying all MOD stations with a timing link we plan to install a timing sub-distribution in one of the FLASH experimental halls, as already successfully implemented at the European XFEL. This sub-distribution will be installed in an tightly temperature and humidity controlled room with solid acoustic shielding walls, to minimize drifts of out-of-loop beam paths. This room will be an excellent location for hosting the mechanical delay lines for setting the pump-probe delays. This location has a clear advantage over the MOD stations, which are enclosed by laser safety curtains only. A schematic picture of length stabilized fiber links is shown in Figure 6.8.

Quantitative tests and measurements of current timing drift and jitter. We plan to measure the arrival time of the optical laser at the MODs via cross-correlation to optical fiber links to the master laser oscillator, measure beamline drifts using cw-laser interferometers or frequency comb metrology (Coddington et al. 2009) and record a multitude of environmental data such as temperature, humidity and pressure but also mechanical vibrations throughout the entire optical beam path. We will also conduct timing test experiments between laser and

FEL XUV beam on a regular basis. Based on this assessment we will determine which one of the measures listed below will have the most impact.

Active optical path length measurement and compensation of the OPCPA amplifier laser beamline and dispersion compensation setup. This can be done for example by retro-reflecting a co-propagating cw or high repetition rate pilot beam. Alternatively we can use fiber-optical timing links at the MODs. Note: We may also need to act on laser timing for FEL XUV beam path length changes – which also have to be measured using co-propagating pilot lasers. Another option is to retroreflect part of the beam from the MOD back to the laser hutch and cross-correlate there with the laser oscillator.

Environmental stabilization of MOD setups. Since better climate control inside the MODs is impractical (only curtain walls) we will cover the optical setups with pressure and temperature controlled enclosures. The enclosures will be purged with temperature-stabilized nitrogen or dry air reducing the impact of temperature and humidity to the beam path. This measure also is beneficial for mid-infrared setups since it eliminates water absorption lines. Modular setups will be installed on low-expansion optical breadboards (invar or carbon fiber).

Acoustic isolation and mechanical stability. The dominant contribution to temporal (and spatial) jitter are acoustic frequencies coupled via sound or mechanical vibrations to the setup. We plan for passively vibration-damped optical tables, massive granite posts and sound-damping enclosures for optical setups at the MODs.

6.5.2 Control of FEL XUV to Optical Laser Time Delay

The time delay between optical ultrafast pump-probe laser and XUV FEL pulses can be coarse and fine controlled via electronic triggers and optical delay lines respectively. The optical delay lines are installed in the pulsed-laser timing system at 1.5 µm center wavelength and allow for up to 4 ns delay at a minimum step-size of 1 fs. Since naturally those delay lines are out of any feedback loop, low expansion invar materials and defined environmental conditions (humidity, temperature, pressure) for the in-air beam path are crucial for ultimate performance. For this reason, all delay lines will be installed in the synchronization sub-distribution hutch, which provides excellent environmental stability. Note: For active monitoring of ultrafast pulse arrival time at the MODs using our all optical pulsed laser timing system, the reference timing link to the MOD needs to be equipped with the identical delay line as the timing link to the laser hutch to allow synchronous scanning of both delay lines during an experiment.

6.5.3 Ultrafast Optical Laser – FEL XUV Timing Tool

While we will be implementing the best possible passive and active timing stabilization system, the ultimate timing performance will have its limits. If these limits – we target 5 fs FWHM for the seeded FEL beamline – will be insufficient, the only further improvement can be achieved by online measurement of the FEL XUV-to-optical laser timing via timing tools. Details of those developments for FLASH2020+ are described in Chapter 8.

6.5.4 Seeded FLASH1 Beamline

The seeded FLASH1 beamline will potentially provide the ultimate timing stability, since the XUV pulse timing is governed by the seed laser and not by the electron beam. The seed laser will be tightly synchronized by all optical timing distribution to the same optical master oscillator as the pump-probe laser. We will explore options and possible benefits of directly stabilizing the timing of the pump-probe laser to the seed laser. We will decide on the implementation of such a direct seed-laser – pump-probe laser link after evaluating the achieved timing jitter using the first implemented standard optical synchronization and estimating potential benefits. Overall we expect that in a seeded FEL beamline the timing jitter could be reduced by a factor of 5-10 compared to the value of 28 fs r.m.s measured in Schulz et al. 2015.

References

Amplitude Systems (2019). „Compress. Industrial pulse compression module.“ In: *Webpage*. Online.

Baum, P. et al. (2004). „Tunable sub-10-fs ultraviolet pulses generated by achromatic frequency doubling“. In: *Opt. Lett.* 29.14, pp. 1686–1688. DOI: 10.1364/OL.29.001686.

Carbajo, S. et al. (2015). „Efficient narrowband terahertz generation in cryogenically cooled periodically poled lithium niobate“. In: *Opt. Lett.* 40.24, pp. 5762–5765. DOI: 10.1364/OL.40.005762.

Christie, F. et al. (2017). „Generation of Ultra-Short Electron Bunches and FEL Pulses and Characterization of Their Longitudinal Properties at FLASH2“. In: *Proc. of International Particle Accelerator Conference (IPAC'17), Copenhagen, Denmark, 14-19 May, 2017* (Copenhagen, Denmark). International Particle Accelerator Conference 8. Geneva, Switzerland: JACoW, pp. 2600–2603. ISBN: 978-3-95450-182-3. DOI: 10.18429/JACoW-IPAC2017-WEPAB017.

Coddington, I. et al. (2009). „Rapid and precise absolute distance measurements at long range“. In: *Nature Photonics* 3.6, pp. 351–356. DOI: 10.1038/nphoton.2009.94.

Dietz, Th. et al. (2018). „Monolithic multi-pass thin-disk laser amplifier providing near fundamental mode 2.3 mJ pulse energy at 1.4 kW average output power and 950 fs pulse duration“. In: *Laser Congress 2018 (ASSL)*. Optical Society of America, AM2A.4. DOI: 10.1364/ASSL.2018.AM2A.4.

Dubietis, A. et al. (1992). „Powerful femtosecond pulse generation by chirped and stretched pulse parametric amplification in BBO crystal“. In: *Optics Communications* 88.4, pp. 437–440. DOI: 10.1016/0030-4018(92)90070-8.

Fritsch, K. et al. (2018). „All-solid-state multipass spectral broadening to sub-20 fs“. In: *Opt. Lett.* 43.19, pp. 4643–4646. DOI: 10.1364/OL.43.004643.

Fuji, T. et al. (2007). „Generation of sub-two-cycle mid-infrared pulses by four-wave mixing through filamentation in air“. In: *Opt. Lett.* 32.22, pp. 3330–3332. DOI: 10.1364/OL.32.003330.

Hauri, Ch. P. et al. (2011). „Strong-field single-cycle THz pulses generated in an organic crystal“. In: *Applied Physics Letters* 99.16, p. 161116. DOI: 10.1063/1.3655331.

Hirori, H. et al. (2011). „Single-cycle terahertz pulses with amplitudes exceeding 1 MV/cm generated by optical rectification in LiNbO3“. In: *Applied Physics Letters* 98.9, p. 091106. DOI: 10.1063/1.3560062.

Homann, C. et al. (2008). „Octave wide tunable UV-pumped NOPA: pulses down to 20 fs at 0.5 MHz repetition rate“. In: *Opt. Express* 16.8, pp. 5746–5756. DOI: 10.1364/OE.16.005746.

Jeong, Y.-G. et al. (2018). „Direct compression of 170-fs 50-cycle pulses down to 1.5 cycles with 70% transmission“. In: *Scientific Reports* 8.1, p. 11794. DOI: 10.1038/s41598-018-30198-y.

Kaumanns, M. et al. (2018). „Multipass spectral broadening of 18mJ pulses compressible from 1.3ps to 41fs“. In: *Opt. Lett.* 43.23, pp. 5877–5880. DOI: 10.1364/OL.43.005877.

Kida, Y. et al. (2011). „Single 10-fs deep-ultraviolet pulses generated by broadband four-wave mixing and high-order dispersion compensation“. In: *Applied Physics B* 105.4, pp. 675–679. DOI: 10.1007/s00340-011-4809-4.

Köttig, F. et al. (2017). „Generation of microjoule pulses in the deep ultraviolet at megahertz repetition rates“. In: *Optica* 4.10, pp. 1272–1276. DOI: 10.1364/OPTICA.4.001272.

Krasilnikov, M. et al. (2012). „Experimentally minimized beam emittance from an L-band photoinjector“. In: *Phys. Rev. ST Accel. Beams* 15 (10), p. 100701. DOI: 10.1103/PhysRevSTAB.15.100701.

Lang, T. (2019). „chi2D & chi3D simulate the frequency conversion processes between femtoscond laser pulses in birefringent nonlinear crystals“. In: *Webpage*. Online.

Light Conversion (2019a). „Optical Parametric Amplifiers for 1030nm Lasers“. In: *Webpage*. Online.

– (2019b). „Optical Parametric Amplifiers for 800nm Lasers“. In: *Webpage*. Online.

Mak, K. F. et al. (2013). „Tunable vacuum-UV to visible ultrafast pulse source based on gas-

filled Kagome-PCF“. In: *Opt. Express* 21.9, pp. 10942–10953. DOI: 10.1364/OE.21.010942.

Müller, M. et al. (2016). „1kW 1mJ eight-channel ultrafast fiber laser“. In: *Opt. Lett.* 41.15, pp. 3439–3442. DOI: 10.1364/OL.41.003439.

Müller, M. et al. (2018). „3.5 kW coherently combined ultrafast fiber laser“. In: *Opt. Lett.* 43.24, pp. 6037–6040. DOI: 10.1364/OL.43.006037.

Nagisetty, S. S. et al. (2018). „High-energy burst mode thin-disk multipass amplifier for laser Compton X-ray source“. In: *High-Brightness Sources and Light-driven Interactions*. Optical Society of America, EM2B.4. DOI: 10.1364/EUVXRAY.2018.EM2B.4.

Palmer, G. et al. (2019). „Pump–probe laser system at the FXE and SPB/SFX instruments of the European X-ray Free-Electron Laser Facility“. In: *Journal of Synchrotron Radiation* 26.2, pp. 328–332. DOI: 10.1107/S160057751900095X.

Pergament, M. et al. (2014). „High power burst-mode optical parametric amplifier with arbitrary pulse selection“. In: *Opt. Express* 22.18, pp. 22202–22210. DOI: 10.1364/OE.22.022202.

Pergament, M. et al. (2016). „Versatile optical laser system for experiments at the European X-ray free-electron laser facility“. In: *Opt. Express* 24.26, pp. 29349–29359. DOI: 10.1364/OE.24.029349.

Russbueldt, P. et al. (2015). „Innoslab Amplifiers“. In: *IEEE Journal of Selected Topics in Quantum Electronics* 21.1, pp. 447–463. DOI: 10.1109/JSTQE.2014.2333234.

Schmidt, B. E. et al. (2017). „Highly stable, 54mJ Yb-InnoSlab laser platform at 0.5kW average power“. In: *Opt. Express* 25.15, pp. 17549–17555. DOI: 10.1364/OE.25.017549.

Schulz, S. et al. (2015). „Femtosecond all-optical synchronization of an X-ray free-electron laser“. In: *Nature Communications* 6.1, p. 5938. DOI: 10.1038/ncomms6938.

Schunemann, P. G. (2017). „New Nonlinear Crystals for the Mid-Infrared“. In: *Nonlinear Optics*. Optical Society of America, NTu2A.1. DOI: 10.1364/NLO.2017.NTu2A.1.

Varillas, R. B. et al. (2014). „Microjoule-level, tunable sub-10fs UV pulses by broadband sum-frequency generation“. In: *Opt. Lett.* 39.13, pp. 3849–3852. DOI: 10.1364/OL.39.003849.

Wallmeier, H. et al. (1988). „Continuously tunable VUV radiation (129-210 nm) by anti-Stokes Raman scattering in cooled H2“. In: *Applied Physics B* 45.4, pp. 263–272. DOI: 10.1007/BF00687155.

Will, I. et al. (2005). „The upgraded photocathode laser of the TESLA Test Facility“. In: *Nuclear Instruments and Methods in Physics Research Section A: Accelerators, Spectrometers, Detectors and Associated Equipment* 541.3, pp. 467–477. DOI: 10.1016/j.nima.2004.12.007.

Winkelmann, L. et al. (2018). „Compact Photo-Injector and Laser-Heater Drive Laser for the European X-ray Free Electron Laser Facility“. In: *Conference on Lasers and Electro-Optics*. Optical Society of America, STu4O.5. DOI: 10.1364/CLEO_SI.2018.STu4O.5.

Winters, D. et al. (2018). „1 MHz Ultrafast Cascaded VUV Generation in Negative Curvature Hollow Fibers“. In: *Conference on Lasers and Electro-Optics*. Optical Society of America, STh1N.2. DOI: 10.1364/CLEO_SI.2018.STh1N.2.

Zapata, L. E. et al. (2018). „One Joule 500 Hz cryogenic Yb:YAG Laser Driver“. In: *Laser Congress 2018 (ASSL)*. Optical Society of America, ATu6A.1. DOI: 10.1364/ASSL.2018.ATu6A.1.

7 Beamlines and Instruments

A main goal of FLASH2020+ concerning beamlines and endstations is the optimization of the scientific user output over the next 10-15 years of FLASH operation. A combination of permanently and semi-permanently (i. e. a few months at a time) installed endstation instruments with some open-port beamlines for specialized user applications has proven very successful in fostering solid scientific applications, attracting and supporting inexperienced users as well as bringing lighthouse experiments into successful operation. Reduction of the machine electron energy working points to two or three will significantly reduce setup times and thus increase user beamtime. Over the past 1.5 decades, state-of-the-art beamlines and endstations have been developed at FLASH1 and FLASH2. A goal of the beamline design proposed for FLASH2020+ is to keep as many of these advanced developments and the overall photon beamline concept while at the same time upgrading photon diagnostics (see Chapter 8), optics and endstations to account for the newest scientific demands of the user community, technical developments and specific experimental requirements where necessary. Thus, these upgrades are fully covering the FLASH2020+ science case.

The machine design for FLASH2020+ has been chosen such that both, FLASH1 and FLASH2, cover a broad wavelength region. FLASH1 will offer a range from 4 nm to 60 nm in seeded or SASE configuration (Chapter 4) while FLASH2 will provide 1 nm to 60 nm in SASE mode with the option of special operation schemes (Chapter 5). These boundary conditions are also reflected in the beamline design for FLASH1 and even more so for FLASH2, where the dedicated short-wavelength (>0.8 nm) beamlines FL24 and FL23 are combined with beamlines for the longer wavelengths (>4 nm with high reflectivity). The latter exhibit larger incidence angles for the beamline optics in order to separate the endstations and optimize their footprint within the available experimental hall space. A high overlap of possible beam parameters for both, FLASH1 and FLASH2, also allows for efficient parallel beamtime scheduling.

As mentioned above, the FLASH user facility is a mixture of open port beamlines and permanent experimental stations as well as semi-permanent instruments operated by the facility and collaboration partners respectively. The semi-permanent instruments can within a short time be attached to one of the open ports. Following user demands, in the future, the option of an (at least partially) open port is foreseen to be offered at four beamlines: the high-resolution monochromator beamline PG2, the THz-XUV pump-probe beamline FL11 (previously BL3), and the dedicated short-wavelength beamlines FL24 and FL23, where FL23 will also provide a monochromator.

Presently, four of the permanent and semi-permanent state-of-the-art experimental stations are the main “workhorses” for experiments at FLASH. The mostly used ones are the permanent installations CAMP at beamline BL1 (for AMO, femto-chemistry and imaging) and REMI at beamline FL26 (for AMO and femto-chemistry) as well as the HEXTOF and WESPE photoemission chambers for condensed matter and surface chemistry experiments. The latter two are typically used at the PG2 monochromator beamline for several experiments in a row and hence stay at the PG2 platform for one to two months about twice a year. With the four mentioned chambers, typically two thirds of the FLASH1 experiments and about 50 % of the FLASH2 experiments are covered. The permanent Raman-endstation at beamline PG1 for high-resolution (time-resolved) RIXS spectroscopy is currently completing the commissioning phase and will soon be added to the FLASH portfolio.

In addition to these five instruments, we have a "pool" of further experimental chambers which are already used or can soon be used for in-house as well as external experiments: the MULTI-P chamber in particular for plasma and warm dense matter as well as AMO physics, the MUSIX chamber for solid-state spectroscopy as well as a planned future endstation for THz related condensed matter experiments at beamline FL11 (former BL3) at FLASH1. The chambers' capabilities, their potential within the FLASH2020+ program and envisioned future upgrades are briefly outlined below, additional details and an in-depth description can be found in the cited references.

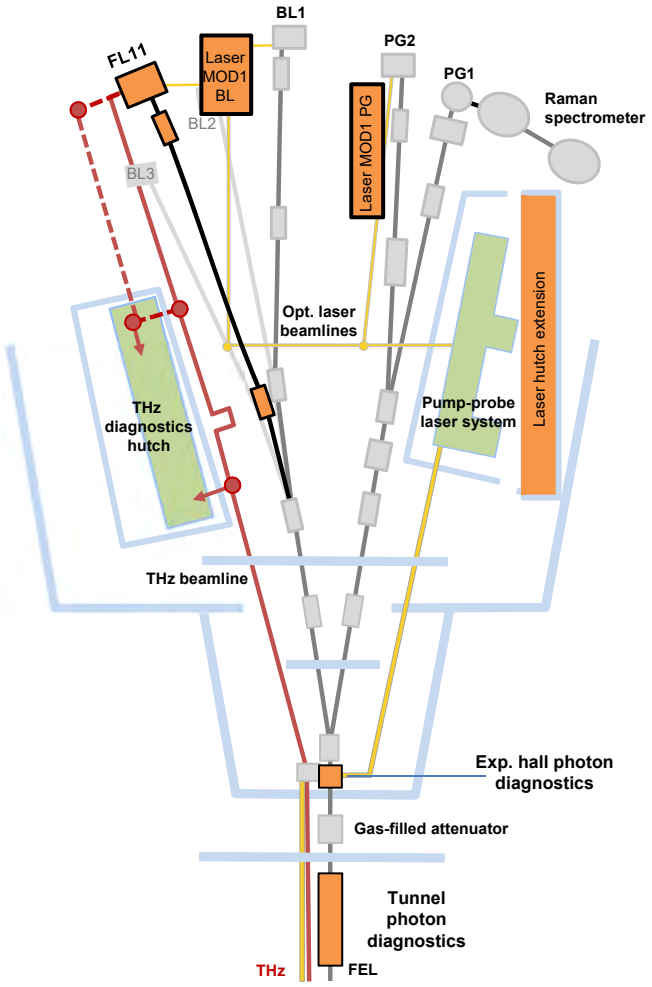

Figure 7.1: *Sketch of the changes and updates of the FLASH1 beamlines within the coming years (highlighted in black and orange). Since the focus in this chapter is on FEL beamlines and their modifications, only the major changes regarding the optical laser are sketched. For more details in this respect, the reader is kindly referred to Chapter 6.*

Summary of Proposed Upgrades for the FLASH Photon Beamlines

As described in detail below and shown in Figure 7.1, the main upgrades envisaged for the FLASH photon beamlines are a complete rebuilding of the FLASH1 photon diagnostics in the FLASH1 tunnel and the beam distribution area (BDA) in the experimental hall. These systems as well as the beamline alignment concept are outdated and will be replaced with new instruments developed for FLASH2.

At FLASH1, the second major upgrade is a new beamline "FL11" joining the options of BL2 and BL3. This will allow for an advanced focusing system for the new beamline, shallower incidence angles for transport of short wavelengths to the new (semi-)permanent THz-XUV pump-probe endstation and advanced pump-probe laser installations. Following user demands, this new endstation will focus on condensed matter experiments, such as THz-enabled magnetism and surface physics/chemistry studies. Together with upgrades in the THz and XUV endstation diagnostics, this will allow to fully profit from the unique THz facility at FLASH and will fill a gap in the FLASH endstation portfolio.

At FLASH2, most installations are state-of-the-art and require only a limited number of adaptions to user needs as well as the new lasing concepts (Chapter 5) over the years. A major focus here will be to complete the pulse-length compensating short-wavelength monochromator beamline FL23, which is currently in the design and procurement phase.

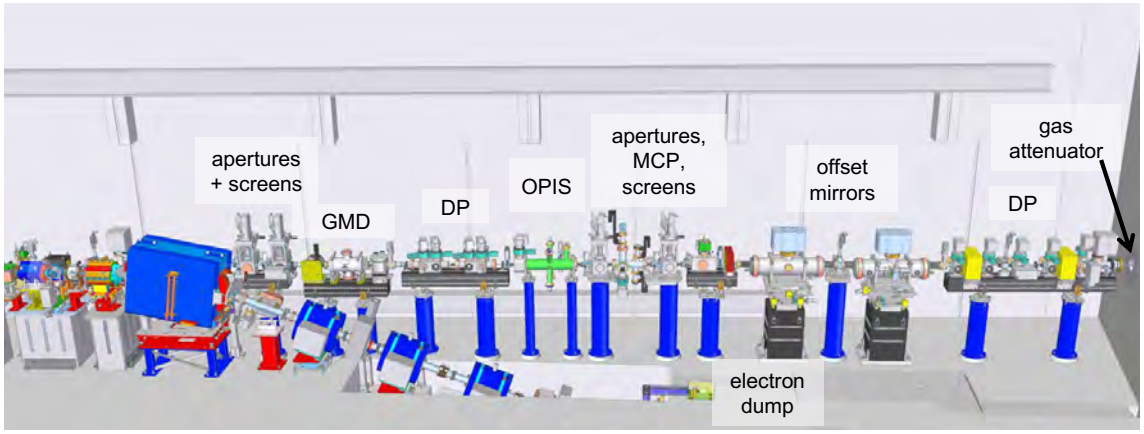

Figure 7.2: *Photon Beamline at the end of the FLASH2 tunnel with the electron beamline in front of it. From left to right: vertical manipulators with apertures and Ce:YAG crystals, respectively, integrated in differential pumping chambers; GMDs (for intensity and beam position) on granite; differential pumping chambers (DP); OPIS (online spectrometer, in green); Aperture unit; MCP (intensity) ; Ce:YAG unit; FEL absorber/shutter; two offset mirror chambers with a pneumatically actuated Ce:YAG screen in between; DP stages for gas attenuator.*

7.1 FLASH1 Beamlines

7.1.1 XUV Photon Beamline in the FLASH1-Tunnel (Planned Upgrades)

The XUV photon beamlines of FLASH1 have to a large extent been designed and built before 2005, are thus nearly 15 years old, and require significant upgrades, which form the main activity of FLASH2020+ for the photon beamlines. Some of the basic photon diagnostics in the tunnel do even stem from the first setup at the "TESLA Test Facility" around the year 2000.

New, more compact and advanced designs for a number of photon diagnostics and beamline components have been developed within the FLASH2 upgrade of FLASH, which will now be transferred to FLASH1 with some adaptions due to space restrictions. In particular, the concept of a pair of alignment mirrors in the tunnel as realized at FLASH2 (Figure 7.2) has proven very effective to provide a stable, reproducible photon beam trajectory into the experimental hall. This concept significantly reduces setup times for complex beamlines and provides excellent focusing quality and a much higher overall stability of the advanced optics systems of the beamlines.

At FLASH1 on the contrary, providing a reproducible photon beam pointing presently has to be realized by the accelerator setup steering the electron beam, which significantly prolongs the machine tuning or requires extensive realignment of the entire beamlines. The advantages of the two alignment mirrors inside the FLASH tunnels outweigh the slightly reduced beamline transmission which results from the two additional reflecting surfaces.

Adapting the two mirror concept to FLASH1 allows the beam to enter the FLASH1 hall on the same beam path as it does now, despite the planned 400 mm horizontal offset of the new undulators (Chapter 4). Therefore, the available FLASH1 beamlines PG, CAMP and BL3 for THz-XUV pump-probe can be operated as before without changes to the beam transport geometry and only require a few upgrades in view of their age and new technological developments. Additionally, it is expected that, similarly to FLASH2, this new design limits all radiation safety issues to the FLASH1 tunnel forgoing the need for a "BDA" area in the FLASH1 hall and allowing free access to the entire beamline system in the experimental hall.

Unlike at FLASH2 (Figure 7.2), for FLASH1 the first tunnel mirror will be placed at the beginning of the photon diagnostics section while the second will stay directly in front of the differential pumping for the gas attenuator to generate the larger offset of 400 mm. The current length of the FLASH1 photon diagnostics section is

approximately 14 m. To be able to compensate the aforementioned 400 mm offset, an incidence angle between about 1.1° and 1.5° is an appropriate choice for the alignment mirror pair. The precise angle will be chosen depending on the detailed technical design and machine geometry, 1.1° would require a distance of 10.4 m from mirror center to mirror center, while at 1.5° this length is 7.6 m, both fitting into the 14 m overall length.

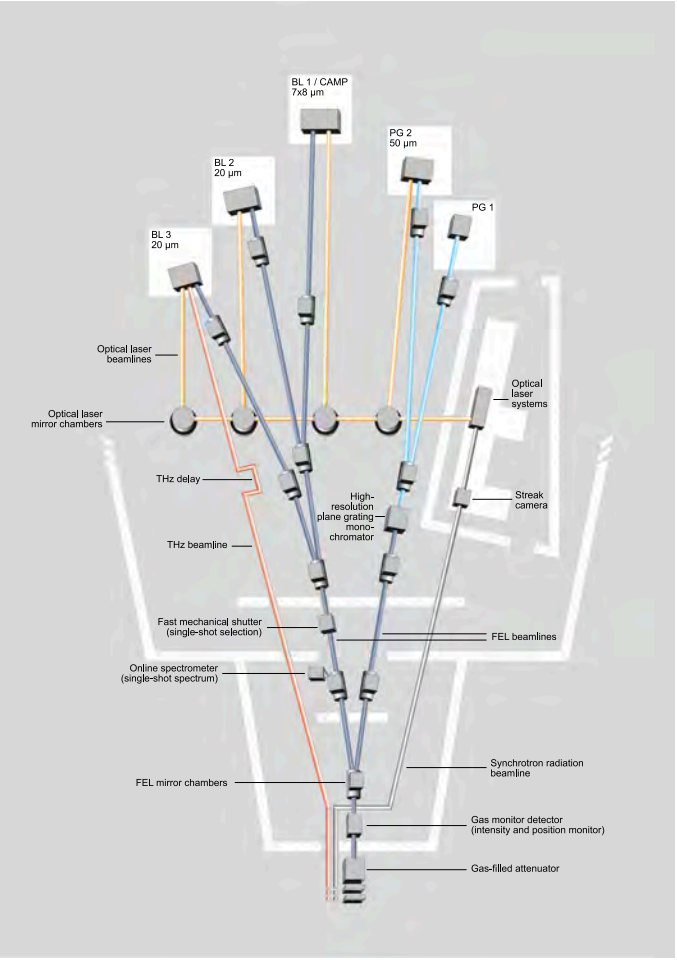

Figure 7.3: *Current status of the FLASH1 experimental hall with beamlines and main components (Tiedtke et al. 2009). For planned changes see Figure 7.1.*

A significant technical challenge is posed by the floor conditions in the electron beam dump area. Currently, the dump is covered by individual concrete blocks with substantial gaps leading to a very unstable ground for the FLASH1 photon diagnostics section, hence improvements on the tunnel floor are mandatory for an advanced photon diagnostics section with improved component stability. The individual photon diagnostics components are described in Chapter 8. Being part of the new machine layout, the 400 mm offset of the new FEL undulators with respect to the THz undulator also leads to a separation of the beam path of the XUV and the THz beams allowing a more independent operation of these two sources. The THz beamline can thus be rebuilt to improve the THz transmission (Section 7.1.5) to the THz hutch and to the THz-XUV pump-probe endstation.

7.1.2 FLASH1 Experimental Hall "Albert Einstein"

Figure 7.3 shows the present layout of the FLASH1 user facility. On this schematic, the FEL, the THz beamline and a synchrotron radiation beamline (originating from the last bending magnet deflecting the electrons into the beam dump) enter into the hall from the bottom. Before and during the separation into the different beamlines, the FEL radiation passes through a set of photon diagnostics and beam manipulation tools, such as a set of four gas-monitor detectors (GMD) for intensity and beam position determination, an attenuation system based on gas absorption, a set of filters and a fast shutter.

The BL beamlines are equipped with a variable-line-spacing (VLS) spectrograph for online determination of the FLASH wavelength spectrum in parallel to the user experiments. The FLASH beam is delivered directly across plane, grazing incidence mirrors to the beamlines BL1 with the CAMP chamber, as well as BL2 and BL3 which mainly offer different beam manipulation tools. The beamlines PG1 and PG2 comprise a high-resolution monochromator allowing for the selection of a narrower spectral width from the FEL pulse with a resolving power up to few 10^4.

At FLASH1, it is a prerequisite to keep the beam path through the PETRA tunnel fixed and thus provide the same entrance into the Albert Einstein hall to avoid the need to adapt and reposition the entire beamline and infrastructure system. As mentioned before, this will be taken care of by installing the new offset mirrors in the FLASH1 tunnel. The PG beamlines (Section 7.1.3) as well as beamline BL1 with the CAMP endstation (Section 7.1.4) offer exciting science possibilities and will be kept with only a number of updates described below. The PG beamline will offer PG1 with the permanent

Raman spectrometer and pump-probe capabilities, while PG2 will maintain an open port for either user supplied endstations or the in-house endstations WESPE and HEXTOF (see Section 7.1.3).

For ultra-fast time resolved studies, the facility provides two additional light sources for femtosecond pump-probe experiments. A femtosecond optical laser synchronized to the FEL (Chapter 6) is situated in a laser hutch (on the right of Figure 7.3) and from there distributed to the end stations in a separate beamline system. A THz source is generated by a dedicated electromagnetic undulator through which the FLASH electron beam passes downstream of the FEL undulators (Section 4.3).

7.1.3 PG Beamlines

For experiments that require a smaller spectral bandwidth than that of the natural SASE radiation or to clean the seeded FEL beam from unwanted higher harmonic spectral components, a monochromator is required. At FLASH1 a high-resolution plane grating (PG) XUV-monochromator with two beamline branches PG1 and PG2 has been in user operation since 2005 (Martins et al. 2006). The beamline can either deliver a highly monochromatic beam with an energy resolution up to a few 10^{-5} or the non-monochromatized FEL radiation. While PG1 hosts a XUV double-stage Raman spectrometer dedicated for time-resolved high-resolution Resonant Inelastic X-ray Scattering (RIXS) experiments as a permanent endstation, PG2 serves as an open port for various types of user experiments. In addition, a XUV split&delay unit integrated in PG2 allows for XUV-pump/XUV-probe experiments (Sorgenfrei et al. 2010). Furthermore, the femtosecond optical laser system can be combined with the FEL radiation for multicolor pump-probe experiments. Conceptually, the open port of the PG2 beamline has proven efficient in housing different (semi-permanent) experimental stations (see below) and it is proposed to keep that flexibility, also to efficiently allow method developments at FLASH (in particular when BL2 and BL3 will be combined into FL11).

Planned Upgrades for the PG Beamlines

For a broad range of user experiments an energy resolution in the order of 10^{-3} to 10^{-4} is needed, which is well provided by the two gratings currently installed. However, all optical beamline components are coated with amorphous diamond-like carbon (DLC) optimized for the fundamental FLASH photon energy range of 20 eV to 270 eV. The high reflectivity of the DLC coating ensures high damage resistance and excellent beamline transmission below 270 eV, but offers only very moderate transmission in the range between the carbon K-edge and oxygen K-edge.

In view of great interest of the condensed matter community to also use higher photon energies – FLASH1 presently reaches far beyond the oxygen K-edge in the 3rd harmonic – and the fact that for all applications the photon flux should be maximized for the selected conditions, it is planned to upgrade the PG2 beamline optics with Ni-coatings to increase the transmission efficiency at high harmonic photon energies.

Furthermore, it is envisioned to upgrade the monochromator unit with a third, low line density grating, acting as a filter to select high harmonics. First grating design studies have already been carried out (Gerasimova et al. 2011) and resulted in a 80 lines/mm variable groove depth grating which would increase the beamline transmission in the range of 600 eV to 900 eV by more than one order of magnitude while keeping the pulse stretching well below 20 fs .

At PG2, the toroidal refocusing mirror unit currently limits the focal spot size to around 50 µm$\times$50 µm at a fixed location. In order to provide a flexible beamline focus and also be able to change the laser fluence at a sample on demand, it is planned to implement variable focusing at PG2 by a suitable Kirkpatrick-Baez (KB, Kirkpatrick et al. 1948) mirror system. Since this modification has implications on the overall beamline layout, a possible reduction of the number of optical elements in the beamline still needs to be studied.

Concerning beamline branch PG1, an upgrade of the existing KB-mirror mechanics based on compact in-vacuum hexapods will improve and guarantee the needed precision and reproducibility of the beamline microfocus on

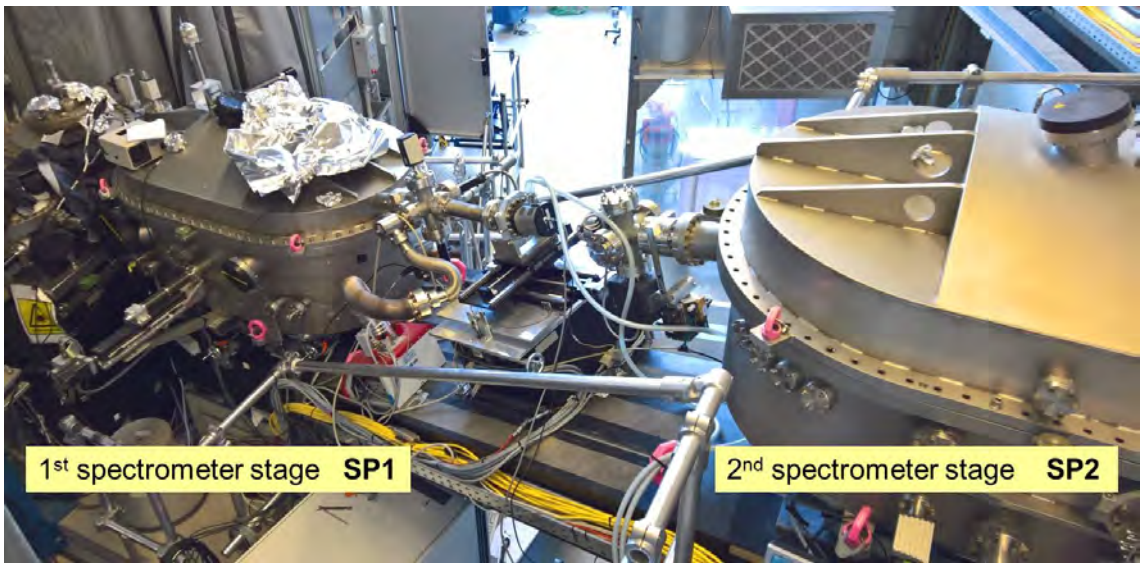

Figure 7.4: *Two stages of the PG1 Raman spectrometer.*

the sample, which directly enters into the XUV Raman spectrometer resolution (Dziarzhytski et al. 2016).

Permanent Endstation at Beamline PG1: RAMAN Spectrometer

Beamline PG1 is permanently equipped with a unique high-resolution XUV double-stage Raman spectrometer (Figure 7.4), dedicated to resonant inelastic soft X-ray scattering (RIXS) experiments in the spectral region from 20 eV to 200 eV. The optical design of the spectrometer is based on a confocal additive coupling of two high-resolution spectrometers (SP1 and SP2) mediated by a middle slit for elastic line and stray light suppression. Each spectrometer is equipped with two off-axis parabolic mirrors and a set of interchangeable plane gratings. The spectrometer has no entrance slit and disperses along the vertical direction, thus the vertical size of the focal spot produced by the PG1 beamline KB-refocusing optics on the sample together with the resolution of the primary monochromator of PG1 defines the resolution of the first spectrometer stage to a large extent. The spectrometer has a design spectral resolution of 2 meV to 20 meV (double spectrometer). Such an energy resolution provides information about the dynamic properties of solid matter approaching the Fourier limit.

Recently, the FLASH1 pump-probe laser beamline has been extended to the Raman spectrometer endstation, now allowing time-resolved RIXS experiments at the transition metal M-edges (20 eV to 210 eV) with an energy resolution of currently $\leq$60 meV (single spectrometer stage) and a time resolution of $\leq$300 fs (FWHM).

Planned Upgrades for the PG1 Endstation

The experimental sample chamber (EC) of the Raman spectrometer has originally been designed to exclusively accept solid samples. In order to extend the instruments capabilities, an upgrade is envisioned to provide the possibility of time-resolved RIXS experiments on liquid jet samples as already requested by interested users. Furthermore, the current chamber is missing appropriate online diagnostics for measuring the incoming FEL intensity, focal spot size and position. To equip the chamber with corresponding diagnostic tools, such as a compact wavefront sensor, a redesign of the EC will be obligatory. Since such an upgrade requires major modifications of the differential pumping section between the KB-mirror pair and the EC, a technical design study needs to be undertaken first.

Semi-Permanent Endstation for PG2: "WESPE" (Wide-angle Electron SPEctrometer)

High repetition rate XUV FELs are an ideal light source for time-resolved photoemission experiments. FLASH offers the best prerequisites, by reaching the oxygen and carbon 1s core-levels, to investigate surface dynamics, e. g. catalytic reactions on solids or ultra-fast magnetization effects as well as charge migration and charge transfer in layered systems. The WESPE endstation (Figure 7.5) offers best conditions to perform such core-level photoemission experiments by providing a combination of a time-of-flight analyzer (Specs, Themis 1000) together with a segmented, position-sensitive delay-line detector (Surface Concept, 3D-DLD-4Q).

In this configuration one benefits from a high detection efficiency of the segmented DLD and its capability of single event detection as well as from the wide detection angle and the high energy resolution (approx. 200 meV) within a large energy window (up to 18 eV). The experimental setup is consisting of a µ-metal measurement chamber, which contains the spectrometer and beam diagnostic tools, as well as a preparation chamber.

The preparation chamber is permanently equipped with standard sample preparation tools such as a sputter gun and a mass spectrometer and provides a LEED/AES to check the sample quality. In addition to the permanent equipment, the setup can be extended by a variety of flexible installations. Depending on the demand of the participating users, evaporators, a quartz crystal balance, a gas-inlet system or a cleaving tool can be inserted.

The sample holder system is designed in a flexible way. A variety of different samples, which differ in material, size and shape and needs of preparation can be transferred into the experiment. Also the measurement conditions are for some experiments very crucial. The manipulator, which serves both chambers, contains a He-cryostat to provide tunable temperatures on the sample environment down to a minimum temperature of approximately 25 K. It is also possible to heat or flash the sample up to about 2000 °C.

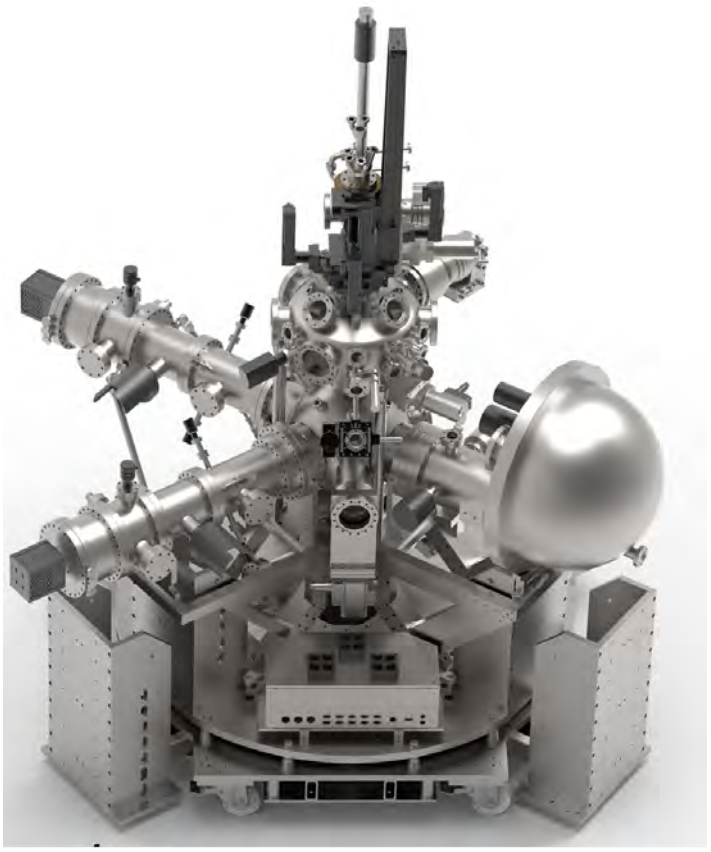

Figure 7.5: *3D model of the WESPE chamber. Courtesy: S. Gieschen and H. Meyer, Universität Hamburg.*

Planned Upgrades for WESPE

In the near future we plan to install a second time-of-flight spectrometer which increases the overall signal intensity and makes, for some systems, even coincidence measurements of bulk- and surface- related dynamics possible.

Semi-Permanent Endstation for PG2: "HEXTOF" ("Momentum Microscope")

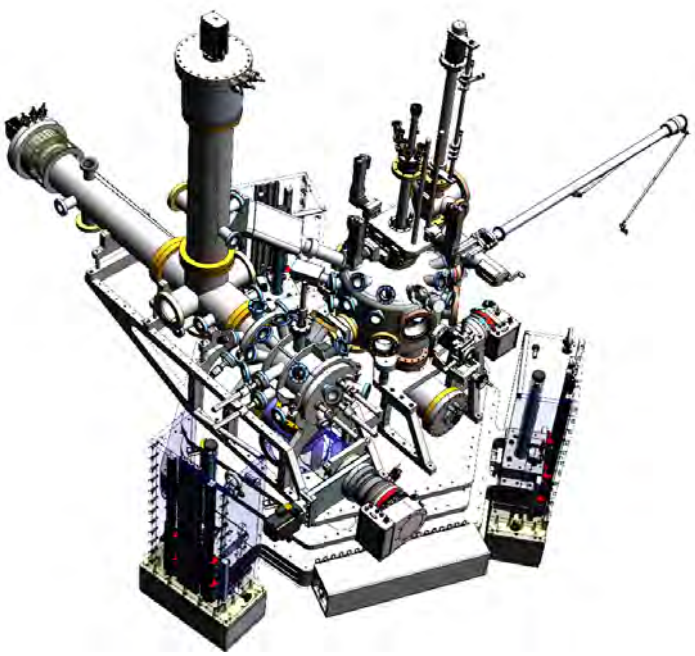

Figure 7.6: *3D model of the HEXTOF chamber. Courtesy: S. Gieschen and H. Meyer, Universität Hamburg.*

A time-of-flight (TOF) momentum microscope is a versatile tool for studies in the area of condensed matter physics, in particular charge carrier dynamics, surface catalysis and chemistry on surfaces via space-, time- and spin-resolved photoemission. The HEXTOF momentum microscope allows simultaneous detection of the entire band structure with unprecedented efficiency in the full surface Brillouin zone with up to 8 $Å^{-1}$ diameter and several eV binding energy range, resolving about 2.5×10^5 voxels, or the angular pattern of core level photoelectrons, respectively, for each time step in a pump-probe experiment. The experimental approach combines time- and momentum-resolved photoelectron, parallel spin detection, X-ray photoelectron spectroscopy (XPS), and X-ray photoelectron diffraction (XPD) as well as time-resolved molecular tomography into a single experiment. The setup consists of a spin-filtered time-of-flight momentum microscope (Kutnyakhov et al. 2016; Schönhense et al. 2017; Kutnyakhov et al. 2020) and a preparation chamber installed on a dedicated adjustable support frame. A fully automatized (x, y, z and Θ directions) frame fits into the laser laboratory with HHG source, FLASH1 / PG2 beamline, PETRA III / P04 beamline (DESY, Hamburg) or the future Soft X-ray Port (SXP) at SASE3 (European XFEL). The main chamber is an all µ-metal UHV chamber equipped with a cryostat as well as an electron beam sample heating system installed on a high precision hexapod for sample manipulation. The preparation chamber is equipped with a cryostat, a mass-spectrometer, a LEED/AES system, a sputter gun, a cleaving tool, evaporators and a quartz crystal balance monitor for *in-situ* sample preparation and characterization.

Planned Upgrades for HEXTOF

A key part of the system is the 3D (k_x, k_y, t)-resolving delay line detector (DLD) (Oelsner et al. 2010). The present single-channel DLD (resolution 150 ps, 80 mm active area, spatial resolution about 80 µm) can only detect one count per microbunch. For the conditions at-FLASH (presently up to 5000 pulses/s) it would be highly desirable to establish multi-hit capability. At present we have used three different detectors, with active area of 60 mm and 80 mm in diameter: a single quadrant DLD (DLD8080), a segmented 4-quadrant DLD (DLD8080-4Q) and an 8 segment DLD (DLD-8s). Moreover, a 256-channel DLD (array of 256 discrete DLD units in a 3D stack), which is developed for this project and currently tested at the manufacturer (Surface Concept 2019), will be used as major upgrade of the setup in order to increase multi-hit capability. A conservative estimate suggests an increase in detection efficiency by at least a factor of 50, retaining the high time resolution.

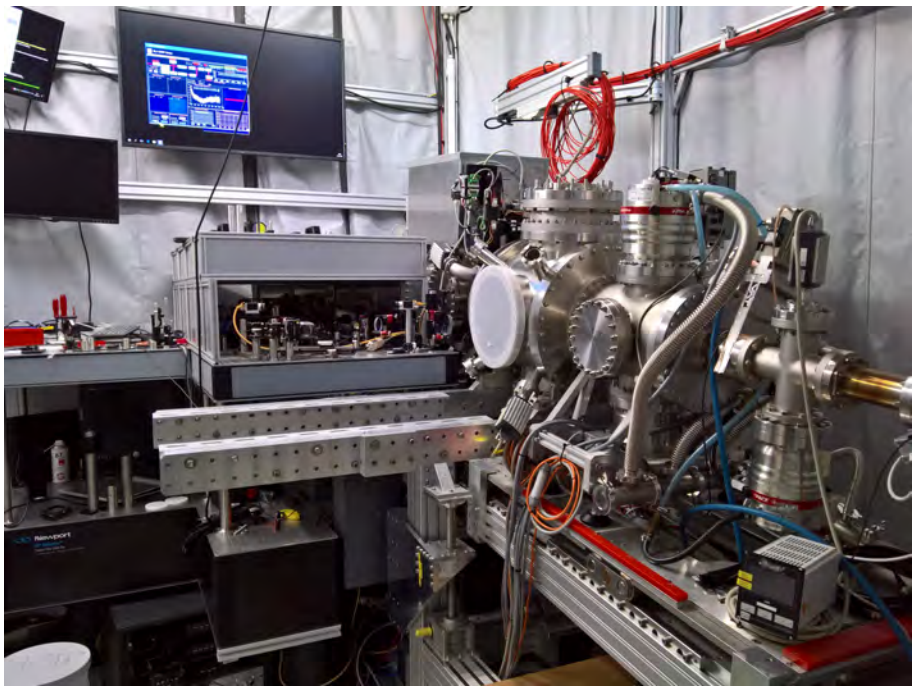

Figure 7.7: *CAMP chamber and pump-probe laser setup inside the CAMP laser safety tent.*

7.1.4 CAMP (CFEL Advanced study group Multi-Purpose chamber) at Beamline BL1

The non-monochromatic beamline BL1 at FLASH was over the last years upgraded with new transport and Kirkpatrick–Baez (KB, Kirkpatrick et al. 1948) focusing optics, and a new permanent endstation, CAMP (Figure 7.7), was installed (Erk et al. 2018). This endstation enables a wide range of experiments from atomic, molecular, and cluster physics to material and energy science, chemistry and biology. The CAMP endstation's modular and flexible layout allows for simultaneous use of large-area single-photon-counting pnCCD photon-detectors and VMI- or COLTRIMS-type electron- and ion-spectrometers, with various (user-provided) solid-state sample holders, gas beams, cluster sources, liquid-jets, (nano-)particle injectors and other sample delivery systems.

For experiments using optical pulses as pump or probe, the endstation has dedicated laser in-coupling optics and diagnostics provided in a permanent laser setup at the BL1 beamline for use with the FLASH1 pump-probe lasers (Redlin et al. 2011). In addition, the beamline is equipped with a dedicated XUV split&delay unit (DESC) (Sauppe et al. 2018) that is based on multilayer mirrors and can provide two pulses with variable delay ranging from (sub-)femtosecond to 650 ps.

The wavelength-independent tight focusing of the KB mirrors of $\approx 7\,\mu m \times 8\,\mu m$ (v x h), in combination with the pnCCD imaging detectors enables scattering measurements, e. g. of single nanoparticles, across the full parameter range of FLASH1.

First experiments included both, measurements of static processes, such as magnetic scattering from magnetic domains and single particles, as well as optical-laser-pump FEL-probe experiments, investigating femtosecond dynamics in thin-films and single particles, with sizes from a few micrometers down to 10 nm in diameter. Other experiments utilize the double-sided VMI spectrometers, in combination with the permanent laser setup and the FEL pulses, to investigate femtosecond molecular dynamics in the gas phase, for example by means of Coulomb explosion imaging, ion-electron correlation spectroscopy or ion-covariance mapping.

The system is ready for future upgrades of the FLASH accelerator towards higher photon energies and for operation with higher harmonics, as the beamline mirrors and detector systems are fully capable of going to the oxygen K-edge photon energy and beyond.

Planned Upgrades at CAMP

One major upgrade at CAMP is the implementation of novel fast optical-imaging cameras, named Timepix3, enabling simultaneous velocity map imaging (VMI) of all ionic fragments and electrons. This approach results in more data per ionization event, the possibility to investigate correlations between the fragments, and the acquisition can run at the full repetition rate of FLASH (up to 1 MHz). The Timepix3 camera – being member of the Medipix family – is the upgraded version of the Timepix camera which has been successfully tested at FLASH (Fisher-Levine et al. 2018). It possesses an improved version of the readout chip, substantially less dead-time and a few nanosecond time resolution. Hence, it is ideally suited for multi-hit VMI measurements at a high repetition rate FEL like FLASH. The Timepix3 CMOS chip has been designed by CERN, NIKHEF and Bonn University. Within the Medipix collaboration, the DESY detector group FS-DS is strongly involved in the Timepix developments, particularly focusing on the readout electronics.

It is furthermore planned for the near future to complement the pnCCDs at CAMP with the newly developed PERCIVAL detector for imaging applications in the soft X-ray range beyond 250 eV. The PERCIVAL (**P**ixelated **E**nergy **R**esolving **C**MOS **I**mager, **V**ersatile **A**nd **L**arge) detector system is a collaborative development of DESY, Rutherford Appleton Laboratory/STFC, Elettra Sincrotrone Trieste, Diamond Light Source, and the Pohang Accelerator Laboratory. The presently tested, frontside illuminated (FSI) version of the 'P2M' (Percival 2 Megapixel) detector (Wunderer et al. 2019) has an imaging area of $4\times4\,\mathrm{cm}^2$ with 1408×1484 pixels of $27\times27\,\mu\mathrm{m}^2$. The sensor module is two side buttable, and allows clover-leaf like arrangements of up to 4 sensors modules. Since its pixel size is about 9 times smaller than the pixels of the pnCCDs, it allows for higher position, respectively q-space resolution (depending on the specific geometry). At FLASH, the backside Illuminated (BSI) version will be employed. Due to its relatively low noise ($<15\ \mathrm{e}^-$ rms), single photon counting would be possible at the 250 eV energy level and above. Moreover, its adaptive gain switching allows each pixel to automatically 'decide' in which gain stage it should work on a frame-to-frame basis. This boosts the dynamic range to 1-50000 photons @250 eV per pixel per frame. This is exceeding the dynamic range of the pnCCDs which work with a manually adjustable gain by about two orders of magnitude. In summary, in view of the planned extension of FLASH towards higher soft X-ray energies beyond the C 1s edge, the PERCIVAL detector will be a versatile addition to the FLASH detector suite.

To profit fully from the high repetition rate of FLASH, two further developments – on a timescale of 5-10 years – are ongoing. The first is to couple an amplifying sensor (LGAD) to the existing AGIPD (Allahgholi et al. 2019) detector in order to extend its sensitivity to lower energies. Secondly, a new $\geq$100 kHz X-ray imaging detector, based on hybrid pixel technology and amplifying sensors, is foreseen to be developed by the DESY detector group FS-DS for CW FELs as well as diffraction limited storage rings (DLSRs).

7.1.5 Upgrade: THz-XUV Pump-Probe Instrument at FL11 (Present BL3)

Development of the New XUV beamline FL11

Over the last years it became evident that, with the new open port beamline FL24, the reaction microscope (REMI) permanently installed at FL26, and due to its large overlap with the capabilities of beamline BL3, beamline BL2 has had a very low occupancy. In other words, one upgraded beamline, to be named FL11, could take the load of BL2 and BL3 while even performing better. For this reason, we propose to reduce the number of BL beamlines and keep only beamlines BL1 with CAMP and FL11 (former BL3) with the THz-XUV pump-probe option (Figure 7.1), both in combination with the upgraded pump-probe laser (Figure 6.2). As shown in Figure 6.6 (laser chapter), the space of the BL2 beamline and endstation will then be used for new, much more efficient laser beamlines and laser infrastructure for CAMP and FL11.

Note that, as is detailed in Chapter 6 and driven by user demands, significant upgrades are needed in the pump-probe laser infrastructure for FLASH1 including a new pump-probe laser with an extension of the laser hutch, new advanced beamlines based on the FLASH2 concept for transporting the laser to the endsta-

tions and user experiments, and in particular the laser infrastructure at the experimental endstations. The additionally required space for this laser infrastructure is, as mentioned above, generated when combining BL2 and BL3 to FL11.

Most of the main drivers of THz-XUV pump-probe experiments are condensed matter and surface physics related, such as studies on magnetism. These experiments will benefit tremendously from the option to reach the 3d-metal L-edges. At the same time, due to space charge limitations XUV intensities required for these experiments are very small, typically in the 100 nJ range per pulse. Therefore, we intend to optimize the beamline transmission regarding shorter wavelengths and change the beamline mirrors of FL11 from the current 3° incidence angles to 2°, but can keep the number of mirrors/deflections in order to still have sufficient distance between CAMP and the FL11 endstation. Extending the wavelength range includes a choice of optimized optics coatings (Pt, Ni and C) which will lead to a total beamline transmission of >15 % down to 1.8 nm and >1 % down to 1 nm.

Furthermore, the focusing concept of BL3 is outdated since it uses a fixed ellipsoidal mirror for focusing or the back-reflecting multi-layer option for combination with the THz undulator beam. The back-reflecting mirror concept will be dispensable with the THz doubler as described in Section 4.3. Hence, in connection with the upgrade of THz performance, we propose to upgrade the XUV FEL beamline with a KB system with variable focus and a semi-permanent endstation for solid state and surface physics/surface chemistry experiments (see below). In dedicated user workshops the detailed configuration of FL11 and the proposed semi-permanent endstation are planned to be finalized.

New Beamline for Transport of the THz Radiation

In the current FLASH1 machine setup, XUV and THz undulators are in line, one after the other. Behind the electron dump magnet, the THz radiation is separated from the XUV and sent to its own beamline by a THz mirror with a 10 mm center aperture for the XUV beam. The concept is based on the fact that the THz divergence is much larger than the XUV divergence, and hence for THz wavelengths larger than about 50 µm, most of the THz beam can be collected despite the hole.

As part of the FLASH1 XUV undulator beamline modifications within FLASH2020+, as described in Chapter 4 and Section 7.1.1, the photon beam path of the THz radiation will be separated from the XUV since the THz sources will be installed in the electron beamline parallel to the XUV photon diagnostics section behind a dogleg for the electron beam (Section 4.3). This will allow completely parasitic operation of “THz-only” experiments independent of the XUV FEL use at potentially another beamline. At the same time, the transmission of shorter wavelengths (in 10 µm to 30 µm range) will be increased by as much as 50 % (cf. Figure 7.8), since the outcoupling mirror with hole can be omitted.

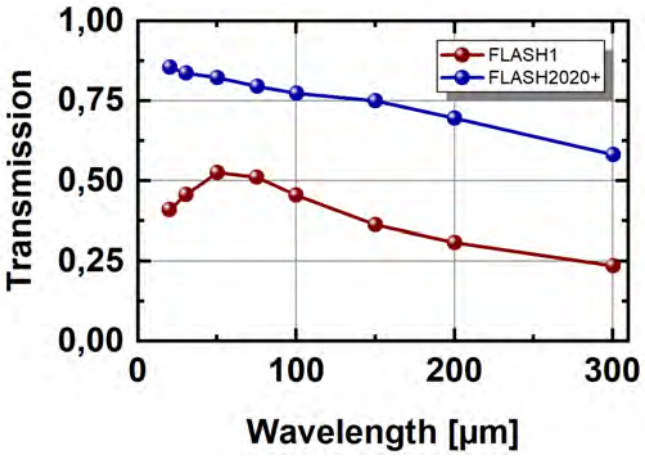

Figure 7.8: *Calculated THz beamline transmission, now (“FLASH1”) and with the described changes within FLASH2020+. Please note that the low transmission at short wavelengths for FLASH1 is due to the aperture in the XUV/THz separation mirror. On the long wavelength side, transmission will benefit from shifting the THz sources (undulator and CTR screen) ≈2 m downstream towards the electron beam dump magnet (see text).*

At the same time, the THz sources (undulator and CTR screen) will be moved ≈2 m downstream, i. e. closer to the electron beam dump magnet. The vacuum chamber of the electron beam dump magnet with its 55 mm×65 mm aperture imposing a high-pass filter for THz transport at FLASH (because of the beam size increase at longer wavelengths) is hence less critical. Moving the sources closer to this aperture will increase transmission at longer wave-

lengths by ≈50 % (cf. Figure 7.8). Finally, two normal incidence THz windows separating the THz beamline from the accelerator vacuum will be replaced by one window at the Brewster angle, further increasing the beamline transmission by almost a factor of 2.

With the above modifications close to the THz source, the overall beamline transmission is significantly improved and optimized. However, a re-building of the THz beamline will be required within the upgrade of the photon diagnostics section in the FLASH1 tunnel. Permanent and advanced online THz diagnostics are essential for understanding user experimental data and will be integrated into the THz beamline and the FL11 endstation instrument based on the recommendations from the THz beamline review panel in April 2018. The new online pulse energy and spectral monitoring and *in-situ* temporal THz pulse diagnostics are planned as described in more detail in Section 8.5.

New THz-XUV Pump-Probe Endstation

According to the recommendation from DESY's Photon Science Committee (PSC) summarizing the THz Beamline review in April 2018 "it is time for management to redirect this effort [THz] to targeted user groups and aim at ultimately increasing the scientific output" and "accommodating specific scientific communities at dedicated semi-permanent end stations". Thus, we plan the development and construction of a dedicated experimental endstation for the THz-XUV pump-probe instrument at the new beamline FL11.

This semi-permanent THz/XUV end-station is intended to focus on femto-magnetism and other solid state and surface physics/surface chemistry experiments. A detailed discussion on the scope of the instrument is planned for the coming months with the respective user community. Efficient provisions will be included to allow fast removal and re-installation of the endstation for a few months of the year, in case a number of users also wishes to use the world-wide unique THz-XUV pump-probe facility with their own instruments for specialized applications.

The semi-permanent endstation will provide tools for fast and efficient overlap (in space and time) of XUV and THz pulses on the sample under investigation, in collinear or non-collinear geometries. In current setups used at BL3 often too much beamtime had to be invested to prepare this task. The incidence angle of the probing XUV beam with respect to the sample will be adjustable to match the sample optical properties (e. g. magnetic asymmetry). XUV intensities at the sample position will be measured with sensitive XUV detectors (e. g. avalanche photodiodes). The FLASH GMDs already allow pulse intensity measurements with ≈1 % relative and better than 10 % absolute accuracy. Nevertheless, due to all the apertures along the beamline, this additional XUV detector needs to be installed to precisely monitor the incoming XUV intensity in the chamber. In combination, this will allow a pulse-to-pulse intensity detection at the sample position with the ultimate dynamic range and precision required by the relatively small magnitude of observed effects ($\approx 10^{-5}$ of the measured XUV signal on the diode). These basic ideas and diagnostic concepts based on our past experience, in combination with the user community input which will be collected, will finally be used to shape a powerful and versatile instrument for the a wide class of THz, XUV and optical laser pump-probe experiments of the condensed matter community.

7.1.6 Laser hutch and beamlines

An optical pump-probe laser is provided to all FLASH beamlines. At FLASH2 a state-of-the-art facility both in terms of laser parameters as well as in beamline and endstation development is currently set up. The laser facilities at FLASH1 will require a significant upgrade within the FLASH2020+ project. Details are described in Chapter 6.

7.2 FLASH2 Beamlines

Since 2014, FLASH2, a second undulator line with its own tunnel and experimental hall, is in operation. FLASH2 offers variable gap undulators which provide the needed flexibility and wavelength scanning options. Special schemes are feasible and will be explored and expanded substantially within FLASH2020+ (e. g. two-color modes, harmonic lasing self-seeding as described in Chapter 5), which will be taken into account in the beamline design.

The FLASH2 beamlines, which have been completed or are under development (Figure 7.13), as well as the photon diagnostics are state-of-the-art including a number of advanced concepts and do not require significant upgrades within the FLASH2020+ project. Already in the existing design, a broad wavelength range of 0.8 nm to 90 nm has been taken into account, the very long wavelengths with a somewhat reduced beamline transmission due to the larger photon beam divergence. The beamlines again combine short and long wavelengths beamlines to make use of the space in the 'Kai Siegbahn' hall most efficiently.

Three beamlines are currently in operation. FL24 with an open port and FL26 with the REMI endstation are available for users, while FL21 is dedicated to photon diagnostics developments. Beamline FL23 is currently under construction as a pulse-length compensating monochromator beamline for short wavelength from $\approx$1 nm to 20 nm, while FL22 and FL27 will be designed for longer wavelengths after having inquired detailed user demands in dedicated workshops. A full set of state-of-the-art photon diagnostics in the accelerator tunnel is used for the optimization of the machine performance by the operators, while diagnostics and photon beam manipulation tools in the experimental hall are dedicated to assist and to be operated by the users. The photon diagnostics as well as the first two mirrors in the tunnel are common to all FLASH2 photon beamlines. As mentioned already in Section 7.1.1, this alignment mirror pair has significantly improved the stability and performance of the FLASH2 beamlines.

The photon diagnostics tools are described in detail in Chapter 8. The photon beam energy is determined by gas monitor detectors (Tiedtke et al. 2008). The wavelength is measured by use of the FLASH Online Photo-Ionization Spectrometer (OPIS) which is positioned in the FLASH2 accelerator tunnel (Braune et al. 2016; Braune et al. 2018). If required, a grating spectrometer is available temporarily at beamline FL22 for an additional spectral distribution measurement with a complementary technique which, however, cannot be used in parallel with user experiments.

Aperture units consisting of circular apertures in combination with fluorescence screens (Tiedtke et al. 2009) are distributed at appropriate positions along the beamlines to assist photon beam diagnostics and alignment of the beamline and optics. Similar to FLASH1, a gas attenuator, which is placed in the photon beamline between the accelerator tunnel and the experimental hall of FLASH2 (inside of the PETRA III tunnel) and can be filled with rare gases or N_2, as well as two filter wheels equipped with foil filters, can be used on demand to attenuate the FEL beam without changing the machine parameters.

A fast shutter allows for a systematic selection of FEL trains and serves as a source for triggering experimental equipment. Data of the photon diagnostics are stored in the FLASH DAQ, linked to a time-stamp (bunch train ID). A state-of-the art ultra-short pulse laser system is available at all beamlines, described in detail in Chapter 6.

7.2.1 Beamline FL21

A new beamline – FL21 – was recently installed in the FLASH2 experimental hall. FL21 features two branches: The straight beamline provides an unfocused FEL beam that can be used for non-permanent photon diagnostics or exploratory experimental setups (Figure 7.9, right beamline). The typical FLASH endstation infrastructure (triggers, ADCs, ethernet, power, cooling water, pressurized air, vacuum interlock etc.) will be installed there. The second branch leads to a dedicated XUV pulse duration lab (on the left in Figure 7.9) in its own $3\times4\,m^2$ laser safety enclosure (not shown). A splitting mirror at the branching can be used to geometrically cut a freely selectable fraction of the incident FEL beam and reflect it towards the pulse length

diagnostics setup based on the THz streaking technique (Ivanov et al. 2018 and refs. therein). Here, the FEL beam is focused by a toroidal mirror into a permanently installed experimental chamber containing a gas jet, several electron time-of-flight (TOF) detectors (see Section 8.4) and other diagnostics. Single-cycle THz pulses generated by an IR drive laser will be used for the pulse duration measurement. Further experience shall be gained here on the THz streaking measurement principle, involved measurement uncertainties and reachable resolution, to provide – medium term – a reliable pulse duration measurement setup. Thanks to the splitting mirror, a parallel online-measurement of the pulse duration together with an experiment in the straight branch is feasible. The final pulse length diagnostics setup will be installed in the main photon diagnostics section to be available online for user experiments at all FLASH2 beamlines.

Figure 7.9: *End of beamline FL21 with two branches: pulse length diagnostics (left) and open port for exploratory setups (right).*

7.2.2 Beamline FL24

Beamline FL24 is a variable micro-focus beamline and operable for the full wavelength range at FLASH2 with its variable-gap undulators. The beamline has an open port (cf. Figure 7.10) to allow for complex and new experimental setups provided by the users.

FL24 is the most 'direct' photon beamline of FLASH2 with the minimum number of beamline mirrors and thus the FLASH beamline best optimized for covering the 'water-window' and wavelengths down to ≈1 nm (Plönjes et al. 2016). The beamline only consists of the tunnel mirror pair for alignment and radiation safety purposes and a Kirkpatrick-Baez (KB) focusing system developed by FERMI (Raimondi et al. 2014). In front of the KB mirror pair, a plane pre-mirror (PM) brings the radiation upwards by 4° to compensate for the vertical deflection introduced by the KB optics. Thus, a horizontal photon beam is delivered to the user-supplied endstations.

The KB system can be moved out of the beam path to provide also an unfocused short wavelength beam to the users on request. The KB optics utilizes a pair of bendable mirrors, which can produce a focus significantly smaller than 10 µm at the standard focal length of 2 m. At the same time, a significantly larger focal spot as well as variable focal distances can also be offered on request. The focal spot dimensions as well as the FEL wavefront are determined using Hartmann wavefront sensors developed at FLASH in a collaboration with the group of K. Mann of the Laser Laboratory Göttingen, Germany (Keitel et al. 2016). A permanent wavefront sensor setup is provided by an outcoupling port in the differential pumping stage behind the KB system.

In-coupling of the optical laser for pump-probe experiments is also provided permanently in the differential pumping unit for a collinear overlap of laser and FEL beam. As described in Chapter 6, a very advanced setup for the pump-probe laser is provided at FL24, which will now serve as a model for new beamlines and upgrades of the existing ones.

A grazing-incidence split&delay unit (SDU) covering the entire wavelength range of FLASH2 including future energy upgrades will soon be installed. It was developed within the BMBF collaborative research ('Verbundforschung') by H. Zacharias et al., Münster Uni-

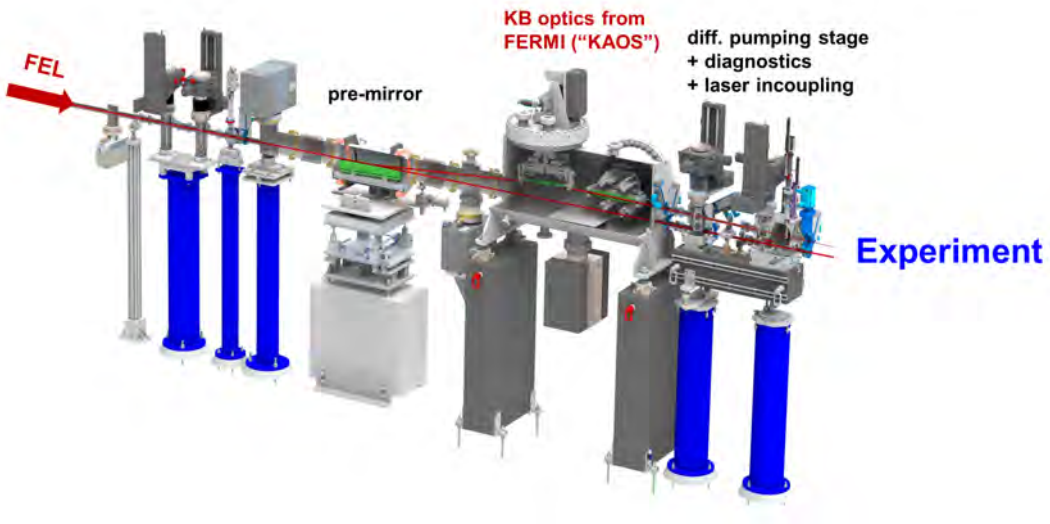

Figure 7.10: *3D model of the beamline end of FL24. From left to right: Aperture and screen units, pre-mirror to provide a horizontal beam behind the KB optics, KB Optics, and differential pumping unit including permanent out-coupling of beam for wavefront sensor and co-linear in-coupling of pump-probe laser.*

versity. The SDU is built for photon energies in the range of 30 eV<$h\nu$<1500 eV with an option to expand this range up to $h\nu$=2500 eV. The SDU is based on wavefront beam splitting at grazing incidence angles. A three dimensional setup allows for the use of two different beam paths. With grazing angles of Θ=1.3° in the fixed beam paths and Θ=1.8° in the variable beam path a good compromise between a sufficiently high reflectivity at short wavelengths (shallow angles) and a large maximum delay (steeper angles) has been chosen. The full delay range is -6 ps<Δt<18 ps. For usage of photon energies in the range of 30 eV<$h\nu$<800 eV the mirrors are coated with nickel providing a total transmission between T=57 % at $h\nu$=30 eV and still T>30 % at $h\nu$=800 eV. For photon energies up to $h\nu$=1800 eV a different beam path with platinum coated mirrors is used enabling a total transmission in the fixed beam path of T>29 % at $h\nu$=800 eV and T=24 % at $h\nu$=1800 eV, respectively. In the variable beam path, the total transmission in this photon energy range is considerably lower but still sufficient with T=13 % at $h\nu$=800 eV and T>6 % at $h\nu$=1800 eV. In view of the new opportunities given by the two-color FEL schemes recently demonstrated at FLASH2 (Chapter 5), future upgrades, implementing gratings in both branches in order to select, split and delay the two different and variable FEL wavelengths are already in the planning phase.

Further Planned Upgrades at Beamline FL24

To complement the capabilities of the CAMP experimental station at beamline BL1 (FLASH1), it is foreseen to employ a second, semi-permanent "CAMP-like" chamber for AMO and femto-chemistry experiments, as well as imaging of nano-particles and thin-films at beamline FL24. This will allow exploiting the short wavelengths beyond the carbon 1s edge with sufficient FEL pulse energies and, in addition, profit from the superior capabilities of the FLASH2 pump-probe laser.

As mentioned before, the CAMP endstation's modular and flexible layout allows for simultaneous use of large-area single-photon-counting pnCCD photon-detectors and VMI- or COLTRIMS-type electron- and ion-spectrometers, with large open ports for user-provided sample delivery systems. In order to be able to use this instrumentation at all "open-port" beamlines at FLASH1 and FLASH2 (BL2/3, PG2, FL23, and in particular FL24), we are presently planning to build a mobile version of the instrument. This endstation (working title "CAMP2") will be fully compatible with all existing instrumentation, and can be used to exploit the unique capabilities of specialized open-port beamlines enabling experiments not possible using the permanently installed CAMP at BL1.

7.2.3 FL26 with REMI (REaction MIcroscope)

Beamline FL26 which is diverging from FL24 employing a 4° incidence plane mirror is equipped with a reaction microscope as a permanent endstation (Figure 7.11). A reaction microscope (REMI) is a state-of-the-art multi-particle coincidence spectrometer. With a REMI, all fragments of a photoionization process can be detected by means of a combination of electron and ion time-of-flight spectrometers and a specific arrangement of electric and magnetic extraction fields (Ullrich et al. 2003). Using a coincident measurement technique, a complete set of all the kinematic properties of the products of a photoionization process can be determined in the experiment. Hence, this device is especially suited to investigate the dynamics of various ionization processes of gas phase and liquid targets.

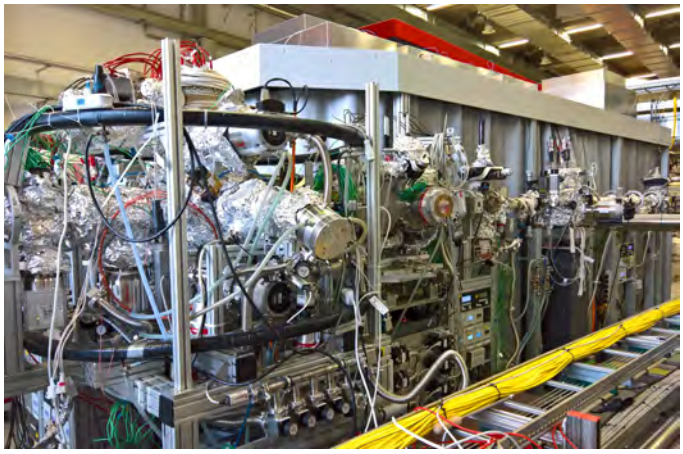

Figure 7.11: *Permanent REMI installation at FL26 including laser hutch (in the back) for pump-probe laser manipulation close to the experiment and housing the HHG VUV source.*

Over the past years, a number of remarkable scientific results derived from REMI experiments at FLASH1 have been published, e. g. regarding the dynamics of inter-molecular Coulombic decay processes in weakly-bound rare gas dimers (Schnorr et al. 2013) and the dynamics in the dissociation of multiply-charged iodine molecules (Schnorr et al. 2014). With a similar apparatus, the COLTRIMS instrument of the group of R. Dörner at the University of Frankfurt, the existence of so-called Efimov-states in the helium trimer could be proven and very precise measurements of the structure and the extremely low binding energies of the He-trimer as well as the He-dimer were successful (Zeller et al. 2016; Kunitski et al. 2015).

In order to improve the efficiency of the scientific work with such a powerful as well as complex instrument, the group of R. Moshammer (MPI-K, Heidelberg) in collaboration with colleagues from DESY, has set up a REMI as a permanent endstation at FL26 (Schmid et al. 2019). This endstation, operated by the MPI-K team, is available to all user groups interested in atomic and molecular science.

With respect to time-resolved experiments employing XUV-XUV pump-probe schemes, a mirror chamber has been added recently which simultaneously serves as an in-line split&delay stage and a focusing device. The time-delay can be adjusted in a range of ± 2.7 ps. A focal spot size of 4 µm $\times$ 5 µm (FWHM) has been achieved. The carbon mirror coating covers the whole FLASH2 wavelength range sufficiently well down to about 6.9 nm, and the reflectivity is larger than 75 % in the wavelength range between 9 nm and 41 nm (Schmid et al. 2019).

Planned Upgrades at the REMI

In addition to the FEL and the optical NIR/UV pump-probe laser, a synchronized HHG laser system providing VUV photons, even in the FEL off-times, is realized in the laser tent close to the REMI. It has been developed within the BMBF collaborative research (“Verbundforschung”) as a project of the Leibniz Universität Hannover (U. Morgner et al.), together with DESY and the MPI in Heidelberg. These three sources together will enable multi-color pump-probe experiments in the near future.

Driven by user demands and based on the successful operation of the fast KALYPSO line detector with the VLS spectrometer (FLASH1) for recording the spectra of all pulses in a pulse train (Section 8.3), we started investigations regarding the realization of a dedicated refocusing optics and a grating spectrometer plus KALYPSO detector behind the REMI.

Parameters	Value
Wavelength / nm	1.2 – 20.0 (including harmonics)
Pulse length / fs	<50
Resolving poer / $\lambda/\Delta\lambda$	$\geq$2000
Flux at the end of the beamline / photons/pulse	1×10^{10}

Table 7.1: *User requirements for the Time-Delay Compensating Monochromator as basis for the FL23 beamline design.*

Regarding the REMI chamber itself, it is foreseen to change the sample delivery part to a modular jet system. A setup on rails is planned by the colleagues around R. Moshammer, to be able to easily switch between different sample injection systems. Since both, FLASH1 and FLASH2 are expected to cover wavelengths up to $\geq$60 nm, we currently assume that the REMI endstation will stay in the FLASH2 hall. If, however, new scientific opportunities encourage the use of the REMI endstation with a fully seeded beam, it would be possible to switch the positions of REMI and CAMP.

7.2.4 FL23 Time-Delay Compensating Monochromator Beamline (ongoing upgrade)

For many research areas which require a narrower spectral bandwidth of the photon pulse than the natural bandwidth of FLASH, ultrashort pulse-lengths <50 fs and high peak brightness are prerequisites. An ultra-short pulse length can be preserved using a two-grating monochromator design (Poletto et al. 2018; Ruiz-Lopez et al. 2019 and references therein). The user requirements for such a time-delay compensating monochromator were evaluated in a workshop in July 2017 and are summarized in Table 7.1.

The simulated performance in Poletto et al. 2018 shows that one can mostly reach these values, but might, at the long wavelength end, have to trade pulse length for resolution, because one reaches the Fourier limit. Beamline FL23 is currently in the design and procurement phase and is expected to be installed and commissioned in 2021. With its medium resolution while preserving the pulse length and with its priority set on the short wavelength range, it will very well complement the high resolution monochromator beamline PG at FLASH1. FL23 is separated off FL24 behind the split&delay unit, thus allowing use of this advanced instrument also at FL23.

To maximize the beamline throughput and the transmission efficiency, the number of optical elements is minimized in the time-delay compensating monochromator (TDCM) beamline. The TDCM is equipped with six optical elements (cf. Figure 7.12): a planar elliptical mirror (EM), two variable line spacing (VLS) gratings in reflection mode, a slit (S), a planar mirror (PM) and a bendable Kirkpatrick-Baez focusing system (KBO). The EM deflects the FEL beam horizontally into the new beamline FL23, and at the same time illuminates the first grating and focuses the horizontally dispersed

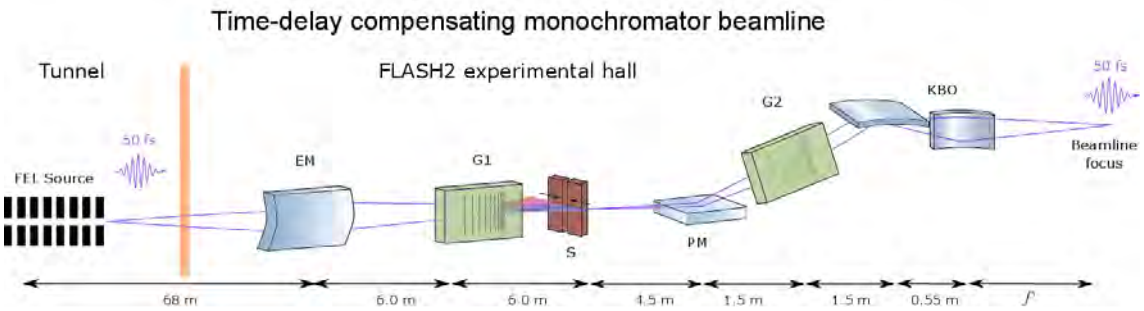

Figure 7.12: *Sketch of the Time Delay Compensating Monochromator beamline FL23. For details see text.*

radiation onto the exit slit of the first monochromator stage. Two sets of gratings are envisaged within this monochromator stage, one for the short wavelength range (λ=1.2 nm to 6 nm) and one for longer wavelengths (λ=6 nm to 20 nm). Space for a third grating pair is foreseen for future upgrades. A second set of gratings (with the same parameters) is installed behind the slit in the second monochromator stage, however, with an important difference: the second grating is working in inside order configuration, whereas for the first grating the outside order is selected. In such a way the optical path difference (OPD) introduced by the grating dispersion – and thus the pulse-front tilt – can be compensated for all wavelengths (Poletto et al. 2009). Upstream of the second grating, the planar mirror (PM) brings the radiation upwards by 4° to compensate the vertical angle introduced by the KB optics. Thus, a horizontal photon beam is provided to the user experiments. The PM is positioned before the second grating keeping the beamline short enough to fit into the experimental hall while providing the desired resolution.

Finally, the photon beam is focused using the KB optics developed by FERMI (Raimondi et al. 2014), which efficiently covers the entire wavelength range envisaged for the FLASH2020+ upgrade. An additional advantage of the TDCM design is that the focus size of the KB optics is dependent only on the FEL source parameters, while the slit width can be varied with respect to desired resolution and throughput without affecting the focal spot dimensions since the monochromator image at the exit slit is small compared to the slit width.

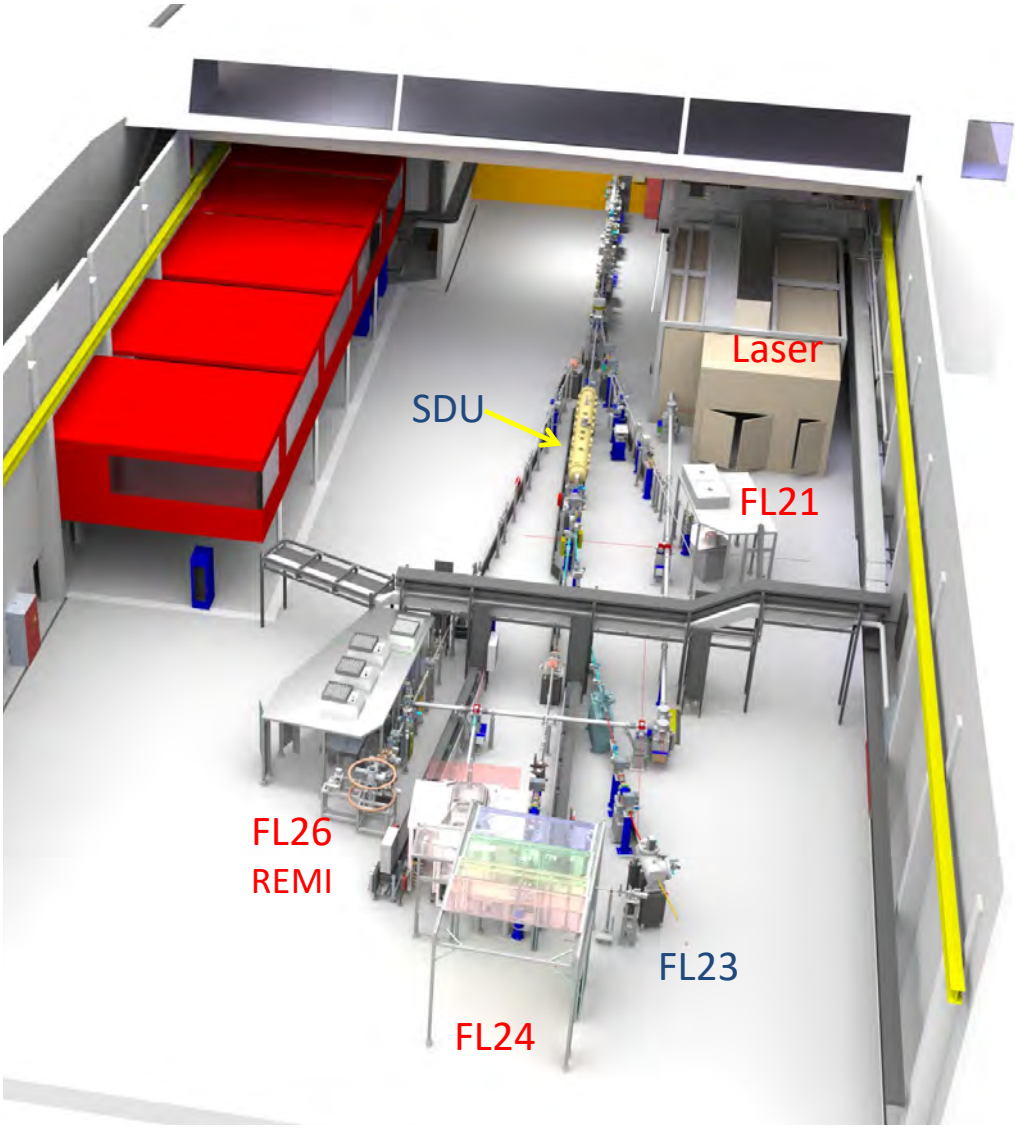

Figure 7.13: *Layout of FLASH2 hall with present beamlines marked in red and upgrades in dark blue.*

7.3 Mobile Endstations for Users (available for all open-port beamlines)

In addition to the semi-permanent endstations (WESPE, HEXTOF, 'THzFL11', 'CAMP2') mentioned before in connection with the respective beamlines, two further instruments are available for users and are briefly sketched here:

MULTI-P (MULTI-Purpose chamber)

Applications: in particular plasma-physics and warm dense matter (WDM) experiments, but also AMO experiments (for science examples see Zastrau et al. 2014; Harmand et al. 2012; Przystawik et al. 2012).

Equipment:

- HiTRaX (Fäustlin et al. 2010) & Knick-Spec spectrometers (Schroedter et al. 2014) for soft X-ray Thomson scattering & fluorescence spectra
- Variety of flanges for manipulators, liquid jet sample delivery and the like
- Residual gas analyzer (RGA = mass spectrometer)
- Breadboard and sample hexapod inside
- VMI and different MCPs
- LHe cryostat
- High turbo pumping speed (>4600 L/s)
- Incl. diff. pumping towards beamline (three orders of magnitude)

MUSIX (MUlti-dimensional Spectroscopy and (In-)elastic X-ray scattering)

The MUSIX chamber (Beye et al. 2018) is open for collaborations with the Helmholtz young investigator group around Martin Beye.

Applications: solid state sample environment for materials science allowing absorption, diffraction and RIXS measurements (separate, similar chamber with liquid jet environment for chemistry in solution foreseen).

Equipment:

- solid state ultra-high-vacuum sample environment
- $\theta - 2\theta$ diffractometer
- flexible grating spectrometer with a resolving power >2000 across the whole photon energy range of FLASH
- in-vacuum CCD
- sample can be rotated around the azimuth upon mounting and can be cooled down to 25 K. Heating up to about 350 K.

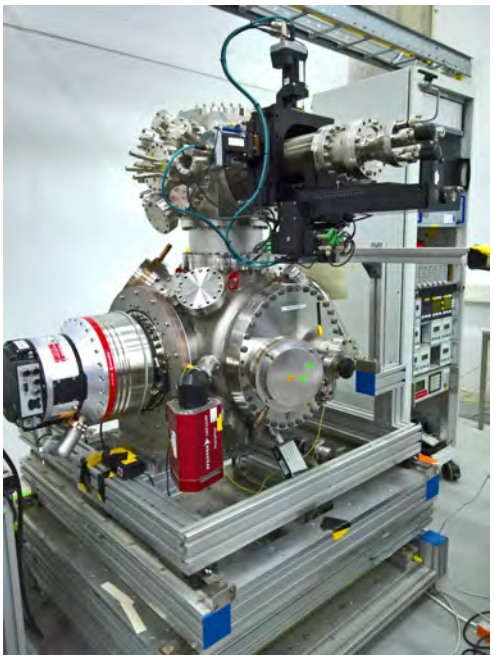

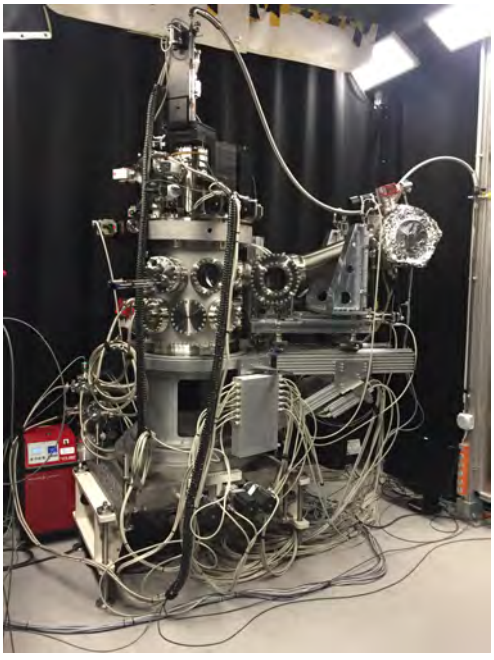

References

Allahgholi, A. et al. (2019). „The Adaptive Gain Integrating Pixel Detector at the European XFEL". In: *Journal of Synchrotron Radiation* 26.1, pp. 74–82. DOI: 10.1107/S1600577518016077.

Beye, M. et al. (2018). „Non-linear soft x-ray methods on solids with MUSIX—the multidimensional spectroscopy and inelastic x-ray scattering endstation". In: *Journal of Physics: Condensed Matter* 31.1, p. 014003. DOI: 10.1088/1361-648x/aaedf3.

Braune, M. et al. (2016). „A non-invasive online photoionization spectrometer for FLASH2". In: *Journal of Synchrotron Radiation* 23.1, pp. 10–20. DOI: 10.1107/S1600577515022675.

Braune, M. et al. (2018). „Non-invasive online wavelength measurements at FLASH2 and present benchmark". In: *Journal of Synchrotron Radiation* 25.1, pp. 3–15. DOI: 10.1107/S1600577517013893.

Dziarzhytski, S. et al. (2016). „Microfocusing at the PG1 beamline at FLASH". In: *Journal of Synchrotron Radiation* 23.1, pp. 123–131. DOI: 10.1107/S1600577515023127.

Erk, B. et al. (2018). „CAMP@FLASH: an end-station for imaging, electron- and ion-spectroscopy, and pump–probe experiments at the FLASH free-electron laser". In: *Journal of Synchrotron Radiation* 25.5, pp. 1529–1540. DOI: 10.1107/S1600577518008585.

Fäustlin, R. R. et al. (2010). „A compact soft X-ray spectrograph combining high efficiency and resolution". In: *Journal of Instrumentation* 5.02, P02004. DOI: 10.1088/1748-0221/5/02/p02004.

Fisher-Levine, M. et al. (2018). „Time-resolved ion imaging at free-electron lasers using TimepixCam". In: *Journal of Synchrotron Radiation* 25.2, pp. 336–345. DOI: 10.1107/S1600577517018306.

Gerasimova, N. et al. (2011). „The monochromator beamline at FLASH: performance, capabilities and upgrade plans". In: *Journal of Modern Optics* 58.16, pp. 1480–1485. DOI: 10.1080/09500340.2011.588344.

Harmand, M. et al. (2012). „Plasma switch as a temporal overlap tool for pump-probe experiments at FEL facilities". In: *Journal of Instrumentation* 7.08, P08007. DOI: 10.1088/1748-0221/7/08/p08007.

Ivanov, R. et al. (2018). „FLASH free-electron laser single-shot temporal diagnostic: terahertz-field-driven streaking". In: *Journal of Synchrotron Radiation* 25.1, pp. 26–31. DOI: 10.1107/S160057751701253X.

Keitel, B. et al. (2016). „Hartmann wavefront sensors and their application at FLASH". In: *Journal of Synchrotron Radiation* 23.1, pp. 43–49. DOI: 10.1107/S1600577515020354.

Kirkpatrick, P. et al. (1948). „Formation of Optical Images by X-Rays". In: *J. Opt. Soc. Am.* 38.9, pp. 766–774. DOI: 10.1364/JOSA.38.000766.

Kunitski, M. et al. (2015). „Observation of the Efimov state of the helium trimer". In: *Science* 348.6234, pp. 551–555. DOI: 10.1126/science.aaa5601.

Kutnyakhov, D. et al. (2016). „Spin texture of time-reversal symmetry invariant surface states on W(110)". In: *Scientific Reports* 6.1, p. 29394. DOI: 10.1038/srep29394.

Kutnyakhov, D. et al. (2020). „Time- and momentum-resolved photoemission studies using time-of-flight momentum microscopy at a free-electron laser". In: *Review of Scientific Instruments* 91.1, p. 013109. DOI: 10.1063/1.5118777.

Martins, M. et al. (2006). „Monochromator beamline for FLASH". In: *Review of Scientific Instruments* 77.11, p. 115108. DOI: 10.1063/1.2364148.

Oelsner, A. et al. (2010). „Time- and energy resolved photoemission electron microscopy-imaging of photoelectron time-of-flight analysis by means of pulsed excitations". In: *Journal of Electron Spectroscopy and Related Phenomena* 178-179, pp. 317–330. DOI: 10.1016/j.elspec.2009.10.008.

Plönjes, E. et al. (2016). „FLASH2: Operation, beamlines, and photon diagnostics". In: *AIP Conference Proceedings* 1741.1, p. 020008. DOI: 10.1063/1.4952787.

Poletto, L. et al. (2009). „Time-delay compensated monochromator for the spectral selection of extreme-ultraviolet high-order laser harmonics". In: *Review of Scientific Instru-*

ments 80.12, p. 123109. DOI: 10.1063/1.3273964.

Poletto, L. et al. (2018). „Double-grating monochromatic beamline with ultrafast response for FLASH2 at DESY“. In: *Journal of Synchrotron Radiation* 25.1, pp. 131–137. DOI: 10.1107/S1600577517013777.

Przystawik, A. et al. (2012). „Generation of the simplest rotational wave packet in a diatomic molecule: Tracing a two-level superposition in the time domain“. In: *Phys. Rev. A* 85 (5), p. 052503. DOI: 10.1103/PhysRevA.85.052503.

Raimondi, L. et al. (2014). „Status of the K-B bendable optics at FERMI@Elettra FEL“. In: *Adaptive X-Ray Optics III*. Ed. by St. L. O'Dell et al. Vol. 9208. International Society for Optics and Photonics. SPIE, pp. 24–34. DOI: 10.1117/12.2062326.

Redlin, H. et al. (2011). „The FLASH pump–probe laser system: Setup, characterization and optical beamlines“. In: *Nuclear Instruments and Methods in Physics Research Section A: Accelerators, Spectrometers, Detectors and Associated Equipment* 635.1, Supplement, S88–S93. DOI: 10.1016/j.nima.2010.09.159.

Ruiz-Lopez, M. et al. (2019). „Wavefront-propagation simulations supporting the design of a time-delay compensating monochromator beamline at FLASH2“. In: *Journal of Synchrotron Radiation* 26.3, pp. 899–905. DOI: 10.1107/S160057751900345X.

Sauppe, M. et al. (2018). „XUV double-pulses with femtosecond to 650ps separation from a multilayer-mirror-based split-and-delay unit at FLASH“. In: *Journal of Synchrotron Radiation* 25.5, pp. 1517–1528. DOI: 10.1107/S1600577518006094.

Schmid, G. et al. (2019). „Reaction microscope endstation at FLASH2“. In: *Journal of Synchrotron Radiation* 26.3, pp. 854–867. DOI: 10.1107/S1600577519002236.

Schnorr, K. et al. (2013). „Time-Resolved Measurement of Interatomic Coulombic Decay in Ne_2“. In: *Phys. Rev. Lett.* 111 (9), p. 093402. DOI: 10.1103/PhysRevLett.111.093402.

Schnorr, K. et al. (2014). „Electron Rearrangement Dynamics in Dissociating I_2^{n+} Molecules Accessed by Extreme Ultraviolet Pump-Probe Experiments“. In: *Phys. Rev. Lett.* 113 (7), p. 073001. DOI: 10.1103/PhysRevLett.113.073001.

Schönhense, G. et al. (2017). „Spin-filtered time-of-flight k-space microscopy of Ir – Towards the “complete” photoemission experiment“. In: *Ultramicroscopy* 183, pp. 19–29. DOI: 10.1016/j.ultramic.2017.06.025.

Schroedter, L. et al. (2014). „Hidden Charge States in Soft-X-Ray Laser-Produced Nanoplasmas Revealed by Fluorescence Spectroscopy“. In: *Phys. Rev. Lett.* 112 (18), p. 183401. DOI: 10.1103/PhysRevLett.112.183401.

Sorgenfrei, F. et al. (2010). „The extreme ultraviolet split and femtosecond delay unit at the plane grating monochromator beamline PG2 at FLASH“. In: *Review of Scientific Instruments* 81.4, p. 043107. DOI: 10.1063/1.3374166.

Surface Concept (2019). In: *Webpage*. Online.

Tiedtke, K. et al. (2008). „Gas detectors for x-ray lasers“. In: *Journal of Applied Physics* 103.9, p. 094511. DOI: 10.1063/1.2913328.

Tiedtke, K. et al. (2009). „The soft x-ray free-electron laser FLASH at DESY: beamlines, diagnostics and end-stations“. In: *New Journal of Physics* 11.2, p. 023029. DOI: 10.1088/1367-2630/11/2/023029.

Ullrich, J. et al. (2003). „Recoil-ion and electron momentum spectroscopy: reaction-microscopes“. In: *Reports on Progress in Physics* 66.9, pp. 1463–1545. DOI: 10.1088/0034-4885/66/9/203.

Wunderer, C. B. et al. (2019). „The Percival 2-Megapixel monolithic active pixel imager“. In: *Journal of Instrumentation* 14.01, pp. C01006–C01006. DOI: 10.1088/1748-0221/14/01/c01006.

Zastrau, U. et al. (2014). „Resolving Ultrafast Heating of Dense Cryogenic Hydrogen“. In: *Phys. Rev. Lett.* 112 (10), p. 105002. DOI: 10.1103/PhysRevLett.112.105002.

Zeller, St. et al. (2016). „Imaging the He2 quantum halo state using a free electron laser“. In: *Proceedings of the National Academy of Sciences* 113.51, pp. 14651–14655. DOI: 10.1073/pnas.1610688113.

8 Photon Diagnostics

Characterization of free-electron laser beam parameters such as the absolute photon flux, beam position, focus size as well as the spectral and temporal distribution is of fundamental importance for most user experiments and equally important for machine operators. Since new state-of-the art photon diagnostics tools have been developed for FLASH2, one of the main objectives of the FLASH2020+ project is to transfer these advanced diagnostics concepts to FLASH1 and thereby replace the existing equipment in the FLASH1 tunnel and the experimental hall – being nearly 15 years old – to cope for the new scientific and technological challenges. In the following sections the main photon diagnostics tools will be briefly described. Additional details can be found in the cited references. Standard diagnostics for general characterization and optimization of the SASE process and the photon beam transport up to the user endstations such as apertures and fluorescent crystals, the MCP tool or alignment lasers will be provided at both FLASH1 and FLASH2. Also, a number of beam manipulation tools such as filter wheels for metal foil filters, gas attenuator, and the fast shutter will be included in the beamline design. Details can be found in (Plönjes et al. 2015; Tiedtke et al. 2009).

8.1 Pulse Energy and Beam Position

For many users the most important FEL parameter is the photon pulse energy, which varies from pulse to pulse. This requires online non-invasive absolute monitoring on a shot-to-shot basis with a sufficiently high temporal resolution. The gas-monitor detectors (GMDs) originally designed for this purpose (Tiedtke et al. 2008) are suited for on-line monitoring of the intensity of the FEL radiation in the wavelength range from 4 nm to 50 nm and with a repetition rate of 1 MHz currently provided at FLASH1. For the wavelength range extended to shorter wavelengths well below 4 nm envisaged within the FLASH2020+ upgrade and to cope with shorter wavelengths resulting from new undulator schemes in FEL operation, upgraded versions of the GMDs with increased sensitivity are required, due to the lower photoionization cross sections for the rare gases used in these monitors. Therefore, we will replace all GMDs by so-called X-ray gas-monitors (XGMDs) (Sorokin et al. 2019) initially developed for hard X-ray FELs (European XFEL and SwissFEL), which have at least 10 times higher sensitivity.

Figure 8.1 shows a scheme and general overview of the configuration of the XGMD. The operation of the XGMD is based on atomic photoionization of rare gases at low pressures in the range from 1×10^{-4} Pa to 1×10^{-2} Pa. The basic principle of the XGMD is that ions and photoelectrons created upon photoionization are simultaneously detected by simple metal plates. Hence, the detector is not only radiation-hard and transparent but also does not suffer from any kind of degradation. From the resulting electron and ion currents the absolute number of photons in each pulse can be deduced with an accuracy of better than 10 %. Moreover, a fraction of ions passes through a small aperture in the respective ion detection electrode and is detected by a commercial open electron multiplier (ETP14880) which allows to further increase the dynamic range for detection to between 1×10^5 and 1×10^{14} photons per pulse.

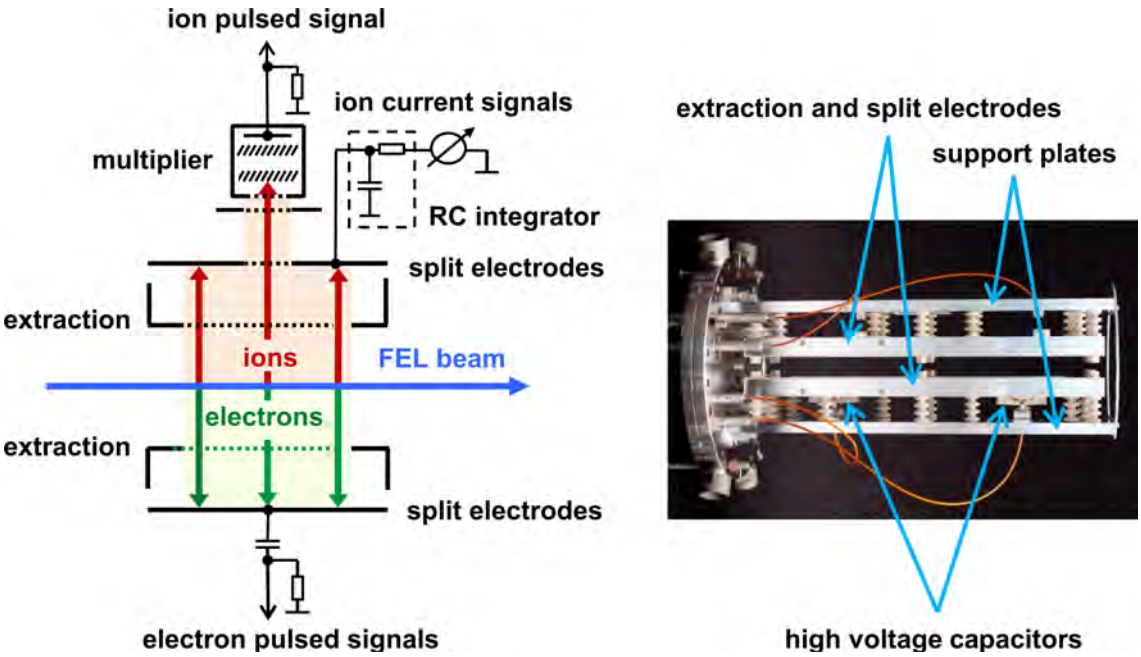

Figure 8.1: *Left: Schematic diagram of the XGMD. Right: Picture of the XGMD (the commercial multiplier depicted in the diagram on the left is not shown in the photo). (Sorokin et al. 2019).*

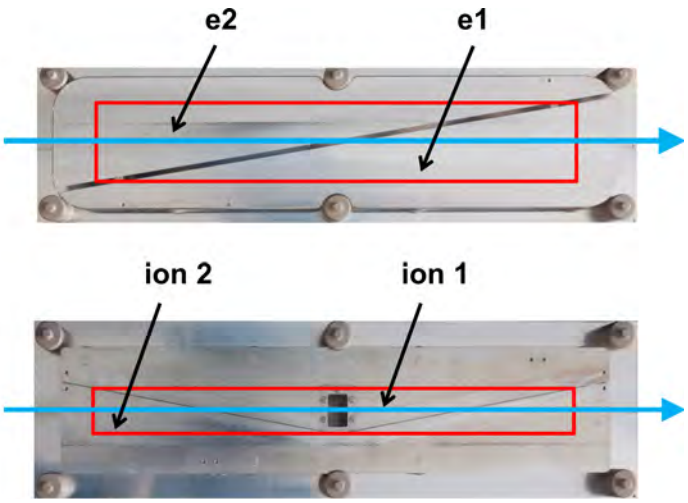

Figure 8.2: *Top: Top view on a triangular split electrode for the electron detection. Bottom: Top view on a linear split electrode for the ion detection with the aperture in the central part which enables the transmission of a fraction of ions toward the commercial open electron multiplier. Blue arrows represent the direction of the FEL beam. For both types of extraction electrodes, the sensitive area which can be hit by charged particles (indicated by red rectangles) is defined by the rectangular entrance aperture of the XGMD. (Sorokin et al. 2019).*

Both, ion and electron detection electrodes consist of a pair of diagonally split plates as shown in Figure 8.2. This allows monitoring of the FEL beam position in one transverse direction with accuracy down to 10 µm. Therefore, two XGMDs rotated by 90° to each other enable measuring the beam position in vertical and horizontal directions. The XGMD provides a temporal resolution of better than 50 ns due to high voltage capacitors manufactured in-house, which are used to decouple the two parts of the electron split electrodes from the readout electronics, respectively. They are mounted in the vacuum chamber directly on the electrode surface. This fulfills demands of all FELs over the world. All XGMDs have been calibrated at the Metrology Light Source (MLS) of the Physikalisch-Technische Bundesanstalt (PTB) (Gottwald et al. 2012; Gottwald et al. 2019).

Planned XGMD Upgrade

• The proposed novel two-color-mode lasing schemes is challenging for the XGMD operation since the latter generally require a monochromatic beam. To overcome this challenge, it is proposed to use the two XGMDs (which are available for all beamlines) operated with two different gases, which have substantially different total photoionization cross sections and mean ion mean charge values for the two lasing

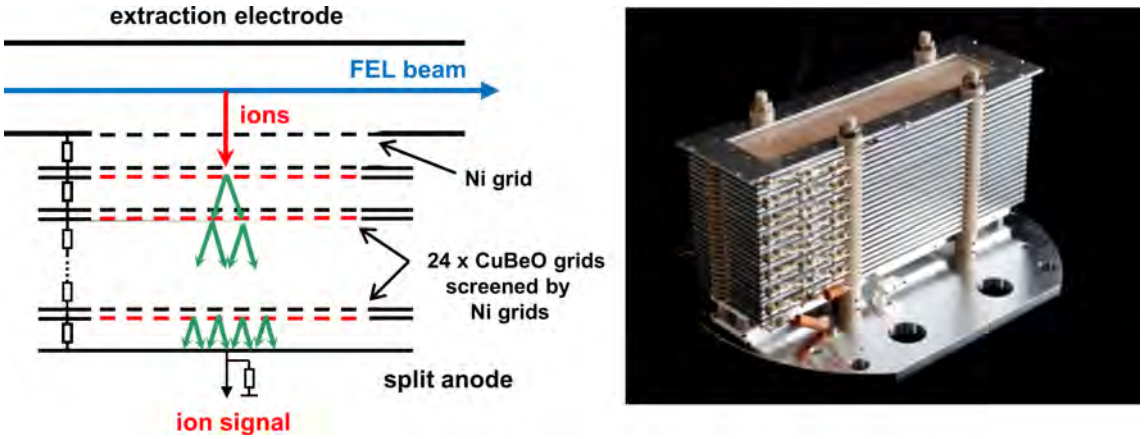

Figure 8.3: *Left: Schematic diagram of the HAMP detector. Right: Picture of the HAMP detector. (Sorokin et al. 2019).*

wavelengths. In this case, the number of photons N_1 and N_2 at the 1st and 2nd wavelength can be derived by solving two equations for the unknown quantities N_1, N_2.

• Small beam-confining apertures or wavelength discriminating elements, such as gratings, in combination with the FEL inherent pointing and spectral fluctuations affect the transmitted intensity behind those elements. Hence, pulse-resolved intensity measurements with the XGMD in front might not be sufficiently reliable. For this reason, we plan to install an additional intensity monitor behind the slit of the monochromator beamline FL23, which is the most critical beamline with respect to intensity monitoring. In order to account for the very limited space, we will use a newly developed intensity monitor based on the XGMD concept which is already operational at very low gas pressures of 1×10^{-5} Pa and thus does not require any elaborate and long differential pressure stages. This Huge Aperture Multiplier detector (HAMP) is a self-made multiplier with an active area as large as 200 mm along the photon beam path and 50 mm in width (Sorokin et al. 2019). An overview of its basic operation principle and assembly is shown in Figure 8.3.

8.2 Spectral Distribution

Measurement of the central wavelength and further spectral characterization of the photon beam provides essential information for the optimization of the SASE process and user experiments. Spectral beam properties can be used for cross-checking the mean electron energy and to determine the bandwidth of the FEL beam as well as the content of higher harmonics. Furthermore, the spectral distribution yields the number of modes in the pulse and can be used to estimate the pulse length. At FLASH2, a non-invasive concept for wavelength measurement was developed and is used, a spectrometer based on photoionization of rare gases (Online PhotoIonization Spectrometer OPIS, Braune et al. 2016; Braune et al. 2018). In this approach, the kinetic energies of photoelectrons are determined by time-of-flight spectroscopy. With the well-known binding energy of the rare gas electron orbitals the photon energy can be determined. The main advantage of this approach is that the photon beam does not pass dispersive or redirecting optical elements, but just traverses a dilute rare gas section with an operation pressure of typically 1×10^{-7} mbar. Hence, the OPIS instrument has practically 100 % transmission and is suited for non-invasive wavelength measurements enabling wavelength monitoring during machine tuning as well as in parallel to user operation. Using fast MCP-detectors and ADCs for data acquisition, pulse train-resolved spectra can be recorded even for the highest repetition rates of the 1 MHz burst-mode operation of FLASH. The OPIS instrument can in principle be used to give further photon beam information

	FLASH1 tunnel spectrometer	FLASH2 XUV spectrometer	FLASH compact spectrometer	FLASH1 VLS spectrometer
spectral range	4 nm – 46 nm	1 nm – 62 nm	1.5 nm – 40 nm	5.8 nm – 60 nm
resolving power	600 – 1500	100 – 1000	150014 nm	2000 – 3000
repetition rate	10 Hz	10 Hz	10 Hz	1 MHz (KALYPSO) 10 Hz (PCO Camera)

Table 8.1: *Basic specifications of grating spectrometers at FLASH.*

such as relative intensities and beam position, and allows for wavelength monitoring tasks not easily achievable with grating spectrometers. Recently, the two different wavelengths generated in a special two-color mode operating scheme and their relative intensities could be monitored simultaneously with OPIS. Using a variety of rare gas electron orbitals and retardation voltages, the OPIS instrument can basically cover the complete XUV spectral range with wavelengths shorter than 87 nm. The relative uncertainty of the derived central wavelength is in the range of 10^{-2} to 10^{-4}. The photon spectral distribution is imprinted on the photoelectron line shape, however, it is broadened by the large photoelectron source volume in the beamline and the MCP detector response function. Hence, the resolving power regarding the spectral distribution is moderate, ranging up to about 700 for short wavelengths around 4 nm. For detailed information regarding the spectral distribution, an XUV grating spectrometer setup (Tanikawa et al. 2016) is available in the FLASH2 experimental hall as a permanent installation at one of the beamlines (currently FL22). An additional mobile spectrometer (compact spectrometer) (Frassetto et al. 2011) can be put into operation at any FLASH1 or FLASH2 beamline on request. Especially for transparent experimental setups, the compact spectrometer can be used for online wavelength monitoring in a pulsetrain-resolved fashion with 10 Hz repetition rate. For specifications of the grating spectrometers see Table 8.1.

In the FLASH1 tunnel an OPIS spectrometer will be included in the main photon diagnostics if space permits, which will be decided in the technical design phase. In addition, the existing variable line spacing (VLS) grating spectrometer, which is currently installed in the BL-branch of FLASH1 and is employed for BL user experiments on request, will be adapted for regular monitoring of the central wavelength and spectral distribution. This VLS spectrometer (Brenner et al. 2011) has got a 2°-grazing incidence design, which allows propagating most of the FEL light in 0^{th} diffraction order towards the user experiment, whereas only a small dispersed fraction (1 % to 10 %) of the 1^{st} order of the incoming light is used for wavelength monitoring (see Figure 8.4).

Recently, a novel detector named KALYPSO (KArlsruhe Linear arraY detector for MHz rePetition-rate SpectrOscopy) in version 2.1 (Rota et al. 2019) was implemented in the VLS spectrometer setup. This fast line detector allows for sampling of all spectra of several hundred individual pulses in a train at 1 MHz readout rate, enabling non-averaged online wavelength monitoring.

The KALYPSO detector has been developed in a collaboration between the Karlsruhe Institute of Technology (KIT), the Paul-Scherrer-Institute (PSI) in Switzerland and DESY. Data transfer of the KALYPSO detector is handled via direct memory access (DMA), based on novel field-programmable gate array (FPGA) readout cards in MTCA.4 crate standard for electronic modules. In the front-end, the detector at FLASH uses Si-strip detectors from PSI with 256 pixels of 50 µm width and 10 mm height, which are sensitive in a wavelength range from 200 nm to 1050 nm, and the GOTTHARD (Mozzanica et al. 2012) ASIC chip, also from PSI, for readout.

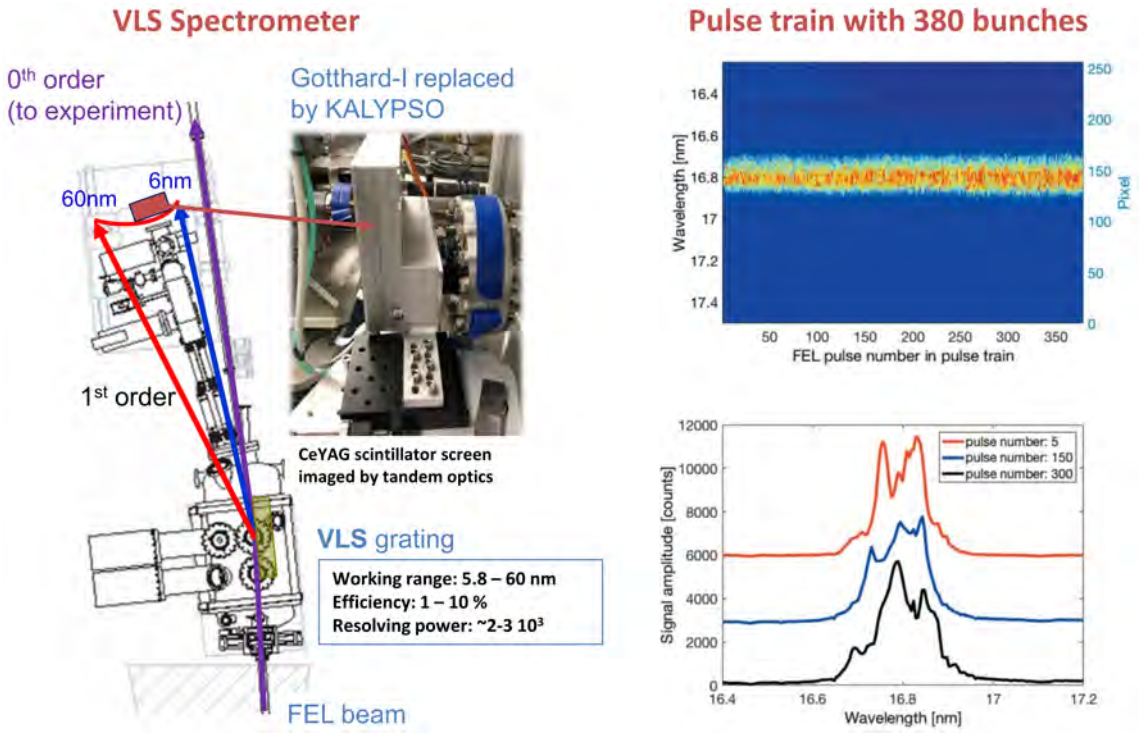

Figure 8.4: *Left: Sketch of the VLS Online Spectrometer, reflecting most of the FEL intensity in 0^{th} order towards the experiment while using about 1 % to 10 % of the intensity to measure spectra online in 1^{st} order, e. g. with the KALYPSO detector. Right: Series of spectra of a full pulse train of – in this case – 380 bunches from the KALYPSO detector. The three individual spectra at right have been offset vertically for better distinction.*

8.3 Wavefront

In the past years, DESY has developed Hartmann wavefront sensors for the soft X-ray spectral range, of approximately 4 nm to 40 nm, in collaboration with the Laser-Laboratorium Göttingen e.V. (LLG). A device is shown in Figure 8.5. The wavefront sensors were shown to be a very valuable tool for characterizing and aligning the photon beam in the various FLASH beamlines and the Kirkpatrick-Baez (KB) optics systems at FLASH. As a next step, wavefront sensors are installed permanently on beamlines with complex focusing optics and tools are developed for a (semi-)automatized optics alignment. The Hartmann wavefront sensors are adapted to the special beam properties of FLASH in terms of wavelength, pulse energy, and coherence (4 nm to 40 nm, ≈15 µJ) (Keitel et al. 2016).

The Hartmann pinhole plate divides the incoming FEL photon beam into sub-rays and illuminates a phosphor coated CCD chip. From lateral deviations in the beam spot pattern, the wavefront for single pulses is reconstructed using a modal approach via a least squares fit with a polynomial basis (software MrBeam from LLG). The measured intensity and phase are used to calculate second moment beam parameters such as beam width, divergence, Rayleigh length, waist position, waist size, and M^2.

A Zernike expansion of the wavefront provides information on the aberrations of the optical system resolved into single coefficients such as astigmatism or coma. Intensity profiles in any plane along the optical axis are accessible using numerical Fresnel-Kirchhoff propagation. A benefit of the Hartmann wavefront sensors is that they provide both intensity and phase information about the beam as well as intensity back propagation in a single shot measurement. Once MHz-rate mega-pixel detector cameras become available, pulse-to-pulse wavefront diagnostics behind a transparent experiment and to study optics deterioration along a pulse train will become feasible.

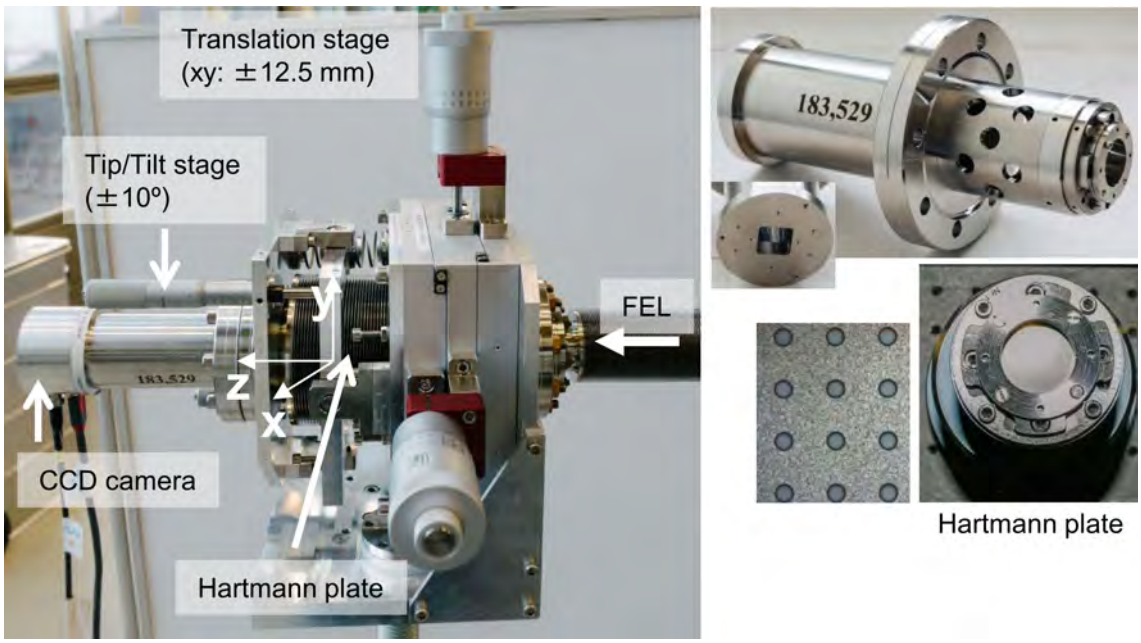

Figure 8.5: *Compact Hartmann sensor with a large field of view (15.2 mm×15.2 mm) including movements (xy direction and tip/tilt). For alignment, this device can be mounted behind a user chamber at FLASH.*

Three wavefront sensors with different characteristics, such as spectral range, spacial requirements, Hartmann plate sizes, camera repetition rates, wavefront repeatability etc. are available at FLASH. An additional wavefront sensor is adapted for the X-ray spectral range of approx. 0.5 nm to 8 nm and is presently successfully in operation at the SQS instrument of European XFEL. More details about the different sensors can be found in (Keitel et al. 2016) and references therein.

8.4 Timing and Temporal Shape

Early experiments by Frühling et al. 2009; Grguraš et al. 2012 showed that a Terahertz (THz) field driven streak camera represents a very suitable diagnostics tool to deliver single-shot pulse duration information. Such an instrument is basically wavelength independent and has a high dynamic range (in pulse duration and FEL energy). Furthermore, it can be operated with repetition rates up to several hundred kHz (potentially even MHz, Frühling et al. 2009; Grguraš et al. 2012) and in addition, it can provide arrival time information between the XUV pulse and the laser driving the THz generation for each single pulse with accuracy well below 10 fs resolution.

The measurement principle is based on a noble gas target being photoionized by the FEL pulse (Figure 8.6). The kinetic energy of the resulting electrons is modified by the electric field of the THz radiation, when it is co-propagating through the target. If the electron wave packet is short compared to the period length of the terahertz field (>600 fs in our case), the temporal structure of the wave packet will be mapped onto the kinetic energy distribution of the emitted electrons (Itatani et al. 2002). The pulse duration can be extracted from the broadening of the peaks measured in the photoelectron spectrum due to the presence of the THz field. The shift of the kinetic energy peaks provides the arrival time.

At FLASH1, a first THz streak camera prototype was build and installed at the PG0 branch of the plane-grating monochromator beamline. This branch has the capability to use the zero-order FEL radiation for the streaking set up while the dispersed radiation can be simultaneously used in the PG2 beamline to measure the FEL spectrum with high resolution.

The THz radiation is generated by interaction of synchronized pulses delivered from the FLASH1 pump-probe laser (800 nm, 80 fs, 6.5 mJ) with a nonlinearly reacting crystal. In detail, the source is based on pulse front tilt optical rectification in a Lithium niobate ($LiNbO_3$) crystal (Hebling et al. 2002). A THz field strength of ≈300 kV/cm has been achieved in the interaction point (Ivanov et al. 2018).

Currently, an improved version of the FLASH1 THz streak camera is installed at the dedicated diagnostic beamline FL21 of FLASH2. This streak camera has at least twice the resolution (with the same THz field source) and in addition to the pulse duration and arrival time, the FEL XUV photon chirp can be determined. To further improve the resolution and to measure short FEL pulses with durations shorter than 10 fs, the device can be operated with different THz sources.

Planned Upgrade

Within the FLASH2020+ project it is envisaged to establish such an improved single shot THz streak camera at the PG0 branch of FLASH1 and furthermore, to move the FLASH2 streak camera from its present position at the diagnostics beamline into the central photon diagnostics section, where it can serve as an online diagnostic tool in parallel to beam in any other of the FLASH2 beamlines. In order to prepare for the planned new options for circular polarization and attosecond operation mode of FLASH, an upgrade to temporal angular streaking (Hartmann et al. 2018) diagnostic is planned.

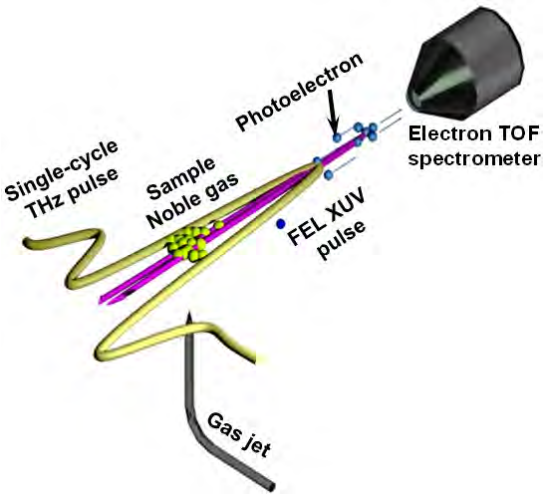

Figure 8.6: *THz streaking basic principle – The FEL pulse ionizes noble gas atoms and the resulting photoelectron kinetic energy distribution is detected by an electron time of flight detector (eTOF). The ionization takes place in the presence of a strong linearly polarized THz field influencing the kinetic energy distribution of the photoelectrons. Thus, the XUV pulse profile and arrival time are mapped on the kinetic energy distribution by the THz field. (Ivanov et al. 2018).*

8.5 Special Photon Diagnostics for the THz Beamline

Based on recommendations by the review panel during the THz beamline evaluation in April 2018, we plan to expand the THz diagnostics around three main components: online pulse energy and spectral monitoring and *in-situ* temporal THz pulse diagnostics. Online pulse monitoring will be accomplished by beam pickoff via a diamond beam-splitter mounted close to the Brewster angle. The beam-splitter serves a double purpose as it also separates the particle-free, ultra-high vacuum of the superconducting accelerator from the high-vacuum of the THz beamline. The pulse energy will be monitored using a hot electron bolometer, which allows for excellent sensitivity and bandwidth to monitor individual THz pulses in FLASH MHz trains. The spectral measurements will be performed with a lamellar grating Fourier Transform Spectrometer (Pan et al. 2019) equipped with a similar bolometer.

Temporal THz pulse diagnostics will be based on Electro-Optic-Sampling (EOS) technology. We already have demonstrated wideband (DC to 7 THz) pulse characterization, based on jitter-corrected scanning EOS. Within FLASH2020+ we aim to transform this technology to a true single-shot THz pulse detection (Russell et al. 2017) (already demonstrated at FLASH, see Figure 8.7) and will double the detection bandwidth towards 15 THz) using polled polymers (McLaughlin et al. 2008).

For the purpose of in-situ EOS THz pulse characterization, a dedicated built-in femtosecond laser system, synchronized to the FLASH

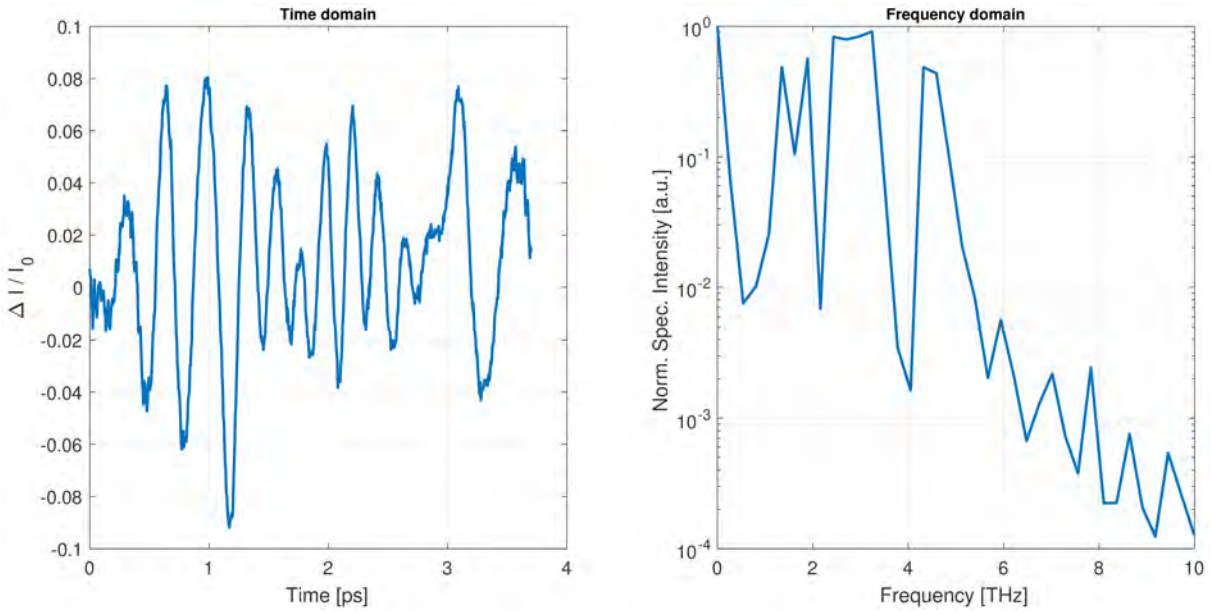

Figure 8.7: *Single-shot THz pulse detection at FLASH1, results from the pilot experiment. By courtesy of Zhiang Chen, SLAC.*

accelerator, and independent of the FLASH pump-probe laser facility (which is dedicated to user experiments) will be installed. A commercial fiber-laser based parametric amplifier system used to probe THz pulses at FLASH in pilot studies has proven to be a robust and reliable solution.

For the ultimate characterization of THz pulses over the complete FLASH THz spectral range (1 THz to 100 THz) we will employ the THz streak camera concept (Ivanov et al. 2018) developed for temporal characterization of FLASH's XUV pulses. For probing, harmonics of the upgraded THz probe laser will be used with fixed pulse durations of 10 fs to 15 fs. A separate probing UV source is needed to decouple the electron beam parameters that define THz and XUV pulses at FLASH (in standard mode of operation the higher the THz pulse energy, the longer the FLASH XUV pulse).

References

Braune, M. et al. (2016). „A non-invasive online photoionization spectrometer for FLASH2“. In: *Journal of Synchrotron Radiation* 23.1, pp. 10–20. DOI: 10.1107/S1600577515022675.

Braune, M. et al. (2018). „Non-invasive online wavelength measurements at FLASH2 and present benchmark“. In: *Journal of Synchrotron Radiation* 25.1, pp. 3–15. DOI: 10.1107/S1600577517013893.

Brenner, G. et al. (2011). „First results from the online variable line spacing grating spectrometer at FLASH“. In: *Nuclear Instruments and Methods in Physics Research Section A: Accelerators, Spectrometers, Detectors and Associated Equipment* 635.1, Supplement, S99–S103. DOI: 10.1016/j.nima.2010.09.134.

Frassetto, F. et al. (2011). „Compact spectrometer for photon diagnostics of the extreme-ultraviolet free-electron-laser radiation“. In: *Nuclear Instruments and Methods in Physics Research Section A: Accelerators, Spectrometers, Detectors and Associated Equipment* 635.1, Supplement, S94–S98. DOI: 10.1016/j.nima.2010.11.004.

Frühling, U. et al. (2009). „Single-shot terahertz-field-driven X-ray streak camera“. In: *Nature Photonics* 3.9, pp. 523–528. DOI: 10.1038/nphoton.2009.160.

Gottwald, A. et al. (2012). „Current capabilities at the Metrology Light Source“. In: *Metrologia* 49.2, S146–S151. DOI: 10.1088/0026-1394/49/2/s146.

Gottwald, A. et al. (2019). „The U125 insertion device beamline at the Metrology Light Source“. In: *Journal of Synchrotron Radiation* 26.2, pp. 535–542. DOI: 10.1107/S1600577518018428.

Grguraš, I. et al. (2012). „Ultrafast X-ray pulse characterization at free-electron lasers“. In: *Nature Photonics* 6.12, pp. 852–857. DOI: 10.1038/nphoton.2012.276.

Hartmann, N. et al. (2018). „Attosecond time-energy structure of X-ray free-electron laser pulses“. In: *Nature Photonics* 12.4, pp. 215–220. DOI: 10.1038/s41566-018-0107-6.

Hebling, J. et al. (2002). „Velocity matching by pulse front tilting for large-area THz-pulse generation“. In: *Opt. Express* 10.21, pp. 1161–1166. DOI: 10.1364/OE.10.001161.

Itatani, J. et al. (2002). „Attosecond Streak Camera“. In: *Phys. Rev. Lett.* 88 (17), p. 173903. DOI: 10.1103/PhysRevLett.88.173903.

Ivanov, R. et al. (2018). „FLASH free-electron laser single-shot temporal diagnostic: terahertz-field-driven streaking“. In: *Journal of Synchrotron Radiation* 25.1, pp. 26–31. DOI: 10.1107/S160057751701253X.

Keitel, B. et al. (2016). „Hartmann wavefront sensors and their application at FLASH“. In: *Journal of Synchrotron Radiation* 23.1, pp. 43–49. DOI: 10.1107/S1600577515020354.

McLaughlin, C. V. et al. (2008). „Wideband 15THz response using organic electro-optic polymer emitter-sensor pairs at telecommunication wavelengths“. In: *Applied Physics Letters* 92.15, p. 151107. DOI: 10.1063/1.2909599.

Mozzanica, A. et al. (2012). „The GOTTHARD charge integrating readout detector: design and characterization“. In: *Journal of Instrumentation* 7.01, pp. C01019–C01019. DOI: 10.1088/1748-0221/7/01/c01019.

Pan, R. et al. (2019). „Photon diagnostics at the FLASH THz beamline“. In: *Journal of Synchrotron Radiation* 26.3, pp. 700–707. DOI: 10.1107/S1600577519003412.

Plönjes, E. et al. (2015). „The Soft X-ray Free-Electron Laser FLASH at DESY“. In: *Optical Technologies for Extreme-Ultraviolet and Soft X-ray Coherent Sources*. Ed. by Federico Canova et al. Berlin, Heidelberg: Springer Berlin Heidelberg, pp. 1–21. ISBN: 978-3-662-47443-3. DOI: 10.1007/978-3-662-47443-3_1.

Rota, L. et al. (2019). „KALYPSO: Linear array detector for high-repetition rate and real-time beam diagnostics“. In: *Nuclear Instruments and Methods in Physics Research Section A: Accelerators, Spectrometers, Detectors and Associated Equipment* 936, pp. 10–13. DOI: 10.1016/j.nima.2018.10.093.

Russell, B. K. et al. (2017). „Self-referenced single-shot THz detection“. In: *Opt. Express* 25.14, pp. 16140–16150. DOI: 10.1364/OE.25.016140.

Schulz, S. et al. (2015). „Femtosecond all-optical synchronization of an X-ray free-electron laser“. In: *Nature Communications* 6.1, p. 5938. DOI: 10.1038/ncomms6938.

Sorokin, A. A. et al. (2019). „An X-ray gas monitor for free-electron lasers“. In: *Journal of Synchrotron Radiation* 26.4, pp. 1092–1100. DOI: 10.1107/S1600577519005174.

Tanikawa, T. et al. (2016). „First observation of SASE radiation using the compact wide-spectral-range XUV spectrometer at FLASH2“. In: *Nuclear Instruments and Methods in Physics Research Section A: Accelerators, Spectrometers, Detectors and Associated Equipment* 830, pp. 170–175. ISSN: 0168-9002. DOI: 10.1016/j.nima.2016.05.088.

Tiedtke, K. et al. (2008). „Gas detectors for x-ray lasers“. In: *Journal of Applied Physics* 103.9, p. 094511. DOI: 10.1063/1.2913328.

Tiedtke, K. et al. (2009). „The soft x-ray free-electron laser FLASH at DESY: beamlines, diagnostics and end-stations“. In: *New Journal of Physics* 11.2, p. 023029. DOI: 10.1088/1367-2630/11/2/023029.

9 Data Concept

9.1 General Considerations and Goals

User experiments at FLASH and at similar FEL and synchrotron user facilities around the world are becoming increasingly dependent on high performance computing to deliver cutting edge science. Looking ahead 10-15 years, we anticipate that both data volumes and data rates from detectors at FLASH will continue to grow significantly, and that ever more sophisticated experiments by researchers will place correspondingly more intense demands on data acquisition, storage, computing and simulation capacity. All this effort is driven to ensure successful experiments and fast publications. Steps to reach the goals will be presented in this chapter.

This involves:

- To enable new experimental techniques and user experiments with optimized output by incorporating novel high speed detectors and online feedback.
- Provide analysis tools and processes including clear documentation to enable efficient preparation of experiments.
- Make the evaluation of user data more efficient by providing sophisticated data reduction algorithms and an advanced scientific computing platform.
- Improve FEL performance and tuning times by providing diagnostic data in combination with machine learning approaches.
- Continued and increased use of centralized storage (currently GPFS), centralized processing (currently Maxwell cluster) and high speed networking (currently 10 Gbit Ethernet and EDR InfiniBand) for high performance computing, storage and data transfer.

9.2 Controls and Online Data Analysis

FLASH operates at intra-pulsetrain repetition rates of up to 1 MHz, which is a challenge for the data acquisition. When operating in SASE mode, each XUV pulse is different in energy, spectrum, pulse duration and structure, arrival time and so on and thus, most experiments cannot simply average data, but rather each XUV pulse property and the result of the user experiment has to be measured and analyzed separately for each XUV pulse – raising very demanding requirements. On the other hand, the natural fluctuations allow covering a large parameter range in short time if they are used efficiently. In contrast to more stable sources (e. g. synchrotron radiation or optical lasers) the parameter space is scanned by the natural fluctuations of the FEL and has not to be scanned independently.

Combining photon diagnostics and experimental data, dependencies with respect to pump-probe delay, wavelength, pulse energy, and so forth can be analyzed on the fly. Thus, experiment control needs immediate visual feedback on pulse-synchronous processed data.

Using flexible, ad-hoc usable, HPC empowered, scriptable Python live visualization toolboxes (like SLAC's psana) as well as the integration of standard analysis software (e. g. Hummingbird, CASS, ONDA) will help in the fast interpretation of the measurement and will increase the experimental outcome significantly.

However, to use the provided infrastructure efficiently, experiment detectors (in particular 2D detectors) have to be integrated closely into the FLASH control system.

9.2.1 The control system (DOOCS, JDDD)

The Distributed Object Oriented Control System (DOOCS) is the accelerator control system for FLASH (and the European XFEL), which has been developed at DESY decades ago and is continuously being developed further. Tens of years of experience ensure a reliable operation.

DOOCS is scalable to larger data rates and increasing number of detectors and will be used to control the electron and photon diagnostics as well as the optical pump-probe lasers for FLASH2020+. DOOCS in addition interfaces to the data acquisition (DAQ) of the FEL and user data. It allows complex calculations with pulse-synchronous data (in middle layer servers) and fast feedbacks.

To visualize DOOCS data, a Java based easy-to-use, drag-and-drop configurable interface “Java DOOCS Data Display” (JDDD) was developed at DESY as well. The beamline controls, photon diagnostics and the user infrastructure provided by FLASH are integrated and operated by JDDD controls. The control panels typically have an easy to use general “user” interface as well as “expert” layers allowing to control and monitor all critical components.

FLASH will supply standard, ready-to-use experiment control and monitoring GUIs via JDDD, self-describing and hyperlinked to the documentation. To utilize all provided IT infrastructure, detectors have to be integrated into the DOOCS system. Within the next few years, all detectors provided by FLASH, like the new detectors planned for CAMP (see Section 7.1.4) Timepix3 and PERCIVAL, will be fully integrated into the DOOCS / DAQ system.

For detectors employed in user experimental setups, we have motivated the users to either fully integrate detectors provided by DESY (including DOOCS controls) into their experimental setups, or work together with the DESY experts on the integration of their special detectors in DOOCS. The goal is to implement also all user detectors into DOOCS and to use the FLASH DAQ system.

9.2.2 Infrastructure

FLASH provides for each endstation the basic signals and commonly used detectors as described in the following:

Timing signals: Different types of triggers and reference frequencies are available to synchronize data acquisition with the FEL pulses. The triggers can be adjusted in sub-ns steps providing a long-term stability with sub-10 ps jitter with respect to the FEL pulses.

Analog to digital converters (ADC): A very common use case is the recording of fast analog electronic signals from MCPs, photodiodes, delay line detectors, and the like that have to be recorded. To serve this need, FLASH will provide at each user endstation access to different types of ADCs via patch panels. Available ADCs will be 108 Msamples per second (16 bit resolution) as well as different options for high resolution TOF spectroscopy ranging from 2 Gsamples up to 10 Gsamples per second (12 bit resolution) ADCs.

The ADCs are operated in the MTCA4 environment and are fully integrated in DOOCS with oscilloscope-like JDDD GUI interfaces. Additional analog and digital in- and outputs to control the experiment or provide feedback are available as well.

Cameras: A large fraction of experiments relies on 2D detectors. Here ,FLASH also provides a collection of cameras that can be plug-and-play integrated into the experiment (standard optical CCD and CMOS cameras). In addition, a limited number of in-vacuum XUV CCDs and other high-end cameras are available with full DOOCS support. Most camera types provided by users also can (with sufficient preparation time) be implemented in DOOCS.

Documentation: Electronic logbooks for experiment documentation are available for each beamline with one-click print options from JDDD and automatic beamline and DAQ status entries documenting the FEL, beamline and DAQ settings during the experiments.

Network: The general network infrastructure is 1 Gbit. Fast detectors will be connected by 10 Gbit lines.

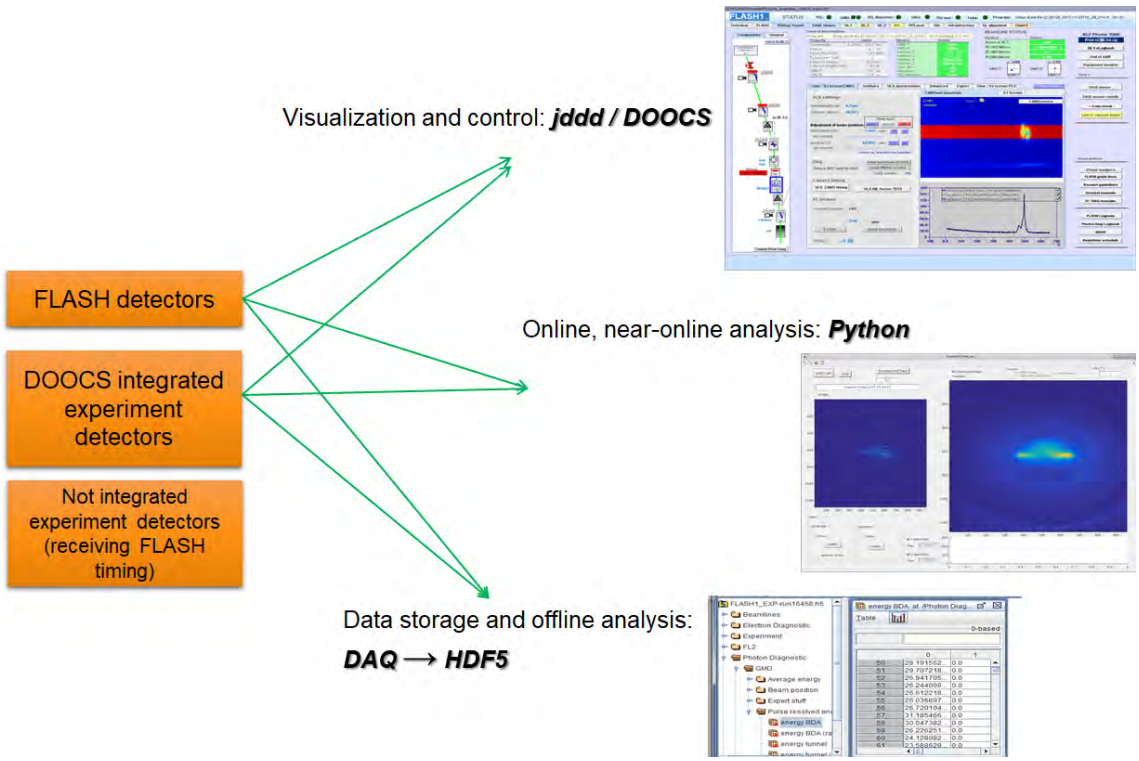

Figure 9.1: *The three pillars of the data analysis at FLASH.*

9.2.3 Online Analysis

In most cases the visual inspection of the recorded data (using JDDD) is by far not sufficient to judge the quality and statistical significance. As pointed out before, pulse-synchronous online data analysis is crucial for the success of the complex experiments performed at FLASH. For many standard analysis situations, which are similar for several user experiments (scans, sorting according to photon diagnostic parameters, correlation plots, covariance mapping, image inversion and reconstruction, ...), FLASH will provide easy to use data analysis GUIs as well as the integration of standard analysis software (e. g. Hummingbird, CASS, ONDA) in the FLASH control system.

Still, every experiment is different and needs specific analysis. User experiments need a well-maintained interface to DOOCS which has been realized as Python API (pydoocs). In order to use this framework efficiently, FLASH will provide pydoocs documentation, example scripts and a "virtual" pydoocs environment to test analysis scripts well before the beamtime. This "data simulator" will provide measured and/or simulated sample data from HDF5 DAQ files to test analysis scripts with real data rates and realistic FEL parameters. The sample datasets will be provided by FLASH for standard detectors. This Python API will allow programmatic access to online pulse-synchronous machine and experiment data.

9.2.4 Data Acquisition and Near-Online / Offline Analysis

The online analysis is crucial to tailor the experiment using a limited number of parameters to ensure high quality data. An extensive and detailed analysis on the other hand cannot be performed during the very limited beamtime. For the careful analysis all saved parameters from user experiments, photon- and electron diagnostics as well as beamline settings have to be easily and in a transparent way accessible to the user for near-online and offline analysis.

All parameters integrated in DOOCS can be recorded in the FLASH DAQ system. Based on the long lasting experience a set of important parameters (>500) from diagnostics and beamline settings has been defined which is permanently recorded whenever the FEL is in operation. In addition, users can, according to their needs, record additional experiment related data (ADCs, cameras, other DOOCS integrated devices) in a dedicated user DAQ system.

The recorded data is continuously converted into HDF5 files which are easily accessible via a provided Python API a few minutes after the data was taken. This scheme allows the pulse-synchronous access to all recorded data already during data taking. The API hides the complexity of gathering data from up to thousands of HDF5 files produced by different DAQs. To perform the final offline analysis in the user home institute, the option is offered to combine the data from different DAQs into large HDF5 files to get easy access also without the FLASH API. In contrast to very hardware specific naming in DOOCS, the HDF5 naming scheme is specifically structured for user needs. The transparent, self-describing and extensively commented data structure helps to easily find the parameters of interest.

The HDF5 files are stored in a data storage system (GPFS) with a large capacity (>3 PB for DESY photon science) which is located in the DESY computer center and is managed by central IT. The access-controlled experiment data (only registered experiment participants have access) is available on disk for analysis for about half a year and will be archived on tape for a period of 10 years. A folder structure is created on this storage system for each beamtime to provide a single point of storage for all experiment-related data.

Apart from storing the HDF5 files from the FLASH DAQ, the result of the data analysis and other meta data, this storage place can also be used to save user data not recorded by the FLASH system e. g. for special detectors with highly specialized analysis software that are not yet integrated into the FLASH control system / DAQ. Here, a sophisticated timing distribution via the sensor network timing protocol ensures that the user detector can acquire programmatic access to the current train ID and thus record the data pulse-synchronously.

Since the data volume per experiment gets larger and larger, the transfer of all the raw data to the home institutes will become increasingly difficult and cumbersome. DESY has to provide sufficient compute resources for an offline (and near-online) data processing on site with fast connection to the storage. Here, DESY's central IT provides and expands a state-of-the-art high performance cluster (Maxwell) for DESY photon science research as well as for users, that is connected with a fast connection (EDR InfiniBand) to the storage. This infrastructure has to be continuously increased and adapted to arising demands.

FLASH follows the DESY guidelines concerning data policies. Currently, strategic discussions on open data access are ongoing. According to the present data policy, the principle investigator is responsible for the data and has the right to change the access permission. Other institutes have already implemented an open access policy, making scientific data publically available after an embargo time, following the recommendations of the PaNdata Europe project ("Common policy framework on scientific data").

Since FLASH has already an authorization management system for stored experiment data (GPFS), it is technically easily possible to provide public access after an embargo time. However, a sensible implementation of an open data model requires a comprehensive metadata catalog supporting detailed data searches, e. g. based on the experimental technique, experimental setup, sample composition and FEL parameters.

9.2.5 Scientific Computing

The main target of data analysis is the extraction of knowledge from the raw data. The analysis concepts used so far, mostly based on analysis codes specifically developed by users, often for a single beamtime, are not efficient for more and more complex experiments. Users will need assistance by experts instructing them how to use the appropriate tools in the DESY computing environment. Experts with computational skills as well as a deeper understanding of the experiment will be required to efficiently optimize the data analysis and extract all information from the raw data.

In addition, FLASH will provide applications for reconstruction, analysis, simulation and modeling with convenient interfaces to be used interactively, in batch mode or by web applications. There will be significant development needed to analyze the raw data from the detectors on the fly to extract the essential data (e. g. principle component analysis), reject insufficient data and thus reduce the amount of saved data significantly. Providing fast analysis for pulse-resolved diagnostics (pulse energy, pulse-resolved wavelength and pulse duration)

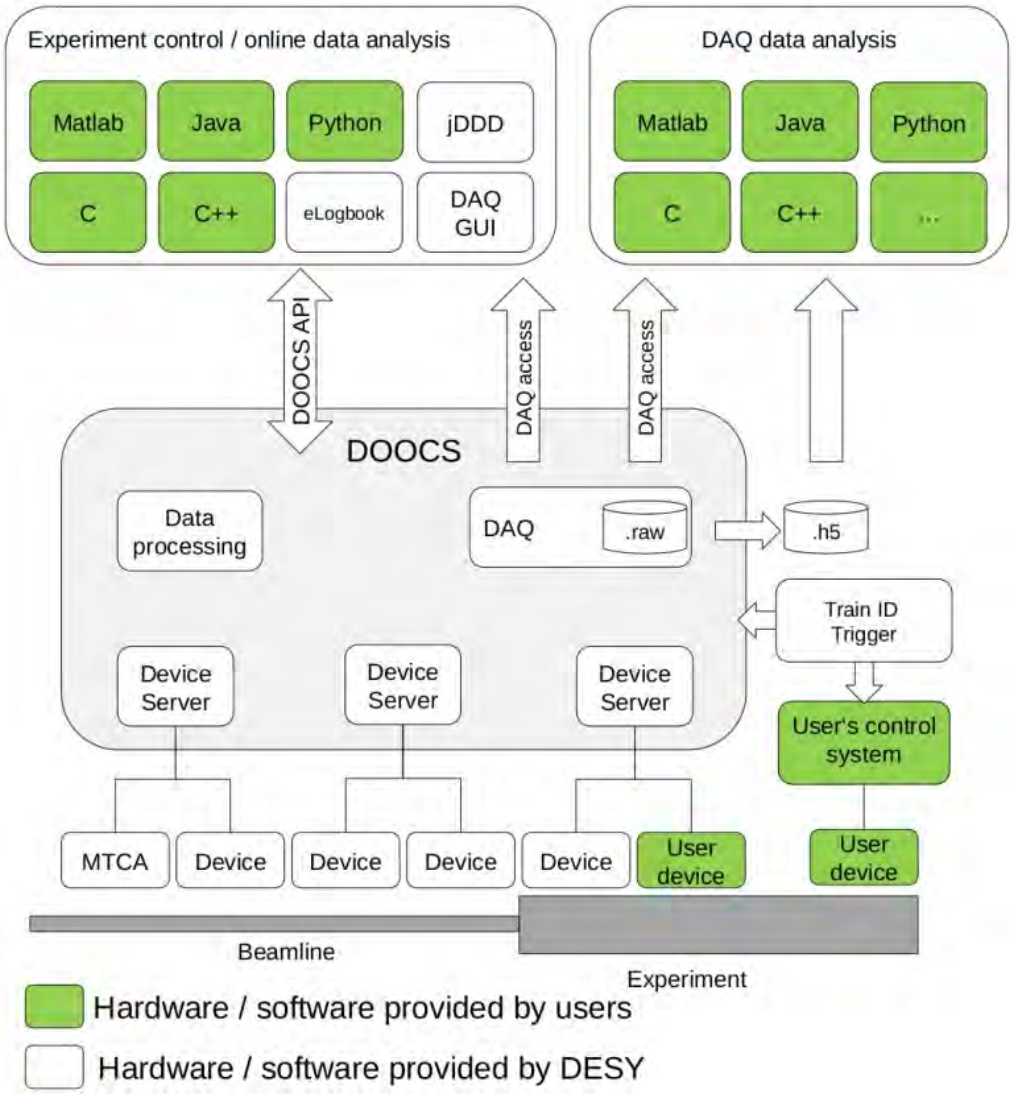

Figure 9.2: *Schematic view of the data flow from diagnostics, beamline and experiment data to controls and analysis options.*

as well as for user data yields an important step for online analysis.

Depending on the signal complexity, hardware related approaches using FPGA and GPUs will be pursued for well-defined scopes while machine learning technologies will be investigated for more complex data. Besides data reduction, machine learning can in particular help to judge the quality of the acquired data for photon diagnostic data as well as for user data.

A currently ongoing evaluation project (in collaboration with the Univ. Kassel and HZB) judges the signal quality and the automatic detection of space charge effects for photoelectron spectroscopy. Similar methods can also be implemented for 2D data as was recently demonstrated in the classification of complex diffraction images recorded with single FEL pulses (Langbehn et al. 2018; Zimmermann et al. 2019). FLASH will build up knowledge and infrastructure to help users implementing machine learning algorithms for similar cases.

Machine learning methods can also help to improve the radiation properties of the FEL. In the accelerator hundreds of parameters are influencing the (highly nonlinear) creation of photon pulses. So far the optimization of the XUV photon parameters (e. g. pulse energy, pointing, spectral distribution, arrival time, pulse duration) are optimized by operators, mainly focusing on one or two parameters. The optimization of all parameters at the same time is an extremely difficult task and mostly not possible in all day operation.

Here, reinforcement learning, a sub-field of machine learning, can be used to fulfill such a complex task. Using the measured photon

and electron diagnostic parameters as input, modern algorithms can in principle be used to find optimum parameters for the accelerator settings.

Such a demanding project will be followed in small implementation steps in close collaboration between the photon diagnostic group and the accelerator group as well as with international partners from other accelerator labs. First results from LCLS show the potential of the new approach (Scheinker et al. 2018; Sanchez-Gonzalez et al. 2017). The field of machine learning however is currently extremely dynamic, thus it is hard to predict the impact in the next few years. We are aware of the great potential and will thus closely follow the development to identify the most promising attempts for our needs.

References

Langbehn, B. et al. (2018). „Three-Dimensional Shapes of Spinning Helium Nanodroplets“. In: *Phys. Rev. Lett.* 121 (25), p. 255301. DOI: 10.1103/PhysRevLett.121.255301.

Sanchez-Gonzalez, A. et al. (2017). „Accurate prediction of X-ray pulse properties from a free-electron laser using machine learning“. In: *Nature Communications* 8.1, p. 15461. DOI: 10.1038/ncomms15461.

Scheinker, A. et al. (2018). „Demonstration of Model-Independent Control of the Longitudinal Phase Space of Electron Beams in the Linac-Coherent Light Source with Femtosecond Resolution“. In: *Phys. Rev. Lett.* 121 (4), p. 044801. DOI: 10.1103/PhysRevLett.121.044801.

Zimmermann, J. et al. (2019). *Deep neural networks for classifying complex features in diffraction images*. Online.

title graphics: Martin Beye, DESY

Deutsches Elektronen-Synchrotron DESY
A Research Centre of the Helmholtz Association

The task of the Helmholtz Association is to pursue the long-term research goals of government and society, including fundamental research, as an autonomous scientific organization. To this end, it identifies and addresses the great and urgent challenges facing society, science and industry by conducting top-class research in line with its strategic programmes. With more than 40 000 employees and an annual budget of €4.8 billion, the Helmholtz Association is Germany's largest scientific organization.

HELMHOLTZ
RESEARCH FOR GRAND CHALLENGES

www.helmholtz.de